EXCIMER LASER RESEARCH

J. H. Parks, C. A. Brau and J. J. Ewing
AVCO EVERETT RESEARCH LABORATORY, INC.
2385 Revere Beach Parkway
Everett, MA 02149

Interim Technical Report for Combined Periods 15 March 1975 to 15 October 1976

Sponsored by

DEFENSE ADVANCED RESEARCH PROJECTS AGENCY
ARPA Order No. 1806

Monitored by

OFFICE OF NAVAL RESEARCH
DEPARTMENT OF THE NAVY
Arlington, VA 22217

FOREWORD

ARPA Order No:	1806
Program Code No:	5E20
Name of Contractor:	Avco Everett Research Laboratory, Inc.
Effective Date of Contract:	15 August 1974
Contract Expiration Date:	14 October 1977
Amount of Contract:	$762,985
Contract No:	N00014-75-C-0063
Principal Investigator: Phone No:	J.H. Parks (617) 389-3000, Ext. 323
Scientific Officer:	Director, Physics Program, Physical Sciences Division, Office of Naval Research, Department of the Navy, 800 North Quincy Street, Arlington, Va. 22217
Short Title of Work:	Excimer Laser Research

UNCLASSIFIED

SECURITY CLASSIFICATION OF THIS PAGE (When Data Entered)

REPORT DOCUMENTATION PAGE	READ INSTRUCTIONS BEFORE COMPLETING FORM
1. REPORT NUMBER	2. GOVT ACCESSION NO. 3. RECIPIENT'S CATALOG NUMBER
4. TITLE (and Subtitle) (6) Excimer Laser Research.	(9) 5. TYPE OF REPORT & PERIOD COVERED Interim Technical Report 15 March 1975 to Oct 1976 6. PERFORMING ORG. REPORT NUMBER
7. AUTHOR(s) (10) J.H. Parks, C.A. Brau and J.J. Ewing	(15) 8. CONTRACT OR GRANT NUMBER(s) N00014-75-C-0063; ARPA Order-1806
9. PERFORMING ORGANIZATION NAME AND ADDRESS Avco Everett Research Laboratory, Inc. 2385 Revere Beach Parkway Everett, Massachusetts 02149	10. PROGRAM ELEMENT, PROJECT, TASK AREA & WORK UNIT NUMBERS
11. CONTROLLING OFFICE NAME AND ADDRESS Advanced Research Projects Agency ARPA Order No. 1806	12. REPORT DATE (11) Oct 76 13. NUMBER OF PAGES 85
14. MONITORING AGENCY NAME & ADDRESS (if different from Controlling Office) Office of Naval Research Department of the Navy Arlington, Virginia 22217	15. SECURITY CLASS. (of this report) Unclassified 15a. DECLASSIFICATION/DOWNGRADING SCHEDULE
16. DISTRIBUTION STATEMENT (of this Report) Approved for public release; distribution unlimited. (12) 77 p.	
17. DISTRIBUTION STATEMENT (of the abstract entered in Block 20, if different from Report)	
18. SUPPLEMENTARY NOTES	
19. KEY WORDS (Continue on reverse side if necessary and identify by block number) 1. Excimer 2. Lasers 3. Electron Beams 4. Rare Gas Halides	

20. ABSTRACT (Continue on reverse side if necessary and identify by block number)

This report describes a theoretical and experimental investigation of the rare gas monohalides. As a class, these molecules show great promise for achieving high power scalable laser action in the near UV portion of the spectrum.

A theory has been developed to describe the structure of these molecules. The predictions of this theory are borne out by fluorescence experiments.

DD FORM 1 JAN 73 1473 EDITION OF 1 NOV 65 IS OBSOLETE

UNCLASSIFIED

SECURITY CLASSIFICATION OF THIS PAGE (When Data Entered)

048430

TABLE OF CONTENTS

LIST OF ILLUSTRATIONS

I. INTRODUCTION

The combined Semi-Annual Technical Reports presented in this report cover the period 15 March 1975 through 15 October 1976. This composite report presents a complete description of AERL research in rare gas monohalide and halogen lasers.

Within this period ARPA/ONR sponsored laser programs at AERL have led to the discovery of two new classes of UV lasers; the rare gas monohalides and the halogen lasers.

The AERL research effort in this area has been three pronged. First, a basic theoretical and experimental understanding of the new molecules, the rare gas halides, has been achieved by studying the kinetics and spectroscopy of these species. Second, lasing experiments, using e-beam excitation, have been performed to demonstrate laser candidates and optimize the laser efficiency. Thirdly, research on electric discharge pumping techniques has been closely coupled with the molecular research to find scalable means to excite these systems. This approach has yielded the following significant results: Laser action was first demonstrated on XeF (335 nm),[1] XeCl (308 nm),[2] KrF (248 nm),[2] and I_2 (342 nm)[3] at AERL (Appendix A); an accurate, predictive, experimentally verified model has been developed to describe the chemical binding and spectroscopy of the rare gas halides[4, 5] (Appendix B); the first electric discharge pumped KrF laser was developed at AERL[6]; an accurate model has been developed to describe the KrF laser discharge;[7] an analysis discharge stability in such systems has been given;[8] high intrinsic efficiency has been demonstrated for KrF,[9] and more recently on XeF; discharge pumping of the Br_2 laser has been demonstrated under IR&D funding[10] and a sound understanding of the kinetics for both rare gas halides and halogen lasers is emerging. Under this contract, theoretical calculations of photoabsorption loss processes in discharge excited noble gases have been made and are reviewed in this report (Appendix C). A comprehensive review paper submitted for publication has been included in Appendix D.

The significance of the AERL effort lies in the fact that this new class of lasers offers the potnetial of both high overall electrical efficiency ($\geq$ 10%) and high average laser power ($\geq$ 100 kW/aperture).

An experimental effort is now underway to test the scaling laws developed for the electric discharge pumped KrF laser. If successful, this work will be a significant stepping stone to the first high efficiency, high average power short wavelength laser.

II. RARE GAS HALIDE SPECTROSCOPY

In appraising laser concepts that could lead to high overall efficiency, three simple criteria stand out. First, for allowed electronic transitions of atoms or molecules in the near UV, the radiative lifetime is generally short, in the range 1 nsec to 1 μsec. Second, the rate of decay of the lower laser level sets a limit in the intra-cavity flux that can be effectively utilized before "bottlenecking" occurs. The rate of populating the lower laser state via stimulated emission is given by $\sigma\phi_c(h\nu)^{-1}$ where σ is the stimulated emission cross section, ϕ_c the cavity flux in watts/cm^2, and $h\nu$ is the energy of the laser quantum. In order to avoid bottlenecking, the rate of decay of the lower state τ_L^{-1} should be larger than $\sigma\phi_c(h\nu)^{-1}$ for a ϕ_c which will efficiently extract the upper laser state population. For strongly allowed transitions, it is desirable to have $\tau_L^{-1} > 10^9$ sec^{-1}. Third, a most important practical consideration, is efficient matching of the laser discharge "load" to any electric pulse-forming network. This consideration places a strong preference on a laser medium that can be discharge pumped in a stable fashion (no rapid increase in electron number density or arc formation) with constant discharge impedance for times longer than roughly 200 nsec. This very germane efficiency consideration places a definite premium on continuously removing the lower level, i.e., removing bottlenecking.

The combination of the above three criteria has encouraged many workers to look for new lasers in which the lower level is rapidly dumped. Rapid removal of the lower level can occur in a variety of ways: collisional quenching, predissociation or, finally, dissociation of the lower laser level. The latter process is by far the fastest and characterizes what are commonly referred to as "excimer" lasers. In such a laser the lower level disappears on time scales of order 10^{-12} sec. If the lower laser level is rapidly removed, large intra-cavity fluxes can be used to efficiently extract every upper laser level formed in the pumping sequence. In this fashion, maximum efficiency can be attained within the limits of kinetic branching ratios and quantum efficiencies with which the upper level is formed.

Figure 1 shows a schematic molecular potential energy level diagram for a rare gas monohalide. One can see that these lasers utilize lower level dissociation. The upper laser level, denoted as MX^*, is bound with respect to dissociation into an inert gas atom M and an excited halogen atom, X^*. It is also bound with respect to $M^* + X$. The ionic nature of these excited states has been discussed.[4, 5, 11, 12] The excited state is nothing more than a positively charged inert gas ion, M^+, and a negative halogen ion, X^-, held together by coulombic rather than covalent forces. Predictions made at AERL under previous ARPA sponsorship of various properties of these excited species are based on the similarity of these excited states to the ionic ground states of the nearly isoelectric alkali halide ground states.[4] These predictions are accurate to within a few percent.[4, 5, 13] The similarity of the excited ionic states of the rare gas monohalides to ground state alkali halides derives from the fact that a rare gas halide ionic excited state differs by only one electron from an alkali halide. KrF^* is simply the ion pair $Kr^+ F^-$. Kr^+ is only different by one electron from Rb^+. Thus, the properties of KrF^* are very close to those of the ionic RbF molecule. A number of other useful analogies exist as well. For instance, the rare gas excited states, such as Kr^*, have low ionization potentials and as a result the chemistry of Kr^*, both kinetically and generically, is very similar to that of Rb.

MX^* has its potential minimum at a radius R_o, and can radiate to lower states that derive from the collision of ground state M and X atoms. Predicted estimates of R_o and other features of the class of rare gas halides are given in Table I. For the schematic potential curve shown in Figure 1, emission is centered near two wavelengths, λ_1 and λ_2. Two kinds of lower dissociative levels are shown, a $^2\Sigma$ state and a $^2\Pi$ state. This is the situation that applies for the collision of an atom with P symmetry and one atom with S symmetry. Spin orbit effects are neglected but are important in rare gas bromides and iodides. The $^2\Sigma$ lower state corresponds to having one halogen "hole" in a p orbital on axis with the rare gas atom. The rare gas halide lasers demonstrated to date have terminated on this $^2\Sigma$ state. The $^2\Pi$ state places the partially occupied p atomic orbital perpendicular to the molecular axis. The $^2\Pi$ state is strongly repulsive at the eqiuilbrium

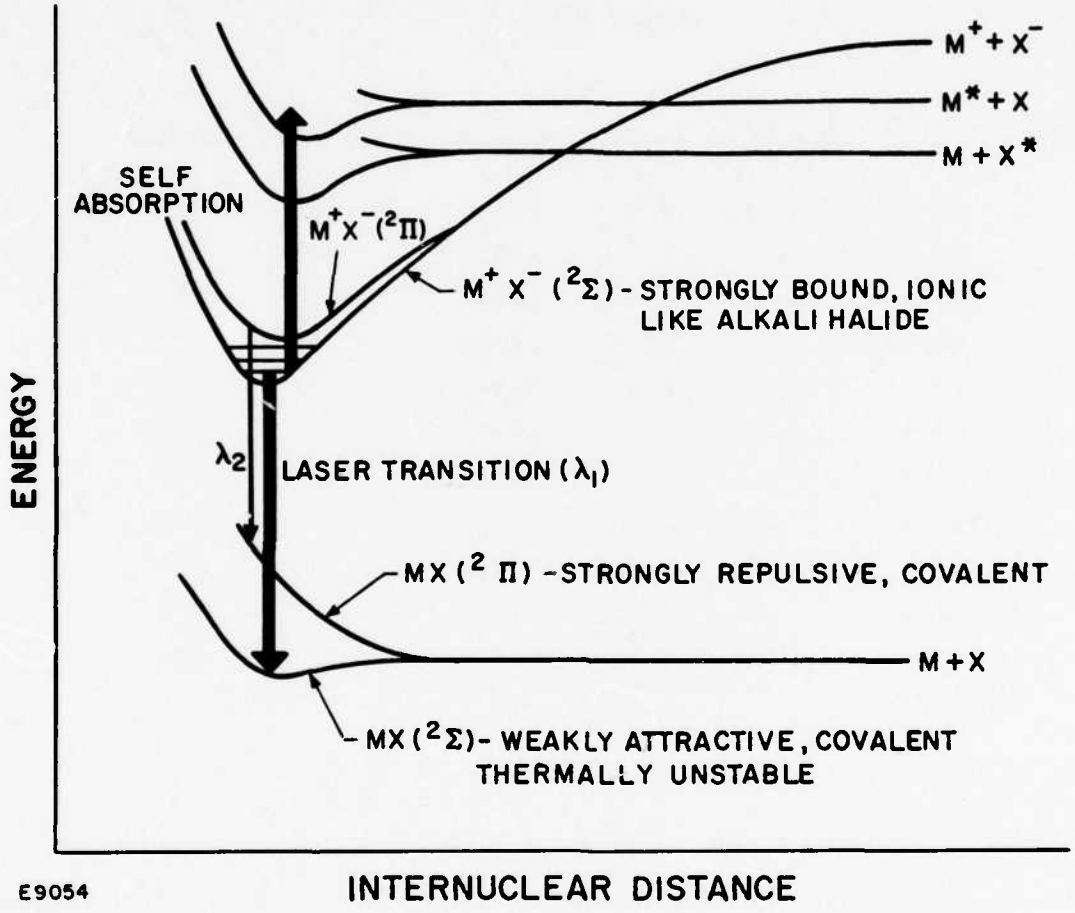

Figure 1 Schematic of Rare Gas Monohalide Potential Energy Curves

TABLE I

PREDICTED FEATURES OF INERT-GAS MONOHALIDES
FROM REF. 4

Molecule	R_A(Å)[a]	R_B(Å)[b]	R_O(Å)	E_M(cm^{-1})	λ_1(nm)	λ_2(nm)	λ_3(nm)[d]
XeI	19.2	6.3	3.3	39135	256	302	342
XeBr	32.0	15.9	3.1	34272	292	354	407
XeCl	71.9	c	2.9	30860	324	402	417
XeF	39.6	c	2.35	25895	386	503	512
KrI	14.1	5.2	2.9	49353	302	231	252
KrCl	30.5	9.8	2.8	45592	219	253	258
KrF	22.7	c	2.27	39229	256	301	305
ArBr	17.0	3.2	2.8	62152	161	178	190
ArCl	24.1	4.5	2.7	58042	172	192	195
ArF	18.9	c	2.17	37484	190	214	218
NeF	9.6	2.6	1.93	93266	197	115	115

a. R_A is the crossing radius of M^+X^- with $M^* + X$.

b. R_B is the crossing radius of M^+X^- with $M + X^*$.

c. These species have halogen excited-state levels only above the inert-gas excitation levels. Hence, no R_B crossing occurs.

d. $\lambda 3$ is the predicted wavelength of the broadband terminating on the $2\pi 1/2$ lower state. For all but XeI, XeBr, KrBr, and KrI, the λ_2 and λ_3 bands are overlapped.

e. For ArI, NeI, NeBr, NeCl, and the helium halides the inert-gas ionization potential is so large that the Coulomb curve does not made up sufficient energy to approach the low-lying halogen excited states. The compounds should only have small well depths and the molecular continua should be near the free atom lines. Possibly ionic states of opposite polarity, viz. $Ne^- + I^+$, could enter into the binding.

internuclear configuration of MX^*, R_o, because more electrons are between the halogen and rare gas nuclei. Emission terminating on the $^2\Pi$ states, near wavelength λ_2, is characterized by a relatively broad continuum bandwidth. Figure 2 shows a microdensitometer trace of the XeI emission spectrum. Note the sharp $\Sigma \rightarrow \Sigma$ band and the two broad $\Sigma \rightarrow \Pi$ bands. Two broad bands are present because of the large spin orbit splitting of the low lying $^2\Pi$ states. The success of the alkali halide model for the rare gas halides is shown by the comparison of existing data given in Table II to the predictions based on the model. Assuming comparable radiative transition rates to both states, the gain, assuming no excited state absorption on the transition near λ_1 will be higher on the $\Sigma \rightarrow \Sigma$ band because the bandwidth is narrower, explaining why existing rare gas monohalide lasers have operated on the sharper, higher gain bands.

The ionic excited state has $^2\Sigma_{1/2}$ symmetry to a first approximation. Higher lying $^2\Pi$ ionic states are also present, and recent calculations by Dunning and Hay show that the substantial spin orbit coupling of Kr and Xe halides can mix these states with the lowest $^2\Sigma_{1/2}$ ionic excited state.[14] Previously, concern that the upper laser level may not be the lowest ionic excited state had been expressed by several workers.[15,16] A recent spectroscopic investigation[17] of the XeF 354 nm band has eliminated this earlier concern and now all workers in the field agree with the earlier assignments of high pressure rare gas halide spectra made at AERL.[1,2,4,5]

The lowest $^2\Sigma$ covalent state, the lower laser level for the existing lasers, is not truly dissociative for XeF and XeCl. The lasing transitions are, in fact, bound to bound[5,17,18] for these species since these molecules have shallow wells in the lowest states. Recent molecular beam scattering experiments at Berkeley apparently show a chemical well depth in these species that is small but somewhat larger than that for a van der Waals interaction.[18] The binding of the XeF ground state was not anticipated theoretically.[19] However, recent calculations at NBS and IBM now give the slight binding ($\sim$700 cm^{-1}) observed in the beam experiments and derived from the XeF spectrum.[20]

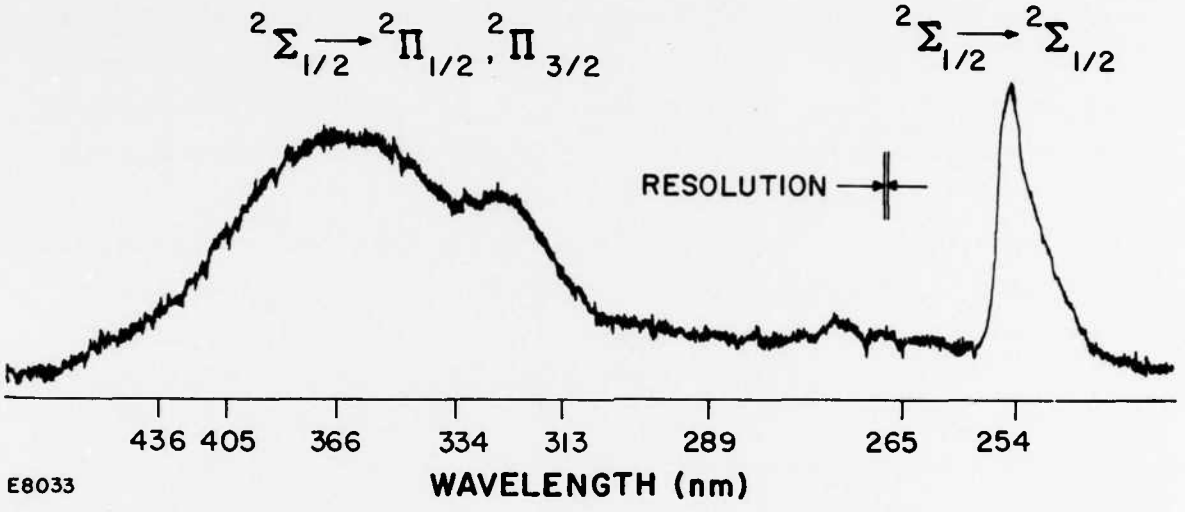

Figure 2 Microdensitometer Tracing of Spectral Plate of Spontaneous Emission Spectrum of XeI. The proposed broad band lasers for XeI would operate on the lower intensity bands assigned as $^2\Sigma \rightarrow {}^2\Pi$.

TABLE II

COMPARISON OF SOME OBSERVED AND PREDICTED FEATURES OF INERT GAS MONOHALIDES (OBSERVED FEATURES SHOWN IN PARENTHESES)[a]

Molecule	R_M(Å)	E_M(cm^{-1})	λ_1(nm)	ω(cm^{-1})
XeI	3.3	39135	256(254)	119
XeBr	3.1	34272	292(282)	150(180)
XeCl	2.9	30860	324(308)	214(210)
XeF	2.35	25195	397(353	365
KrI	3.2	54000	185	138
KrBr	2.9	49353	203	170
KrCl	2.8	45592	219	233
KrF	2.27	39229	256(248)	370(400)
ArBr	2.8	62152	161	220
ArCl	2.7	58042	172(170)	280
ArF[f]	2.17	51679	193	430
NeF	1.93	93266	107	536

[a]From Ref. 5.

As seen in Figure 1, there are higher lying potential curves that derive from $M^* + X$ and $X^* + M$. Not drawn are the potential curves for th ion MX^+, which are typically at higher energies. The exact energy and shape of the curves coming from $M^* + X$ has an important impact on the possibility of self absorption. Xenon bromide is probably a fine example of a rare gas halide that fluoresces very efficiently but lases very poorly.[21] This is probably due to self absorption[9] as pictured in the potentia curves given in Figure 3. Note that the self absorption is aphotodissociation process rather than the photoionization which plagues the rare gas excimer lasers such as Xe_2^*. The positions of the upper and lower laser levels can be determined by the wavelength and shape of the $XeBr^*$ emission bands. The exact R dependence of the upper potential curves and the wavelength dependence of the self absorption bands relative to the stimulated emission is not known. However, it is reasonably clear that absorption is possible in the $XeBr^*$ case for the $^2\Sigma \rightarrow {}^2\Sigma$ lasing transition. Rough consideration of the atomic orbitals that the electrons occupy in the various states suggests that absorption plays a major role in decreasing gain and efficiency in this system. Recall that the upper laser level is an ion pair $Xe^+ Br^-$. In making a transition to the lower laser level, an electron hops out of a p orbital of Br^- into the lowest vacant orbital of Xe^+, a 5 p orbital. This produces ground state Xe and Br atoms. However, in making a transition upward to $Xe^* + Br$, the electron hops from Br^- into a large 6s orbital of Xe. By virtue of the fact that the final electron orbitals centered on xenon for states of Xe^* are larger than those in which a ground state Xe atom is produced, one expects that the total transition dipole moment for absorption is larger than that corresponding to the lasing transition. The absorption is probably spread out over a broader band than the sharp laser transition, as in the alkali halides,[22] thus allowing for some net gain to occur.

One can see from the approximate potential curves for XeBr that emission on the broadband, near 400 nm, terminating on the $^2\Pi_{1/2}$ state would not add sufficient energy to the $XeBr^*$ excited state to allow a transition up to states deriving from $Xe^* + Br$. $Xe\,Br^*$ is at about 35,000 cm^{-1} and addition of a 25,000 cm^{-1} photon to this species is not sufficient to produce an excited state which dissociates into $Xe^* + Br$ or $Xe + Br^*$. This

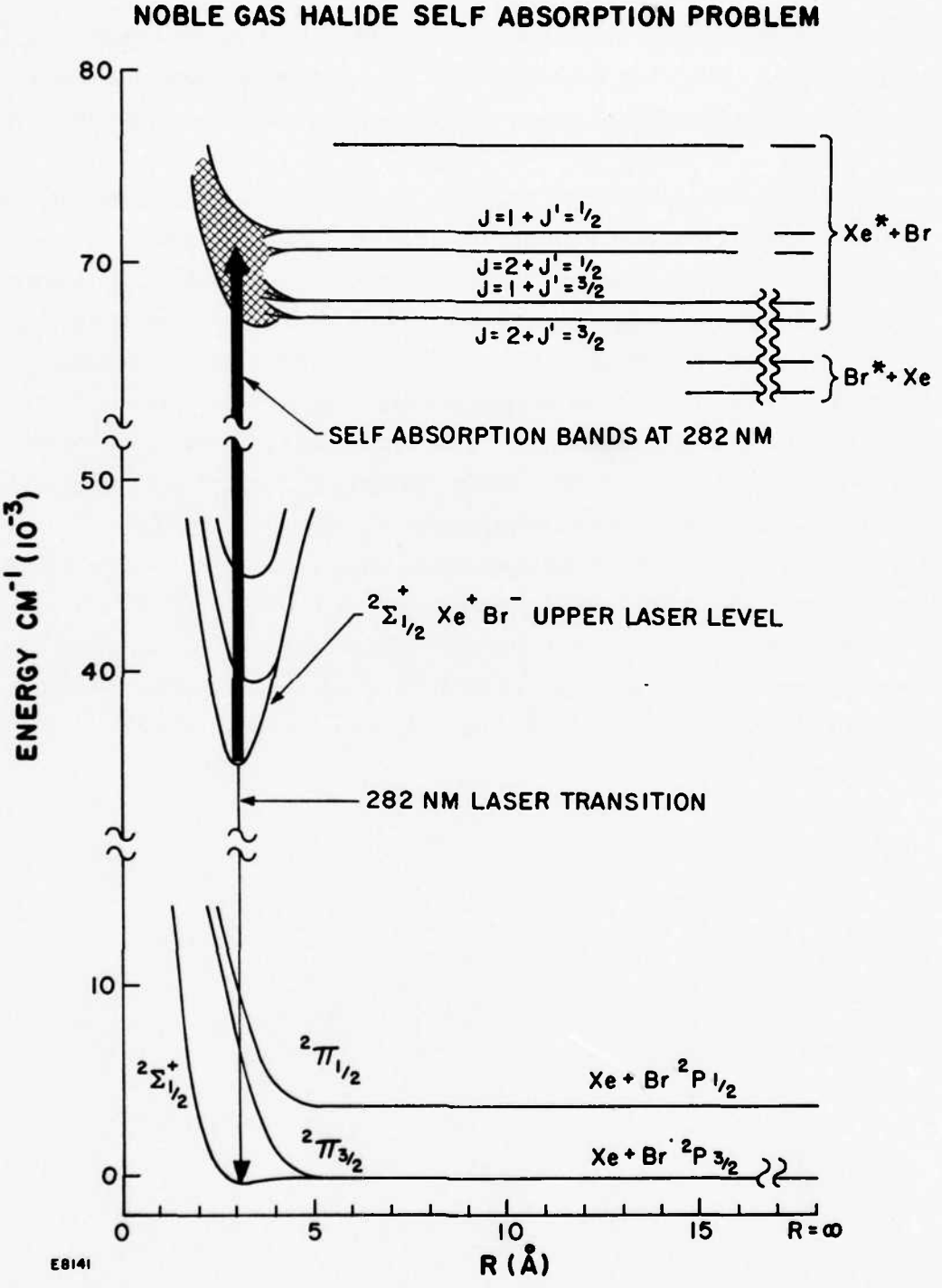

Figure 3 Estimated Potential Curves for XeBr Showing the Possibility of Strong Absorption Band Overlapping the Lasing Transition

is the basis for our conjecture that the broadbands of XeBr could lead to a UV/visible laser. It must be noted here that Br_2 would not be a good source for $XeBr^*$ for the broadband transition since Br_2 absorbs strongly in this band.

An important point to be made is that fairly high quantum efficiency is intrinsic to the rare gas monohalide lasers. Assuming the process begins with production of an excited metastable, such as Kr^*, quantum efficiences of order 50% can be achieved. The lost energy goes into chemical potential by dissociation of the weakly bound halogen molecules, such as F_2, and excess vibrational energy initially invested in producing the rare gas monohalide excited state. The latter loss, corresponding to about 2 eV per laser photon, goes into heavy particle translational energy of the laser mixture on a nanosecond time scale, whereas the energy stored in breaking halogen bonds does not appear as heat until a time scale greater than a microsecond. Neglecting heating due to recombination, a 1 μ sec laser pulse producing 30 J/liter specific output in KrF will heat the gas mixture the order of 30°C. The neglect of gas heating due to F atom recombination is valid because such recombination is very slow[23] compared to the pulse length.

III. RARE GAS METASTABLE PHOTO-IONIZATION

During this contract period, the theoretical effort was directed toward photoabsorption processes in the KrF discharge laser. In a typical laser mixture[24] consisting of ~0.1% F_2/2% Kr/97.9% Ar at atmospheric pressures, the most important of such processes are: (1) F_2 absorption, (2) photo-ionization of excited states of argon and krypton, and (3) possible absorption in the rare gas-halide "molecules" themselves. Absorption due to F_2 is fairly well understood,[25] and constitutes the major loss mechanism, while process (3) cannot be treated theoretically until accurate potential energy curves for the high-lying excited states of KrF and ArF are available. Photo-ionization of Ar^* and Kr^* is amenable to theory, and we have therefore calculated the relevant cross sections. Besides representing a loss mechanism for the λ = 2486 Å laser radiation, the photo-ionization process produces additional free electrons, and may thus affect the discharge kinetics.

To our knowledge, no data or previous calculations exist for these cross sections. Dunning and Stebbings[26] have reported measured values for the upper limit of the photo-ionization cross sections at threshold for the Ar^* and Kr^*, $^3P_{0,2}$ metastable states. Although these are only upper limits, their accuracy is considered to be better than a factor of two,[27] and so they allow some comparison to be made between the theory and experiment. The agreement is very good for Kr^*, but the Ar^* theoretical value is considerably too low. Further analysis indicates that the calculations for the Ar^* and Kr^*, s state cross sections are extremely sensitive to the details of the model, particularly near threshold where the cross section is falling rapidly to zero. This, however, is not the case for the Ar^{**} and Kr^{**}, p state calculations. They are quite insensitive to the detailed model and therefore the theoretical values should be reliable. To obtain the absorption coefficient, we have renormalized the Ar^* theoretical curve so as to agree with the experimental, upper-limit value at threshold.

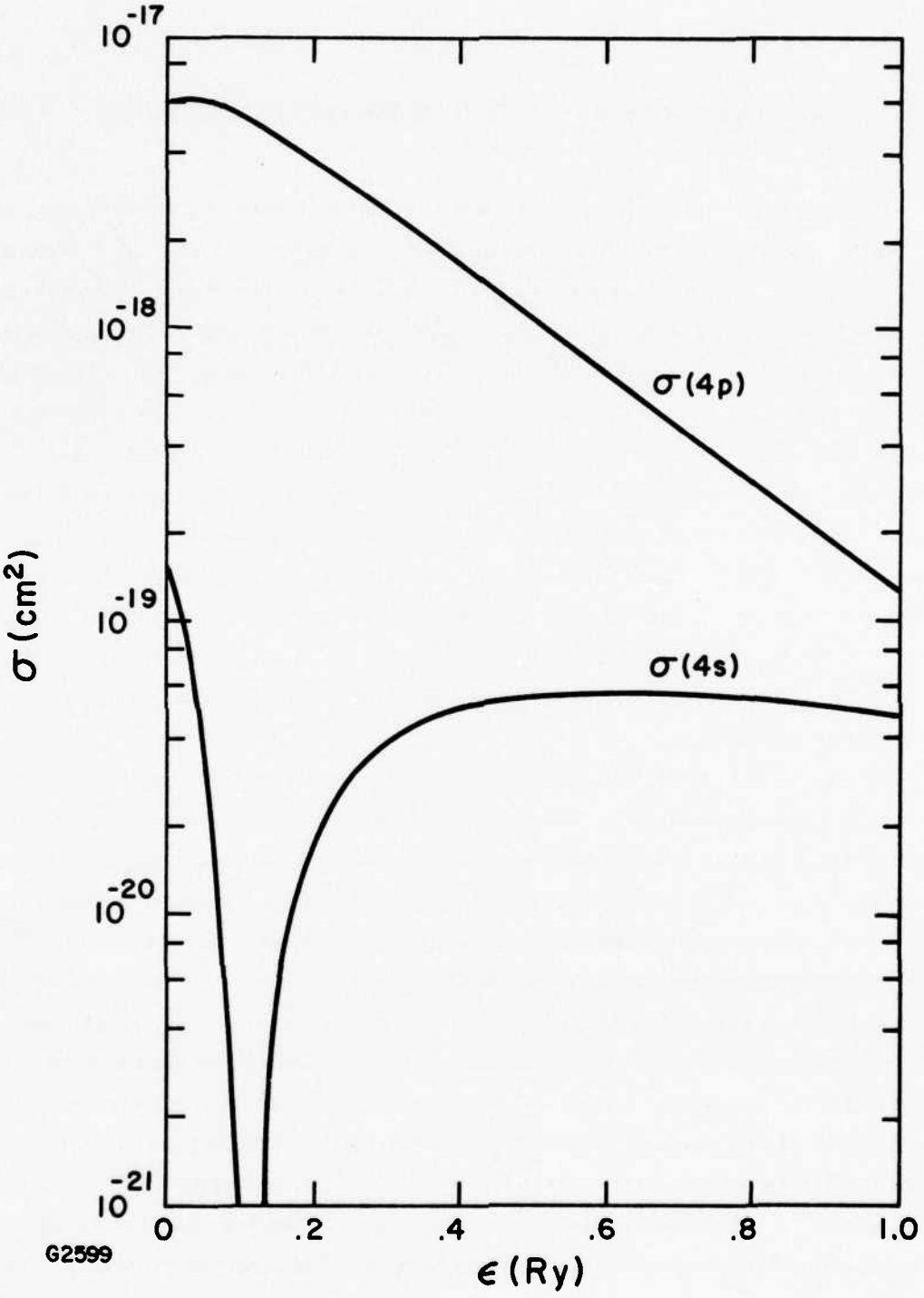

Figure 4 Photo-Ionization Cross Sections for the Ar* State, σ(4s), and the Ar** State, σ(4p)

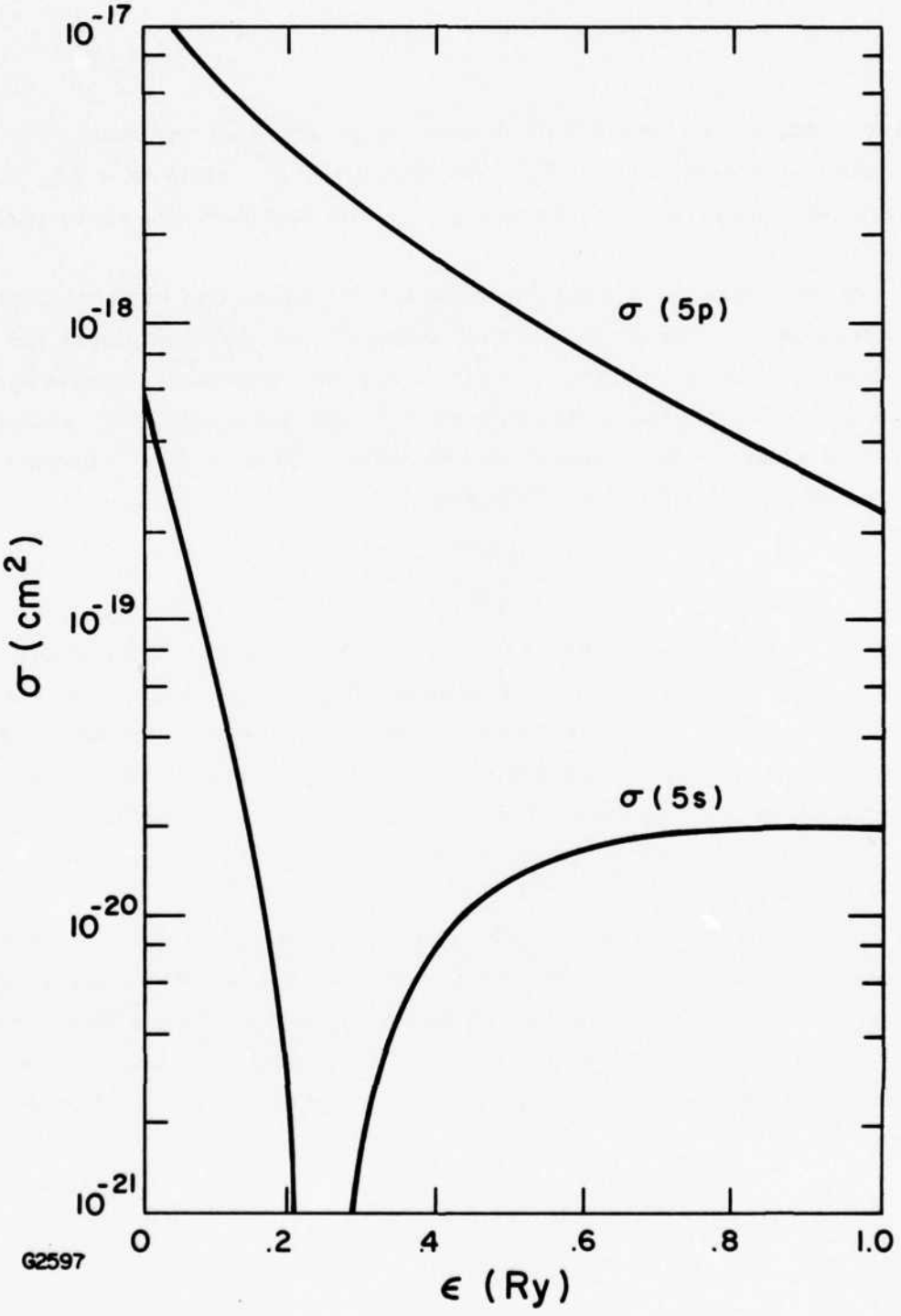

Figure 5 Photo-Ionization Cross Sections for the Kr* State, σ(5s) and the Kr** State, σ(5p)

The key result of the calculation is that, at $\lambda = 2486$ Å, the ratio of p state to s state cross sections is ~30:1, so that if the X^{**} state (X = Ar, Kr) is significantly populated in the discharge, it will dominate the photo-ionization process.

To calculate the absorption length in the laser due to photo-ionization, it is necessary to know the population of the various excited states for the appropriate discharge conditions. Since this information is not available, we have plotted in Figure 6 the absorption length L (in cm) at $\lambda = 2486$ Å vs the total excited-state number density N(s) + N(p) (in cm^{-3}) for various possible relative populations. Defining

$$\eta = \frac{N(p)}{N(s)} \equiv \frac{[X^{**}]}{[X^{*}]} \quad (X = Ar, Kr)$$

we show in Figure 6 the results for $\eta = 0.01$, 0.1 and 1.0 for argon (dashed lines) and krypton (solid lines). It is estimated[14] that $0.1 < \eta < 1$ and $N(s) + N(p) \sim 5 \times 10^{14}$ cm^{-3} for both argon and krypton combined, so that $L \sim 2 \times 10^{3}$ cm, giving an absorption of 5%/m per pass; this is within a factor of 2 of the F_2 absorption loss. Since the major absorption due to the photo-ionization process is due to the X^{**} state, it is desirable to operate at fairly low values of $[X^{**}]/[X^{*}]$.

To summarize, we have calculated the photo-ionization cross sections for several excited states of argon and krypton. The absorption loss due to this process is found to be siginficant under typical discharge laser operating conditions, but the effect can be minimized by running at relatively low excited-state densities, a condition that is compatible with discharge stability.[28]

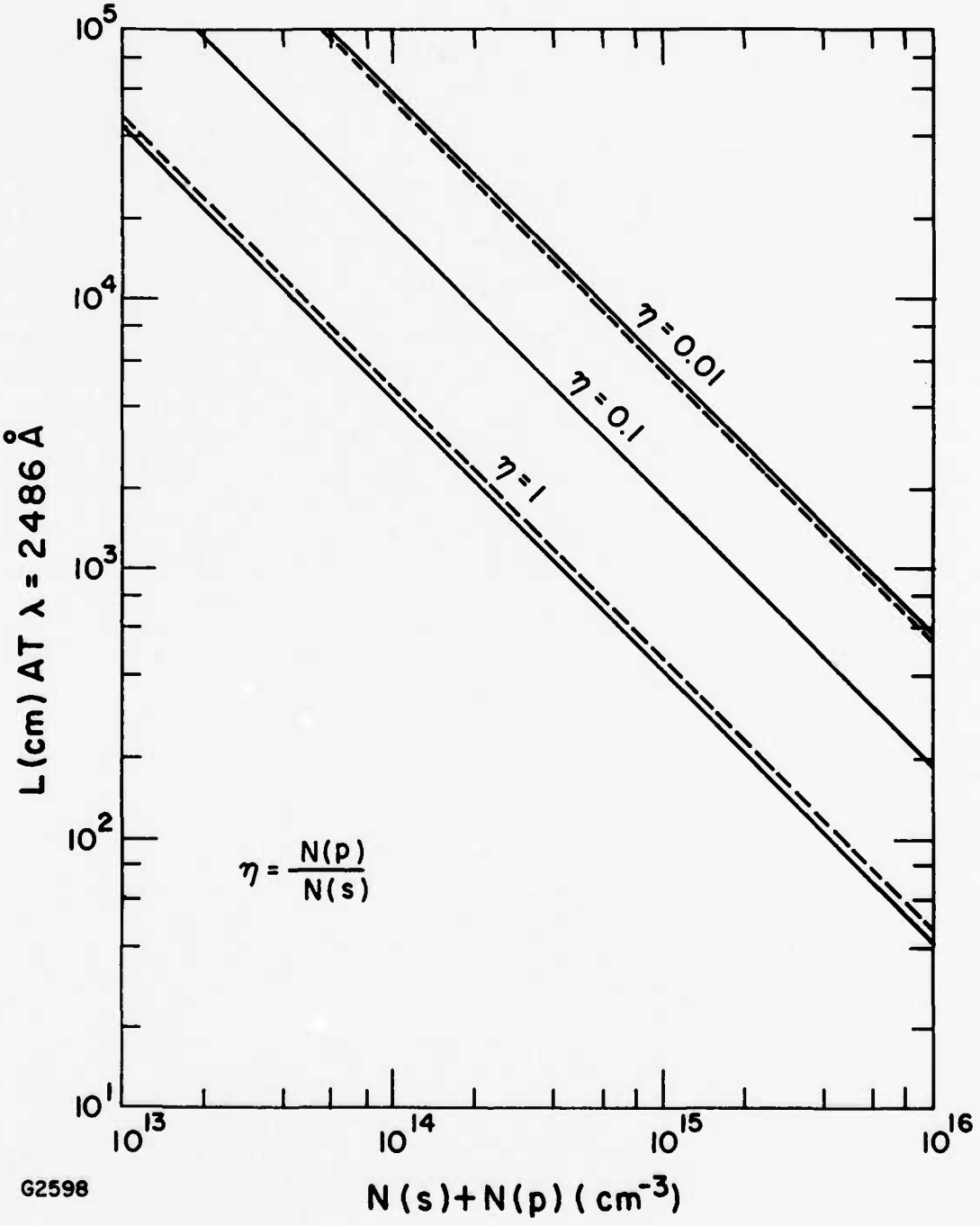

Figure 6 Absorption Length at λ = 2486 Å vs Total Excited-State Number Density. The dashed lines are for argon and the solid lines for krypton.

IV. RARE GAS HALIDE KINETICS

The excited-state chemistry that leads to excited rare gas halogen molecules involves a set of competing kinetic paths. The importance of each mechanism can vary with the means of excitation, pressures and mixture mole fractions. In certain mixtures, the rare gas halide emission is dominant. In other mixtures emission on certain bands of halogen molecules is derived or dominates. This brief discussion and the accompanying tables will show the similarities and complementarities of the kinetic chains that can lead to the various emission spectra. Detailed modeling of these lasers is currently under way in several laboratories, and a thorough review of this is premature and not given here.

Table III gives an overview with short comments on the various reactions which can produce the upper laser levels. Table IV gives an overall kinetic mechanism for rare gas halides. The principal reaction mecahnisms are the alkali-like direct reactions, displacement reactions and ion reactions. The other mechanisms are listed for completeness.

As pointed out above, species such as KrF^* are nothing more than short-lived "pseudo-alkali halides," i.e., diatomic molecules in which one electrical charge has been transferred from the rare gas atom to the halogen. The halogen lasers also operate on transitions from ionic excited states. That is, the upper laser level Br_2^* is the ion pair Br^+Br^-. The formation of alkali halide molecules, halogen ionic excited states and rare gas halide excited states can all proceed along chemically similar pathways. This similarity derives from the fact that metastable rare gas atoms, Kr^* for example, or highly excited halogen atoms have low ionization potentials and chemically behave like ground-state atoms that have low ionization potentials, viz the alkali atoms.[10, 11, 12, 29] The chemical kinetics of alkalis reacting with halogen molecules has a long history and this chemistry is understood in much detail. The mechanism for such alkali/halogen reactions is discussed in detail elsewhere.[29] The reaction of a Kr^* or Br^* with a halogen containing molecule should produce an ionic species. Reactions 1a,

TABLE III

SIMPLIFIED KINETICS FOR FORMING EXCITED STATES OF RARE GAS HALIDES OR HALOGEN LASERS

Rare Gas Halides		Halogens	
1a	$Ar^* + X_2 \rightarrow ArX^* + X$	Ia	$X^* + X_2 \rightarrow X_2^* + X$
1b	$\rightarrow Ar + X^* + X$		
	Branching can lead to either a rare gas halide laser via 1a or a halogen laser via 1b followed by Ia. Large rate constants measured.		Could also branch to lower states of X_2 causing inefficiencies. Large rate constants predicted.
Ion Reactions			
2a	$Ar^+ + F^- + M \rightarrow ArF^* + M$	II	$I^+ + I^- + M \rightarrow I_2^* + M$
2b	$Ar^+ + Br^- + M \rightarrow Ar + Br^* + M$		
	Extremely rapid and of utmost importance in pure e-beam excited mixtures with rapidly attaching halogens.		Extremely rapid, and could be important in systems in which positive halogen ions are formed.
Displacement Reactions			
3	$ArF^* + Kr \rightarrow KrF^* + Ar$	III	$X_2^* + Y \rightarrow XY^* + X$
	Exothermic Ionic displacement in which Kr^+ ion replaces Ar^+ ion. A major channel in e-beam sustained discharges. Large rates estimated.		For exothermic reaction combination could lead to inner halogen emission viz: ($ClBr^*$). Probably not important since large density of free atoms hard to come by.
Recombination of Excited Halogens			
4	$Br^* + Xe + M \rightarrow XeBr^* + M$	IV	$I^* + I + M \rightarrow I_2^* + M$
	Reactions such as this important in $Ar/Xe/X_2$ mixtures where reactions 1b or 2b are fast and produce the excited halogen rather than the rare gas halide.		Rate of this reaction limited in a halogen laser by smaller amounts of I present. Obviously important when source of I atoms is completely dissassociated.
Direct Pumping-Electrons or Energy Transfer			
5	$e + XeF_2 \rightarrow XeF^* + F$ $\rightarrow XeF^* + F^-$ $Xe^* + XeF_2 \rightarrow XeF^* + Xe + F$	V	$e + X_2 \rightarrow X_2^* + e$ $Ar_2^* + X_2 \rightarrow X_2^* + 2Ar$
	Potential limited.		Possibly important in certain rare gas halogen mixtures.

TABLE IV

SIMPLIFIED MECHANISM/RARE GAS HALIDE LASERS

Discharge Pumping/Mixture

- Metastable Formation

$$e + Ar \rightarrow Ar^* + e$$
$$e + Kr \rightarrow Kr^* + e$$

- Reaction with Halogen

$$Ar^* + F_2 \rightarrow ArF^* + F$$
$$Kr^* + F_2 \rightarrow KrF^* + F$$

- Displacement

$$Kr + ArF^* \rightarrow KrF^* + Ar$$

E-Beam Pumping

- All of the Above
- Ion Recombination

$$e + F_2 \rightarrow F + F^-$$
$$F^- + Ar^+ + M \rightarrow ArF^*$$
$$F^- + Kr^+ + M \rightarrow KrF^*$$

1b and Ia of Table III are examples of such reactions. These reactions are thought to proceed by way of an ionic covalent curve crossing, often called the "harpooning" mechanism.[11, 12, 29] In such reactions, the low ionization potential of the alkali or excited species and the high electron affinity of the halogen molecules allows an ionic potential curve of the form $M^+ + X^-_2$ to cross that of $M^* + X_2$ at fairly large internuclear separations, distances of order 5 Å. The X^-_2 ion formed by an electron hop, when the ionic and covalent potentials become degenerate, is unstable with respect to dissociation into $X^- + X$ in the presence of the large electric field of the M^+ ion. As a result, the $M^+X_2^-$ temporary triatomic specie falls apart into an ion pair M^+X^- leaving behind an X atom. The term "harpooning" mechanism derives from considering the electron that hops from the M^* over to X_2 as the harpoon that creates an extremely large coulombic source that pulls the old X_2 molecule apart and forms the new ionic, M^+X^- species. The prime difference between reactions of halogen molecules with alkali metal atoms and the corresponding chemistry with excited states such as Kr^* or Br^* is that in the alkali reactions only one electronic state can be formed whereas several potential product channels can exist in certain excited state/halogen molecule reactions. A similar multiple product channel situation exists in the reaction of halogen atoms with diatomic alkali molecules. In this case, usually several low lying states of alkali atoms are produced by the chemical reaction.[30]

The cross sections and exit channel branching ratios for a number of excited metastable inert gas atoms reacting with halogens are now being measured.[31] The bulk of this work is being done at low pressures. The spectra observed are similar but not identical to those at high pressure as in e-beam or discharge excited lasers. A brief compendium of some of the published relevant reaction rates for reaction of metastable inert gases with halogen containing compounds is given in Table V.

TABLE V

SOME KINETIC RATE CONSTANTS FOR
RARE GAS METASTABLE/HALOGEN REACTIONS

		a. k_Q	b. σ_Q	Comments
$Xe^* (^3P_2)$ +	HBr	6.1	173[a]	
	HCl	5.6	119[a]	
	Cl_2	6.5	193[a]	
	Br_2	6.0	202[b]	
	CF_3I		184[b]	
	F_2	7.3	156[c]	Should produce XeF^* with near unit quantum yield
	NF_3	0.86	23[c]	
$Kr^* (^3P_2)$ +	F_2	8.1	163[c]	Should produce KrF^* with near unit yield
	Cl_2	6.0	147[c]	
	NF_3	1.6	39[c]	
	Xe	1.6	46[c]	
$Ar^* (^3P_2)$ +	Br_2	6.5	147[d]	Produces Br^*
	Cl_2	4.7	95[e]	
		7.1	142[d]	Produces $ArCl^*$ and Cl^*
	F_2	8.5	148[c]	Should produce ArF^* with near unit yield
	NF_3	1.4	28[c]	
	Kr	0.06	1.3[f]	
	Xe	1.8	40[f]	

a. Rate constants, k_Q, given in units of 10^{-10} cm/molecule sec.

b. Cross sections, σ_Q, given in units of 10^{-16} cm^2.

(a) = Reference 32
(b) = Reference 12
(c) = D. Setser, Private Communication
(d) = Reference 31
(e) = Reference 11
(f) = Reference 33

V. EXPERIMENTAL APPARATUS

The experimental results observed at AERL were obtained with a high-intensity e-beam which was used to pump high-pressure mixtures of Ar, Xe and the halogens. The e-beam gun is shown in Figures 7 and 8. The e-beam produced by this gun has an energy of ~400 keV/electron, and an intensity of about 30 A/cm^2 passing through the foil, over an area of ~1 cm by 15 cm. For laser experiments the intensity is increased to about 150 A/cm^2 through the foil at the expense of lowering the energy to about 300 keV/electron. The duration of the e-beam pulse is ~100 nsec, with a 10 nsec rise time and a 20 nsec fall time. The gun has proved to be very reliable, and dozens or hundreds of shots are generally obtained between foil failures.

The cell is mounted directly on the e-beam gun as shown in Figure 9. Several cells are available, including stainless steel cells with brazed sapphire windows capable of operating at temperatures up to 900°F and pressures up to 100 psia. In the present experiment an aluminum cell is used which is compatible with fluorine. The valves are stainless steel and the windows are sapphire or quartz. For maximum reliability, a .001 in stainless steel foil is generally used. Titanium is corroded by the halogens and aluminum is not as strong as stainless steel. However, for maximum e-beam transmission, aluminized kapton films are used. The cell can be warmed up using built-in cartridge heaters to provide a mild bakeout. The cell can be pumped out to an ultimate vacuum of better than 10^{-5} torr with a leak rate better than 10^{-4} torr/hr. Therefore, purity is not a problem.

The gases, except I_2 vapor, are premixed in stainless steel tanks and allowed to stand for several hours, or even several days, to assure that they are fully mixed when they are used. The iodine crystals were obtained from Merck and are claimed to be > 99% pure. They were placed in a small stainless steel sample cylinder attached to the cell through a stainless steel valve. The crystals and sample cylinder were repeatedly allowed to outgas at room temperature (under vacuum but valved off) and then cooled with

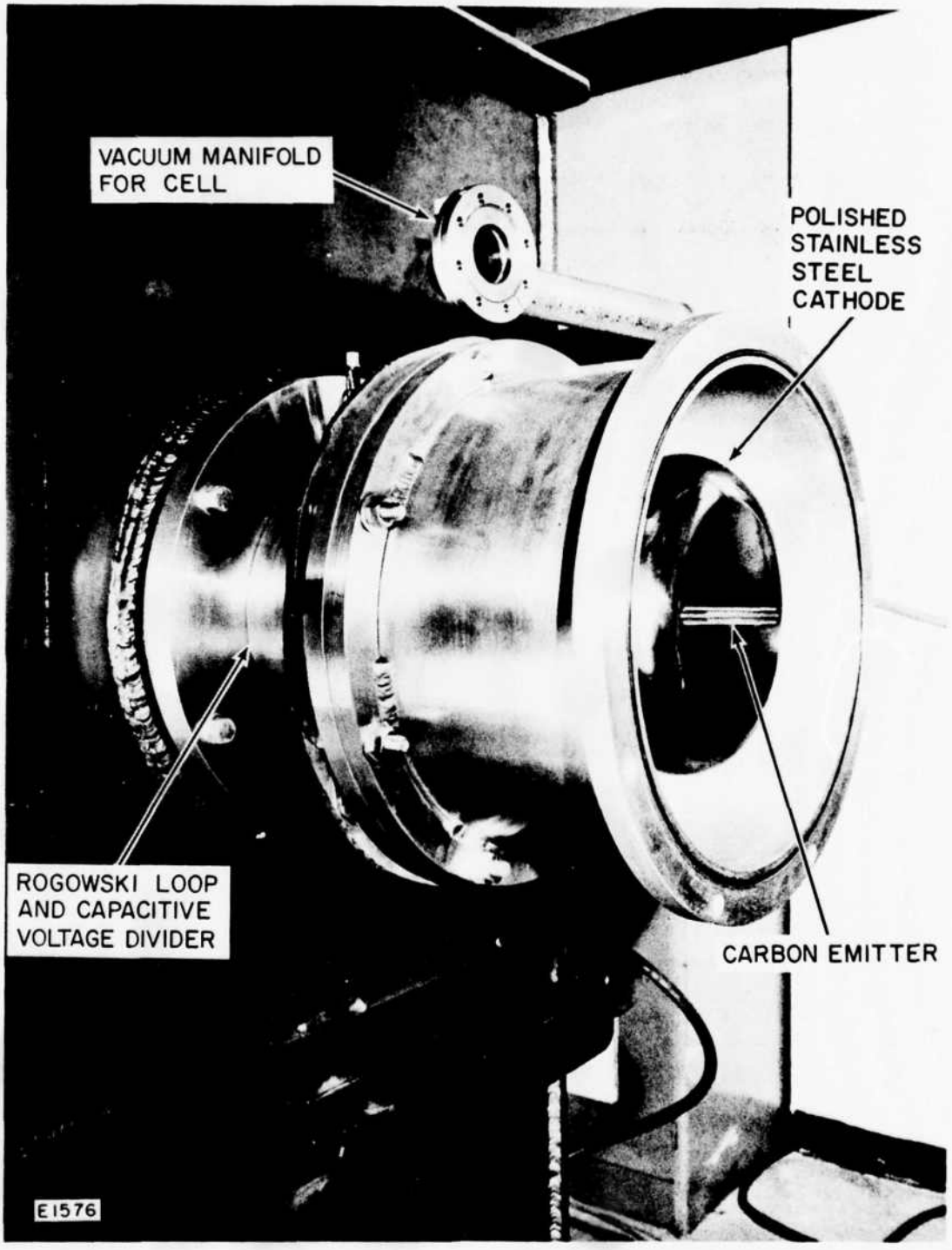

Figure 7 Photograph of the AERL High Intensity Electron Beam Gun

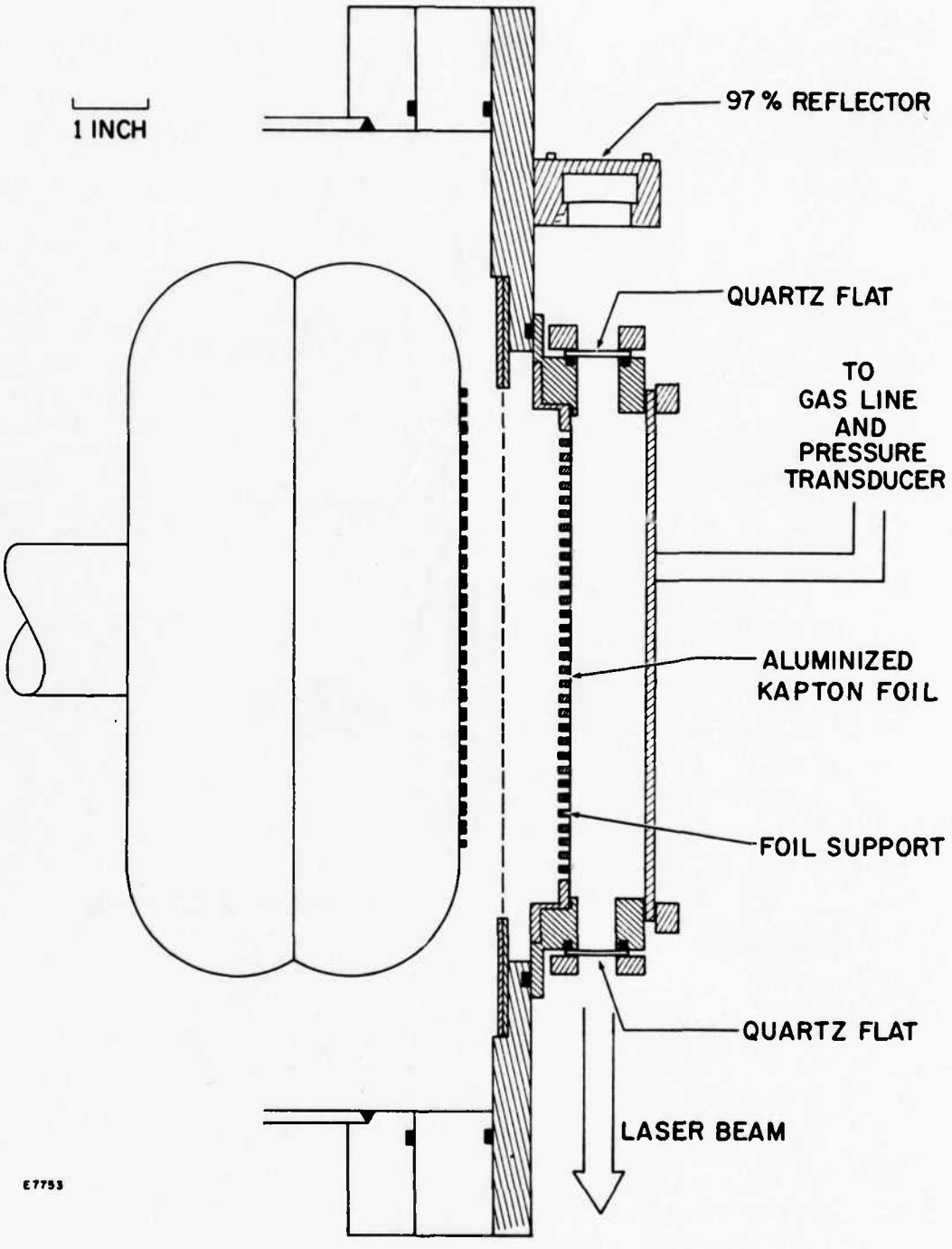

Figure 8 Cross-Sectional View of the High Intensity Electron Beam Gun and Laser Cell

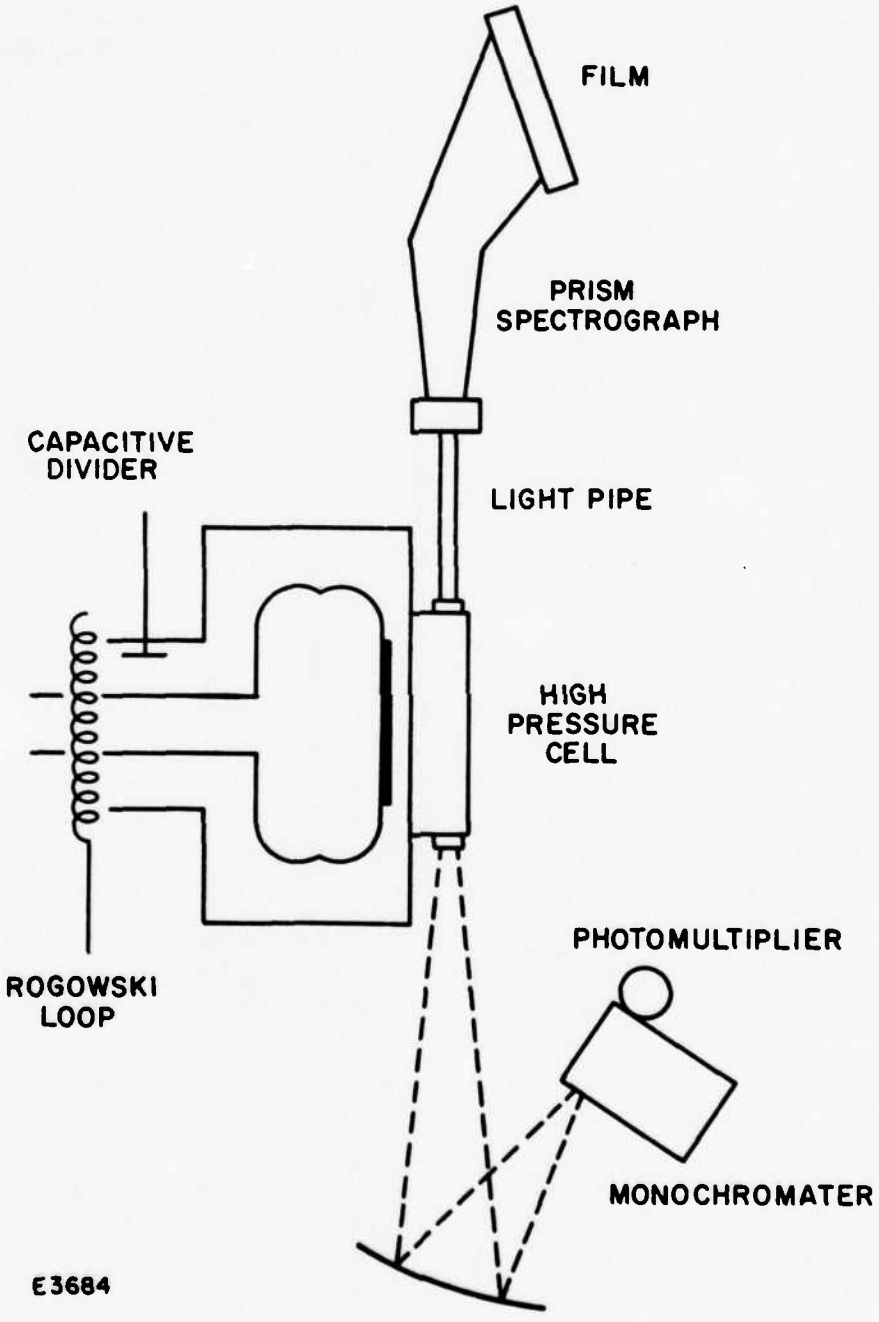

Figure 9 Schematic Diagram of Emission Diagnostics for Fluorescence Experiments

liquid N_2 and pumped out. The I_2 vapor is introduced directly into the evacuated cell and allowed to come into equilibrium. The rare gases are then admitted to the desired pressure and allowed to mix. Mixing is occasionally stimulated by firing the e-beam gun to warm the gas in the irradiated region. The liquid bromine was similarly outgassed by repeated freeze, pump, thaw cycles. Prior to making the measurements with F_2, the cell and mixing manifold were passivated by filling them with an F_2-rich mixture at low pressure (a few torr to half an atmosphere) for several hours.

The diagnostics, shown in Figure 9 include time-integrated and time-resolved emission measurements, as well as laser absorption measurements. The time-integrated emission measurements are made with quarter-meter and half-meter Hilger quartz prism instruments, using film. Generally, at high pressures, one shot is sufficient to provide a medium resolution spectrum using 50 μm slits. This corresponds to a wavelength resolution of $\sim$0.1 nm. The time-resolved emission measurements are made with a Jarrel-Ash one-quarter meter f/3.5 Ebert monochromater with a 1P28 photomultiplier tube, and Tektronix 551 oscilloscopes with type K and L preamps. The spectral resolution of this system is about 0.1 nm. The time resolution is limited by the oscilloscopes to $\sim$10 nsec. To provide an adequate signal-to-noise ratio, it has been found necessary to provide adequate lead shielding around the photomultiplier to screen out X-rays. In addition, it has been necessary to place the oscilloscopes in a screen room and provide careful grounding and shielding of the photomultiplier. Because of the intense emission observed from the rare gas halides it has been found necessary to take extreme care to prevent saturation of the photomultiplier.

Finally, laser optics and alignment equipment are available for laser experiments. The optical cavity consists of two high-reflectivity mirrors separated by about 25 cm. A stable resonator configuration is used in which one mirror has a 1 m radius of curvature and the other is flat. To reduce the losses, the normal incidence windows are aligned with the cavity. The alignment is carried out with a Davidson Optronics alignment telescope. Alignment accuracy of about 0.1 mrad is easily achieved, although much larger misalignments have no observable effect on the results.

VI. REFERENCES

1. C.A. Brau and J.J. Ewing, Appl. Phys. Lett. 27, 435 (1975).
2. J.J. Ewing and C.A. Brau, Appl. Phys. Lett. 27, 350 (1975).
3. J.J. Ewing and C.A. Brau, Appl. Phys. Lett. 27, 557 (1975).
4. J.J. Ewing and C.A. Brau, Phys. Rev. A12, 129 (1975).
5. C.A. Brau and J.J. Ewing, J. Chem. Phys. 63, 4640 (1975).
6. J.A. Mangano and J.H. Jacob, Appl. Phys. Lett. 27, 495 (1975).
7. J.H. Jacob and J.A. Mangano, to be published.
8. J.D. Daugherty, J.A. Mangano, J.H. Jacob, to be published, Appl. Phys. Lett. June 1976.
9. C.A. Brau and J.J. Ewing, "Rare Gas Monohalide Lasers: Performance and Spectroscopy," Second Summer Colloquium on Electronic Transition Lasers, Woods Hole, Massachusetts, Spet. 1975.
10. J.J. Ewing, J.H. Jacob, J.A. Mangano and H. Brown, "Discharge Pumping of the Br_2 Laser," Appl. Phys. Lett. June 1976.
11. M.F. Golde and B.A. Thrush, Chem. Phys. Lett. 29, 486 (1974).
12. J.E. Velazco and D.W. Setser, J. Chem. Phys. 62, 1990 (1975).
13. M.F. Golde, J. Mol. Spectry 58, 261 (1975).
14. T.H. Dunning, Jr. and P.J. Hay, Los Alamos Scientific Laboratory Report LA-UR-76-411, and Appl. Phys. Lett. (to be published).
15. J. Tellinghuisen, J.M. Hoffman, G.C. Tisone, and A.K. Hays, J. Chem. Phys. 64, 2484 (1976).
16. R.G. Gordon, Harvard University, private communication.
17. J. Tellinghuisen, Vanderbuilt University, private communication.
18. Y.T. Lee, (U.C. Berkely), private communication.
19. See Reference 5 for a complete discussion.

20. M. Krauss, National Bureau of Standards, private communication.

21. S.K. Searles and G.A. Hart, Appl. Phys. Lett. 27, 243 (1975).

22. P. Davidovits and D.C. Broadhead, J. Chem. Phys. 46, 2968 (1967).

23. P.S. Canguli and M. Kaufman, Chem. Phys. Lett. 25, 221 (1974).

24. J.A. Mangano and J.H. Jacob, Appl. Phys. Lett. 27, 495 (1975).

25. J.G. Calvert and J.N. Pitts, Jr., Photochemistry, (Wiley, New York, 1966), p. 184.

26. F.B. Dunning and R.F. Stebbings, Phys. Rev. A9, 2378 (1974).

27. R.F. Stebbings (Rice University), private communication.

28. J.A. Mangano (AERL), private communication.

29. For a discussion of the alkali/halogen reactions see for example Kieth J. Laidler, "Theories of Chemical Reaction Rates," McGraw Hill Book Co. New York (1969).

30. J.R. Krenos and J.C. Tully, J. Chem. Phys. 62, 420 (1975).

31. L.A. Gundel, D.W. Setser, M.A.A. Clyne, J.A. Coxon, and W. Nip, "Rate Constants for Specific Product Channels from Ar($^3P_{2,0}$) Reactions and Spectrometer Calibration in the Vacuum Ultraviolet," to be published.

32. J.E. Velazco and D.W. Setser, Chem. Phys. Lett. 25, 197 (1974).

33. L.G. Piper, J.E. Velazco and D.W. Setser, J. Chem. Phys. 59, 333 (1973).

APPENDIX A

354-nm LASER ACTION ON XeF

LASER ACTION ON THE $^2\Sigma^+_{1/2} \rightarrow {}^2\Sigma^+_{1/2}$ BANDS OF KrF AND XeCl

LASER ACTION ON THE 342-nm MOLECULAR IODINE BAND

354-nm laser action on XeF†

C. A. Brau and J. J. Ewing

Avco Everett Research Laboratory, Inc., Everett, Massachusetts 02149
(Received 29 May 1975; in final form 4 August 1975)

This letter reports laser action on the xenon monofluoride $^2\Sigma_{1/2} \rightarrow {}^2\Sigma_{1/2}$ band at 354 nm. Lasing on discrete vibrational bands has been achieved by pulse excitation of high-pressure mixtures of F_2/Xe/Ar with an electron beam. XeF is a member of a new class of diatmoic molecules, the noble gas monohalides, which all exhibit similar molecular structure and spectra, and laser action should be attainable on the various bands of other members of this class of molecules. The kinetics and loss mechanisms of these laser candidates are briefly discussed.

PACS numbers: 42.60.C, 32.20.F, 82.40.T

We have recently been studying the spectroscopy,[1] kinetics, and laser potential of a new class of molecules, the noble-gas monohalides. The possibility of laser action on bound-free transitions in molecules of this type was first suggested by Setser and co-workers.[2,3] Recently, Searles and Hart demonstrated laser action on the 282-nm transition in XeBr.[4] This letter reports e-beam–excited laser action on XeF at 354 nm. The laser transition originates on an excited state formed directly by chemical reactions in e-beam–excited Xe/F_2 mixtures. It terminates on a high vibrational level of the slightly bound XeF ground state. XeF is the one member of this class of molecules which, theoretically, should have both the highest intrinsic grain and the lowest intrinsic loss of this class of molecules.

The salient features of these diatomic molecules can be understood in terms of the approximate XeF potential-energy curves shown in Fig. 1. The lowest states of XeF and the other inert-gas halides are covalent in nature and have molecular symmetry $^2\Sigma_{1/2}$, $^2\pi_{3/2}$, and $^2\pi_{1/2}$. The covalent $^2\Sigma$ state is slightly bound while the $^2\pi$ states are repulsive. The binding energy of the $^2\Sigma$ state of XeF is probably of the order of 8000 cm^{-1}.[5] Transitions from the higher-lying excited states can be either bound to bound, as in the $^2\Sigma_{1/2} - {}^2\Sigma_{1/2}$ 354-nm XeF lasing transition, or bound to free, as in the $^2\Sigma_{1/2} - {}^2\pi_{1/2,3/2}$ transitions.

The higher-lying excited states of XeF, and the other noble-gas monohalides, are predominantly ionic in nature, having the polarity Xe^+F^-.[1] This ion pair is entirely analogous to an alkali halide both in binding energy and in gross structural properties. The ionic excited states have molecular symmetry $^2\Sigma_{1/2}$, $^2\pi_{3/2}$, or $^2\pi_{1/2}$, with the $^2\Sigma_{1/2}$ ionic state lying lowest.

The possibility of laser action on these species is apparently enhanced by a large reactive cross section for producing excited species by chemical reactions of the type

$$Xe^* + F_2 \rightarrow XeF^* + F. \qquad (1)$$

The measured rates for the analogous reactions of Xe^* + Cl_2 or Br_2 are quite large.[3] Apparently these chemical reactions, which start on an excited potential-energy surface of the $Xe + X_2$ triatomic system, have a high probability of staying on an excited potential surface, producing the electronically excited species with a large rate constant.

The estimated stimulated emission coefficient for the $^2\Sigma_{1/2} - {}^2\Sigma_{1/2}$ band in XeF is about 2×10^{-16} cm^2. This estimate is based on the measured spontaneous emission spectrum and the radiative lifetime, whose measurement will be described in a separate article. We have studied the spontaneous emission spectrum of XeF as a function of pressure and find that at pressures above about one-half atmosphere the upper state remains in vibrational equilibrium. The laser transition evidently originates from the lowest vibrational level of the excited state. Since the equilibrium bond length of the excited state[1] is apparently larger than that of the ground state,[5] it is believed that the laser transition terminates on a high vibrational level of the lower state, as shown in Fig. 1. The bandwidths of the $^2\Sigma - {}^2\Sigma$ transitions in the other xenon halides are somewhat larger. This is due to the fact that the other xenon halides have more closely spaced vibrational levels in both lower and upper states, and the spectra appear more like continua. The $^2\Sigma - {}^2\pi$ transitions in both XeF and the other xenon halides are considerably broader since these transitions are truly bound to free. Stimulated emission coefficients of the order of 10^{-18} cm^2 are calculated for these broad bands.

The lasing experiments were carried out in a high-vacuum high-pressure cell constructed of aluminum. Quartz optical windows, sealed to the cell with Viton o

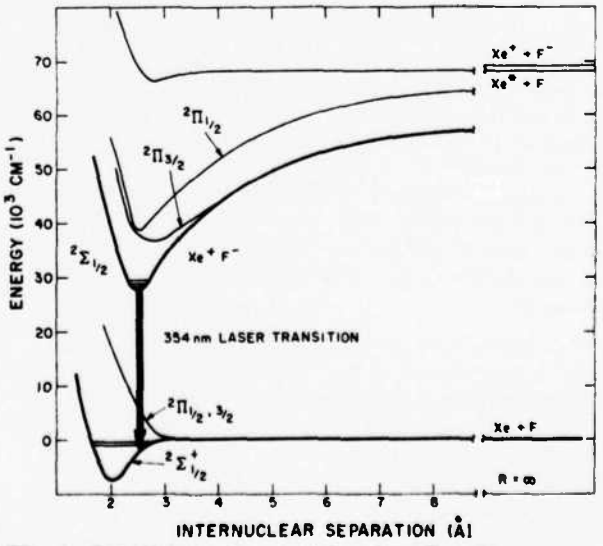

FIG. 1. Potential-energy curves for xenon fluoride.

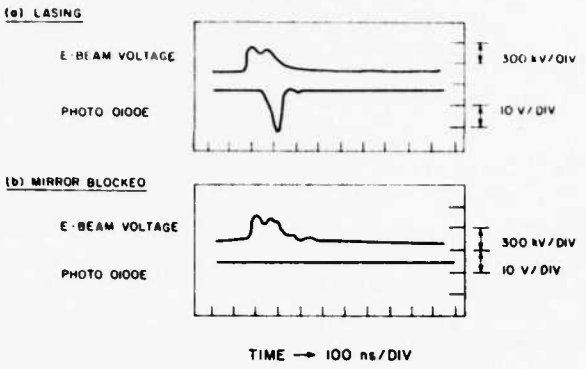

FIG. 2. XeF laser time history.

rings and a support structure, were located at the opposite ends of the cell. The optical aperture was about 1.2 cm in diameter. The volume between the windows was irradiated by a 100-ns pulsed e beam. The e beam, roughly 1×15 cm in area, was injected into the gas transverse to the laser cavity optical axis through a 2-mil aluminized kapton foil. The foil was supported by high-transparency aluminum-foil support. Pressures in the cell could be varied from high vacuum to pressures in excess of 5 atm. Since high pressure caused a measurable movement of the optical windows, as well as more frequent foil ruptures, most lasing experiments were performed at pressures under 4 atm. Gas mixtures were made up in a fully fluorine passivated stainless-steel system. The final gas mixes were placed in high-purity passivated stainless-steel sample bottles and allowed to stand for several hours before use.

During the mixing period, at room temperature, there is very little conversion of the Xe/F_2 mixtures into XeF_2. This has been determined by spectrophotometric measurements of the F_2 absorption in the uv. Irradiation of a sample with the e beam, however, converts a large fraction of the irradiated mixture into stable species such as XeF_2.[5] Thus, gas samples were discarded after being excited by the e beam. Typical mixture mole fractions were 0.001 F_2/0.003 Xe/0.996 Ar. Use of such Xe/Ar mixtures minimizes the amount of Xe_2^* and Ar_2^* that can be present during the e-beam pulse.

The e beam was formed between a cold-cathode electron-gun pulse charged to over 300 kV by an elght-stage Marx generator (Ion Physics Corporation). With an anode-cathode spacing of 1.3 cm, the current density impinging on the foil support structure was roughly 200 A/cm^2. Because of resistive and inductive voltage drops in the Marx generator, the beam voltage dropped by about 20% during the 100-ns pulse duration. The high voltage applied across the diode and the e beam formed therein was terminated after 100 ns by a spark-gap crowbar.

The optical cavity was formed by two curved mirrors (1 m in radius) having 99.97% reflectivity and 97.50% reflectivity at the wavelength of the XeF emission. The mirrors were external to the cell and separated by 30 cm. By carefully aligning the quartz optical windows, losses due to these surfaces could be minimized. Because of the proximity in wavelength of the Ar/N_2 ($C-B$) 358-nm laser transition, alignment could be readily and independently checked by producing laser action on this well studied molecular band.[6,7] Laser action on XeF could also be achieved using an 8% output coupling mirror. However, the laser power output and the gas-mixture pressure range over which one could achieve laser action was much more limited than was the case with the lower output coupling mirrors.

The output of the laser was directed onto a photodiode (ITT FW 128) and onto a spectrograph for temporal and spectral analysis of the laser-beam pulse. The laser beam was attenuated by a factor of 500 by passing through two 11% transmitting screens and a 350-nm filter ($\Delta\lambda = 35$ nm) before reaching the photodiode. The beam emerging from the other mirror was attenuated by a factor of 5 before reaching the entrance slit of an $f/10$ Hilger medium-resolution quartz spectrograph. Spectrograph slit widths of 20 μ were utilized, giving a resolution of about 0.1 nm at 354 nm. Spectra were recorded on Kodak 103-O plates.

Figure 2 shows typical photodiode and e-beam voltage signals obtained in lasing and nonlasing experiments. The stimulated emission intensity was a factor of 100 times brighter than the spontaneous emission intensity in the same band as measured by the photodiode signals. The stimulated emission typically started about 50 ns after the beginning of the e-beam pulse and lasted about 50 ns, at which time the electron beam was turned off. Peak powers of the order of 6 kW were attained. The intensity of the XeF laser beam was comparable to that from a mixture of 5% N_2 in Ar at the same pressure. A complete parametric optimization of the XeF system remains to be done. The spontaneous emission spectrum is considerably different from the stimulated emission spectrum. A comparison of the spectral plates and their microdensitometer tracings shows that the spontaneous emission band contains many vibrational bands while the laser spectrum shows two very pronounced and two weak vibrational bands. The strongest lines in the laser are also the strongest lines in the spontaneous emission spectrum. The integrated photodiode signal corresponds to a laser efficiency of the order of 0.01%. This efficiency is based on the energy deposited in the gas by the e beam, which is estimated from the incident e-beam current density using the stopping power tables of Berger and Seltzer.[8] Optimization of the laser mixtures, pumping power, and output coupling should increase this number.

The population inversion on XeF is caused by reactions of two kinds. First, F_2 can react with electronically excited xenon, Xe*, reaction (1). The Xe* is formed by rapid energy transfer[9] from Ar* and Ar_2^* which are produced by the electron beam.

The XeF* ionic excited state can also be formed by the rapid termolecular recombination of Xe^+ ions with F^- ions:

$$Xe^+ + F^- + M \rightarrow XeF^* + M. \tag{2}$$

These ion neutralization processes can have huge three-body rates.[10] The F^- is formed by dissociative attachment of electrons to the F_2 in the gas:

$$e^- + F_2 \rightarrow F + F^-. \tag{3}$$

Detailed modelling of the kinetics of this new laser needs to be completed however.

It is possible that the inversion can be sustained in this laser transition by the vibrational relaxation of the high-lying vibrational levels which are the lower laser levels in this transition. We do not yet know if this is possible.

Of this class of molecules, XeF stands out as having the potential for the highest gain and the lowest loss. It has higher gain than other species such as XeI because of its longer wavelength and distinctly structured spectrum. More important, however, this band in XeF is not overlapped by self-absorption by the XeF^* to higher-lying states, it does not have halogen-molecule absorption, as does the $XeCl/Cl_2$ system, and it is below the threshold for photoionization of both Ar^* and Xe^* metastables. Although laser action on the $^2\Sigma - ^2\Sigma$ bands of other xenon halides is apparently possible, we anticipate that XeF will have the lowest intrinsic loss of this family of molecules.

The authors wish to thank James Dodge for invaluable and expert assistance in the experimental phases of this work. Discussions with other members of the AERL staff, especially Dr. R.E. Center and Dr. J.D. Daugherty, are gratefully acknowledged.

[†]Work supported by ARPA/ONR.

[1]J.J. Ewing and C.A. Brau, Phys. Rev. A **12**, 129 (1975).
[2]J.E. Velazco and D.W. Setser, in 4th Conference in Chemical and Molecular Lasers, St. Louis, 1974 (unpublished).
[3]J.E. Velazco and D.W. Setser, J. Chem. Phys. **62**, 1990 (1975).
[4]S.K. Searles and G.A. Hart (private communication).
[5]N. Bartlett and F.U. Sladky, *The Chemistry of Krypton, Xenon and Radon in Comprehensive Inorganic Chemistry*, edited by J.C. Bailar (Pergamon, London, 1973).
[6]E.R. Ault, M.L. Bhaumik, and N. Thomas Olson, IEEE J. Quantum Electron **10**, 624 (1974).
[7]S. Searles and G.A. Hart, Appl. Phys. *Lett.* **25**, 79 (1974).
[8]M.J. Berger and S.M. Seltzer, National Academy of Science Report No. 1133 (1964) (unpublished).
[9]O. Cheshnovsky, B. Raz, and J. Jortner, J. Chem. Phys. **59**, 337 (1973).
[10]J.J. Thompson, Philos. Mag. **47**, 337 (1924).

Laser action on the $^2\Sigma^+_{1/2} \rightarrow {}^2\Sigma^+_{1/2}$ bands of KrF and XeCl†

J. J. Ewing and C. A. Brau

Avco Everett Research Laboratory, Incorporated, Everett, Massachusetts 02149
(Received 17 June 1975)

This letter describes two new lasers operating on the $^2\Sigma^+_{1/2} \rightarrow {}^2\Sigma^+_{1/2}$ bands of XeCl (at 308 nm) and KrF (at 249 nm). Pumping was achieved by high-intensity electron beam excitation of high-pressure Ar containing small amounts of Xe and Cl_2 or Kr and F_2. An efficiency of about 0.4% was observed in the initial experiments on KrF, and higher efficiencies appear possible.

PACS numbers: 51.70., 42.60.C

Recently we reported stimulated emission on the $^2\Sigma^*_{1/2} - {}^2\Sigma^*_{1/2}$ band of XeF at 353 nm.[1] Searles and Hart have also reported laser action on the comparable band of XeBr at 282 nm.[2] This letter reports laser action on corresponding bands of two other members of this class of new molecular lasers, namely, XeCl (at 308 nm) and KrF (at 248 nm).

The experimental apparatus has been described previously.[1] A Marx generator is used to impulse charge a cold-cathode electron beam gun to about 350 kV for about 100 ns. This produces a pulsed electron beam having a current density of roughly 150 A/cm^2 into the gas over an area 15×1 cm. At an Ar pressure of 50 psia, the power deposited in the gas is about 1.3 MW/cm^3, corresponding to a total energy of about 2 J in the 15-cm^3 laser volume. The laser optical cavity was formed by two reflectors positioned outside the cell and separated by about 30 cm. uv-grade quartz flats were used for the cell windows, and were optically aligned normal to the laser axis to minimize reflection losses. Absorption by the windows at 250 nm was about 1% per window. The output of the laser cavity was viewed at one end with a planar photodiode [ITT F4000(S5)], and at the other end of the cavity by either a $\frac{1}{2}$-m Hilger quartz spectrograph or a Scientech model 360203 energy meter.

Laser action from XeCl was obtained with a mixture of Ar, Xe, and Cl_2 in the ratio 89.9:10:0.1. The cavity output coupling was 0.5% out of each mirror, for a total output coupling of 1%. Lasing could be achieved only at pressures in excess of 30 psia. Laser action could not be achieved with a mixture containing substantially more Cl_2, viz., 89:10:1. This is not surprising since the XeCl band is overlapped by Cl_2 absorption.[3] This introduces a loss of about 6% per pass in the 0.1% Cl_2 lasing mixture. However, this loss might be avoided by using a different chlorine-bearing compound in place of Cl_2. Figure 1 shows an oscillogram of the photodiode signal from the XeCl laser. The laser intensity was attenuated by a factor of 100 before reach-

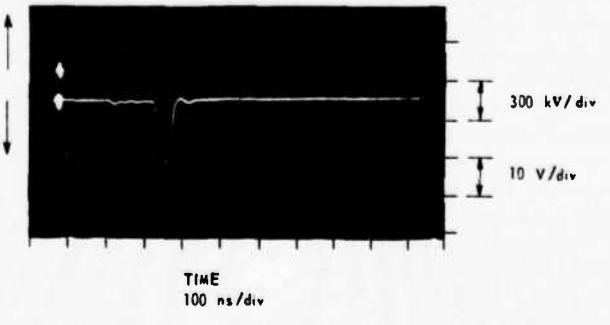

FIG. 1. Oscillogram of XeCl laser emission intensity. Upper trace, e-beam voltage. Lower trace, photodiode signal. Laser intensity attenuated by 10^2.

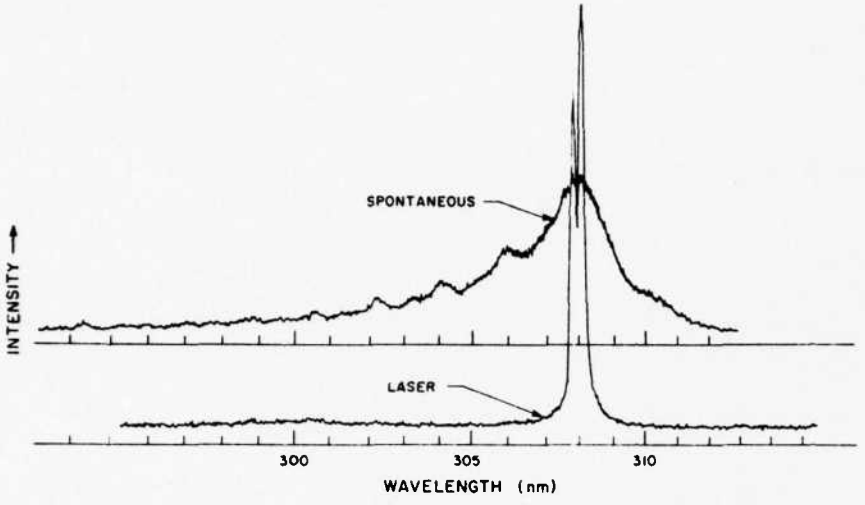

FIG. 2. Comparison of spontaneous and laser emission spectra from XeCl.

ing the photodiode. Note that the e-beam is on for about 100 ns before laser oscillation begins. The small photodiode signal appearing before the laser pulse is spontaneous emission leaking through the 0.5% transmitting laser reflector at wavelengths where the mirrors have larger transmission, $\lambda < 300$ nm, $\lambda > 350$ nm. The peak laser power as measured by the photodiode was roughly 3 kW. Measurements of the total energy output were difficult because they were small, of the order of 50 μJ or less. Laser action could not be achieved with one mirror blocked. Figure 2 shows a comparison of the XeCl spontaneous and stimulated emission spectra. We do not yet understand the origin of the two peaks in the laser spectrum. The spectroscopy of these molecules at high pressure is discussed in a lengthier paper.[4]

In contrast to XeCl, KrF laser action was easily achieved over a broad pressure range from 15 psia to 60 psia with laser reflectors having $\lesssim \frac{1}{2}\%$ output coupling. As in the XeF and XeCl lasers, the power output increased with increasing pressure. The most intense laser emission was obtained from mixtures of Ar, Kr, and F_2 in the ratio 98.9:1:0.1. Figure 3 shows a typical oscillogram of the KrF laser intensity as monitored by the photodiode. The laser turns on very soon after the e-beam has reached full voltage, and stays on for the duration of the e-beam pulse. The KrF laser pulse durations are longer than those observed from XeF, and show no sign of bottlenecking in the lower laser level. In comparing the weak XeCl laser signal shown in Fig. 1 to the KrF signal shown in Fig. 3, it should be noted that the KrF laser beam intensity has been attenuated by a factor of 2×10^4 before reaching the photodiode. The KrF laser intensity is 5000 times brighter than the unattenuated spontaneous emission intensity as measured both with the photodiode and on film. Laser action could not be achieved with one laser reflector blocked. The output of the KrF laser was easily measured with the energy meter. We reproducibly measured energy outputs in the range 3–4 mJ from one end. Since both reflectors had the same nominal output coupling, the total energy output was of the order of 6–8 mJ. This corresponds to a laser efficiency of about 0.4%, based on the energy deposited into the gas in the optical cavity. This efficiency can probably be increased with greater output coupling, since the transition appears to be saturated and the window losses exceed the output coupling. Figure 4 shows a comparison of the spntaneous and stimulated emission spectra of KrF. To our knowledge, this is the first published spectrum of this molecule, and the band position agrees well with predictions.[4,5]

The potential efficiency of the rare-gas halide lasers may be much higher than we have obtained in these preliminary experiments. Initially, the electron beam ionizes and excites the argon buffer. However, the ions rapidly recombine to form excited states[6] which transfer their energy to the krypton or xenon.[7] The excited rare-gas halides are then formed by reactions of the type

$$Kr^* + F_2 \rightarrow KrF^* + F. \qquad (1)$$

Additional excited rare-gas halides may be formed by dissociative attachment of electrons to the F_2, followed by three-body Thompson recombination of the F^- ions with Kr^+ ions. The ultimate efficiency will depend on the efficiency of reaction (1) for producing excited states. Since the energy required to form an argon ion or excited state with an electron beam is roughly 20.6 eV,[6] the effective quantum efficiency of a KrF laser, for example, is 24%. If a discharge were used to pump the krypton metastable levels directly, the effective

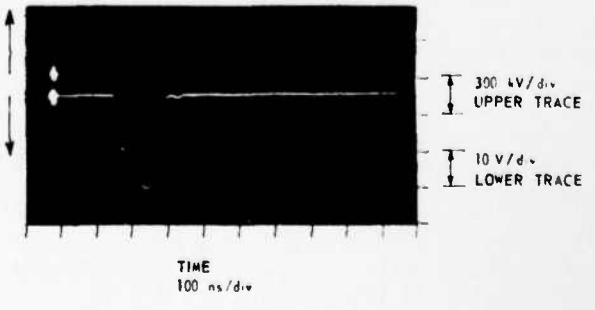

FIG. 3. Oscillogram of KrF laser emission intensity.

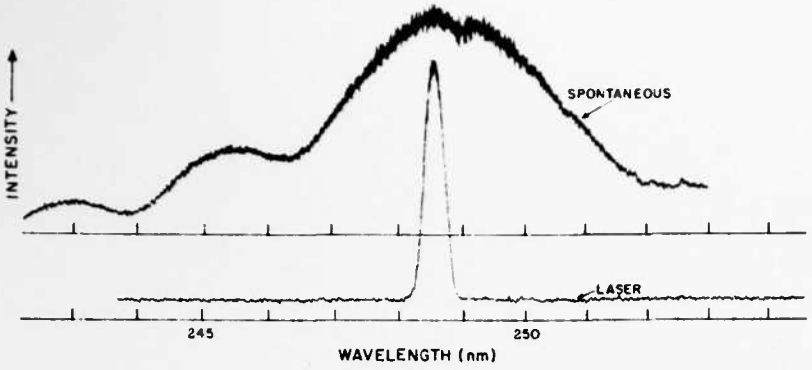

FIG. 4. Comparison of spontaneous and laser emission spectra from KrF.

quantum efficiency is roughly 50%. The ultimate efficiency of these lasers depends on the details of the molecular kinetics.

To provide an experimental indication of the possible efficiency, we have made relative fluorescence efficiency measurements in mixtures of Ar with N_2 (97:3), Ar with Xe and F_2 (99.6:0.3:1), Ar with Xe and Cl_2 (89.9:10:0.1), and Ar with Kr and F_2 (98.9:1:0.1). All the measurements were made at a total pressure of 40 psia. Taking into account the relative transmission of the broad-band interference filters used to isolate the bands of interest and the photodiode response, the peak fluorescence intensities relative to the 358-nm band of N_2 were found to be in the ratio 2:3:16 for XeCl, XeF, and KrF, respectively. These may be converted to rough estimates of the absolute fluorescence efficiencies by using the known kinetics of the Ar/N_2 system,[8] and the Franck-Condon factors for the N_2 $C \rightarrow B$ bands.[9] In the Ar/N_2 system, the energy is deposited in the form of Ar^* and Ar^+ ions. The latter rapidly recombine to form Ar^*. Overall, 20.6 eV must be deposited to form one Ar^*.[6] Under our conditions, 40% of this energy is transferred to N_2, the remainder being lost to Ar_2^*. Of the energy transferred to the N_2, approximately 40% goes to the $N_2(C)$ state either directly or through $N_2(E)$. Of the energy in $N_2(C)$ approximately 25% is radiated, the remainder being quenched by Ar and N_2. Of the $N_2(C)$ fluorescence approximately 33% appears within the bandpass of the interference filter utilized. Thus, in steady state the Ar/N_2 fluorescence efficiency for the mixture cited above is about 0.2%. From this the fluorescence efficiencies are estimated to be 0.4, 0.6, and 3% for the XeF, XeCl, and KrF mixtures, respectively. The difference between the observed fluorescence efficiency and the effective quantum efficiency may be due to the branching ratio for reaction (1), and part may be due to quenching of the excited rare-gas halide molecules by the parent halogens. For example, preliminary data indicate that the XeF^* radiative lifetime is 50 ns and that the rate of quenching of XeF^* by F_2 is 8×10^{-10} cm^3/s. Thus, under the conditions described above, approximately 73% of the XeF^* molecules are quenched before they fluoresce. In a laser, most of this wasted excitation may be recovered by making the stimulated emission time short compared with the quenching time. Thus, these lasers show promise for higher efficiencies than has been heretofore achieved in the visible and uv.

[†]Work supported by ARPA/ONR under Contract No. N00014-75-C-0062.

[1]C.A. Brau and J.J. Ewing, Appl. Phys. Lett. (to be published).
[2]S.K. Searles and G.A. Hart, Appl. Phys. Lett. **27**, 243 (1975).
[3]D.J. Seery and D. Britton, J. Phys. Chem. **68**, 2263 (1964).
[4]C.A. Brau and J.J. Ewing (unpublished).
[5]J.J. Ewing and C.A. Brau, Phys. Rev. A **12**, 129 (1975).
[6]D.C. Lorents and R.E. Olson, Stanford Research Institute Project PYU-2018, Semiannual Report, 1972 (unpublished).
[7]A. Gedanken, J. Jortner, B. Raz, and A. Szoke, J. Chem. Phys. **57**, 3456 (1972).
[8]R.M. Hill, R.A. Gutcheck, D.L. Huestis, Stanford Research Institute Report MP 74-39, 1974 (unpublished).
[9]R.N. Zare, E.O. Larsson, and R.A. Berg, J. Mol. Spectrosc. **15**, 117 (1965).

Laser action on the 342-nm molecular iodine band*

J. J. Ewing and C. A. Brau

Avco Everett Research Laboratory, Incorporated, Everett, Massachusetts 02149
(Received 23 July 1975)

A new laser operating on the 342-nm band of I_2 is reported. Electron-beam-excited mixtures of argon with CF_3I and HI produced this I_2 laser. The excited state of this laser is probably formed by ion recombination reactions, and a plausible mechanism is given.

PACS numbers: 42.60.C, 82.40.T

This letter reports a new electron-beam-pumped uv laser operating on the molecular iodine $D - X$ bands at 342 nm. This laser was obtained by pulsed e-beam irradiation of noble gas mixtures containing primarily Ar buffer gas and trace amounts of the iodine containing species HI and CF_3I. Laser action was also obtained from mixtures of Ar/Xe/*RI* (R = H, CF_3).[1] The highest I_2 laser output occurs with no xenon present. Very weak laser action has also been observed in Ar/I_2 mixtures utilizing room-temperature iodine vapor.

The possibility of electron-beam-pumped laser action on this molecular iodine band has been suggested by Wilkerson and Tisone[7] and by McCusker *et al.*[8] An optically pumped I_2 laser, $\lambda \approx 325$ nm, has also been proposed.[9] McCusker *et al.*[8] measured the fluorescence efficiency for the 342-nm I_2 emission band in e-beam-excited Ar/I_2 mixtures, and found it to be rather high, ~13%. This work gave no definitive kinetic mechanism for formation of I_2 (D), but the formation of this state was presumed to involve energy transfer from Ar^* to I_2. The new laser reported here clearly shows that molecular I_2 need not be initially present at all to produce fluorescence and laser action on this I_2 band. A plausible mechanism for the rapid production of this I_2 excited state in Ar/*RI* mixtures is given. A key feature of the mechanism is that I_2 (D) is formed by ion recombination reactions. This mechanism may also apply in part to Ar/I_2 mixtures. An analogous ion recombination mechanism may also be important in forming the ionic upper laser level of the noble gas halide species.

The broad banded I_2 emission spectrum, extending from 300 to 345 nm, has been the subject of numerous investigations.[9-13] Mulliken's classic paper thoroughly reviews the spectroscopy of I_2,[10] and it seems to be agreed that this I_2 transition has an excited state which dissociates to the separated ion pair $I^+ + I^-$. Thus, recombination of I^+ and I^- ions should yield this excited state. The identification of the 342-nm emission observed from e-beam-excited Ar/*RI* mixtures with the I_2 342-nm band is clear from a comparison of our

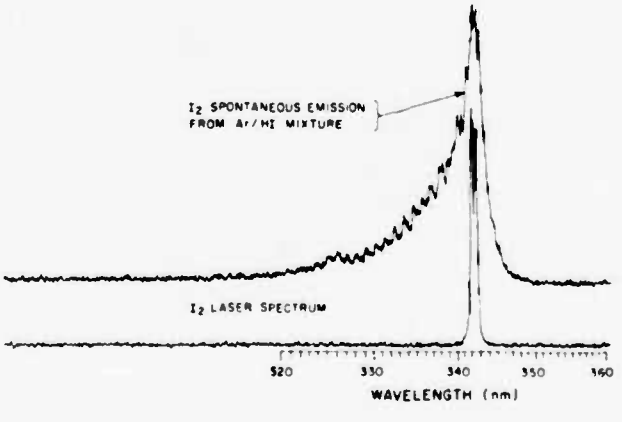

FIG. 1. Densitometer tracings of I_2 emission produced when Ar/HI mixtures are excited with an electron beam.

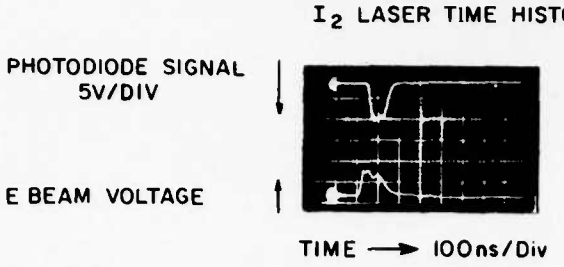

FIG. 2. Oscillograms of the photodiode viewing the laser output and the voltage pulse producing the electron beam. The laser intensity was attenuated by a factor of 160 before striking the photodiode. The signal corresponds to a peak power of about 1 kW.

spontaneous emission spectra with the spectra described by previous workers.[8-13] The prominent 342-nm band with its regularly spaced fluctuations and the weaker I_2 bands at 287, 430, and 450 nm are clearly seen on our plates. Figure 1 shows densitometer traces of the 340-nm band under conditions of spontaneous and stimulated emission. The laser spectrum shows definite narrowing of the band. More than one vibrational band appears to be oscillating, and the laser wavelength could presumably be discretely tuned.

The spectra and laser action were obtained in a device previously described.[2,4,14] Briefly summarizing, an electron beam (~350 kV, 150 A/cm^2 over an area 1×15 cm, 100-ns pulse duration) is injected into high-pressure premixed gases[15] through a 1-mil aluminized kapton foil. Between shots the cell is evacuated and a fresh mixture is introduced. The irradiated volume is inside a laser cavity formed by two 1-in.-diam 1-m-radius-of-curvature mirrors having >99% reflectivity over the 300–350-nm region. The laser reflectors are 30 cm apart and positioned outside the cell. The cell has two uv-grade quartz laser-quality windows. The cell windows are aligned to be parallel and perpendicular to the cavity axis to minimize reflection losses in the cavity. The output from one end of the laser cavity is directed onto an ITT F4000 photodiode (S-5 response) while the output from the other end is used for recording

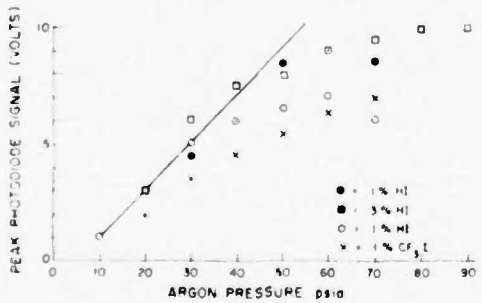

FIG. 3. Pressure dependence of I_2 laser peak power for several different mixtures of Ar/*RI*.

TABLE I. Simplified mechanism for I_2 (*D*) formation from excited Ar.

(1)	$e + RI \rightarrow R + I^-$	$R = CF_3$, H
(2)a	$Ar^* + RI \rightarrow RI^*$	
b	$\rightarrow Ar + R + I^*$	
c	$\rightarrow ArR^+ + I$	
(3)	$Ar^* + I \rightarrow Ar + I^*$	
(4)	$I^* + I^- + Ar \rightarrow I_2^* + Ar$	
(5)	$I^- + RI^+ + (M) \rightarrow I_2^* + R + (M)$	
(6)a	$Ar^* + RI \rightarrow Ar + R + I$	
b	$\rightarrow Ar + RI^+ + e$	
(7)	$Ar^* + I \rightarrow Ar + I^+ + e$	

spectra or making energy measurements. Blocking one mirror clearly spoils lasing action. Peak laser powers of the order of 1 kW have been obtained from ~50 psia Ar/HI mixtures containing 0.3% HI. Figure 2 shows a sample oscillogram of the photodiode signal. Typically, the laser turns on about 40 ns after the e-beam. The turn-on time is not strongly dependent on the pressure and lasts for about 80–100 ns. Since this time is longer than the estimated radiative lifetime,[9] this suggests that lower-level relaxation is fast and that quasi-cw operation is possible. The total energy output corresponds to an efficiency of ~10^{-3}% for converting deposited e-beam energy into laser light through the 1% transmitting mirrors. If the lasing transition is saturated and there are losses in the gas, greater powers and laser efficiencies could be obtained by coupling more light out of the cavity. McCusker *et al.* project considerably higher efficiencies for the e-beam-pumped Ar/I_2 systems.[8] However, we have observed only weak laser action in Ar/I_2, possibly because of the low vapor pressure of I_2 at room temperature.

A plot of the peak laser power vs total pressure for various Ar/*RI* mixtures is given in Fig. 3. The laser power rises linearly with Ar pressure and is not sensitive to the mole fraction of HI used. Use of CF_3I as an iodine source reduces laser power somewhat, but the same general behavior is observed. At higher pressures, the laser output power ceases to rise, possibly due to quenching of one of the reactants which leads to the excited state, or of the excited state itself.[7] The laser could be brought over threshold at lower Ar pressures with higher HI mole fractions.

The production of I_2 (*D*) from Ar/*RI* mixtures was unexpected and the mechanism for its formation is certainly one of the more fascinating aspects of this new laser. Table I summarizes the principal reactions of a plausible mechanism for producing I_2 (*D*) from the excited species, ions, and electrons which are formed when high-pressure argon is excited by an electron beam. The mechanism given in Table I lists only the reactions of the monoatomic species Ar^* and Ar^+. For brevity the analogous reactions which can be written for the dimer ions and excimers, which are also present, are omitted from the table.

The addition of an iodine-containing species to excited argon opens up a number of additional reaction pathways for the energy flow. The most important fact to note is that the iodine-containing species can react to form

both positive and negative ions, and that ion recombination can yield excited I_2. I^- ions can be rapidly formed by dissociative attachment to the RI molecules of the low-energy electrons present in the e-beam-excited gas mixture, reaction (1).[16] Electron scavenging should occur on time scales of 1–10 ns at the RI densities used in this laser. I^* ions can be formed directly from Ar^* or Ar_2^* by charge exchange reactions. I^* ions can also be formed by reactions involving the excited Ar neutrals. Ar^* and Ar_2^* can transfer energy to RI causing either RI bond rupture or Penning ionization. I atoms formed by bond rupture can then be ionized by the positive ions or the excited states of Ar. Three-body recombination of I^* with I^- can occur on a time scale of 10 ns or less.[17] Since the upper laser level correlates to the $I^* + I^-$ ion pair at infinite internuclear separation of the I atoms, recombination of these ions should give the upper laser level with high yields. Reaction of I^- with RI^* could also conceivably lead to I_2^*.

All of the reactions given in Table I are expected to be rapid. The branching ratios into individual product channels in these reactions are not known, however, and could be difficult to measure for reactions involving the excimers. Clearly the over-all kinetic efficiency for making I_2 (D) will depend on the details of the actual mechanism. Our data do not allow us to distinguish, at this time, among the various potential mechanisms, for example whether Ar^* is effective in producing ions in one or two steps. More kinetic information is needed to properly identify the mechanism.

*Work supported by DARPA/ONR through Contract No. N00014-75-C-0063.

[1]Xe was initially added to the gas mixtures in an attempt to lase the xenon iodide bands (Refs. 2 and 3) in analogy to the previously reported XeF (Ref. 4), XeCl (Ref. 5), KrF (Ref. 5), and XeBr (Ref. 6) lasers. Addition of Xe to these mixtures decreases the I_2 $D \rightarrow X$ spontaneous and lasing intensities while bringing out the expected xenon halide spectra.

[2]J. J. Ewing and C. A. Brau, Phys. Rev. A **12**, 129 (1975).
[3]J. E. Velazco and D. W. Setser, J. Chem. Phys. **62**, 1990 (1975).
[4]C. A. Brau and J. J. Ewing, Appl. Phys. Lett. **27**, 435 (1975).
[5]J. J. Ewing and C. A. Brau, Appl. Phys. Lett. **27**, 350 (1975).
[6]S. K. Searles and G. A. Hart, Appl. Phys. Lett. **27**, 243 (1975).
[7]A. K. Wilkerson and TIsone, Thirtieth Symposium on Moleeular Structure and Spectroseopy, Columbus, Ohio, 1975, Paper No. TH10 (unpublished).
[8]M. V. MeCusker, R. M. Hill, D. L. Huestis, D. C. Lorents, R. A. Gutchek, and H. H. Nakano, Appl. Phys. Lett. **27**, 363 (1975).
[9]J. Tellinghuisen, Chem. Phys. Lett. **29**, 359 (1974).
[10]R. S. Mulliken, J. Chem. Phys. **55**, 288 (1971).
[11]P. Venkateswarlu, Phys. Rev. **81**, 821 (1951).
[12]A. Elliott, Proc. R. Soe. (Lond.) A **174**, 273 (1940).
[13]R. D. Verma, J. Chem. Phys. **32**, 738 (1960).
[14]C. A. Brau and J. J. Ewing, J. Chem. Phys. (to be published).

[15]The gases were used as provided by the suppliers without further purification. The stated purity levels were as follows: Ar, 99.999%, Matheson; xenon, 99.95%, Matheson; HI, 98%, Matheson; CF_3I, no stated purity, PCR, Inc. Gainesville, Fla.

[16]L. G. Christophorou, R. N. Compton, and H. W. Dickson, J. Chem. Phys. **48**, 1949 (1968).
[17]J. J. Thompson, Philos. Mag. **47**, 337 (1924).

APPENDIX B

EMISSION SPECTRA OF XeBr, XeCl, XeF, AND KrF*

Reprinted from The Journal of CHEMICAL PHYSICS Vol. 63, No. 11, 1 December 1975

Emission spectra of XeBr, XeCl, XeF, and KrF*

413

C. A. Brau and J. J. Ewing

Avco Everett Research Laboratory, Inc., Everett, Massachusetts 02149
(Received 16 July 1975)

The emission spectra of XeBr, XeCl, XeF, and KrF at high pressure are reported and discussed. The spectra were obtained by observing spontaneous emission from electron beam excited mixtures of argon containing lesser amounts of xenon with the halogens or krypton with fluorine. The emitting state in these species is best described as an ionic species Xe^+X^- or Kr^+F^-. The wavelengths of these emission bands are in good agreement with a theoretical model in which the ionic binding energy of the noble gas halide ion pair is roughly equal to that of the nearest alkali halide. Our high pressure spectra imply that the lowest potential energy curve for XeF is bound.

I. INTRODUCTION

The rare gas monohalides comprise an interesting group of molecules. From a fundamental point of view, they have an important place in the understanding of chemical bonding.[1,2] Recently they have achieved practical importance as well with the demonstration that XeBr,[3] XeCl,[4] XeF,[5] and KrF[4,6] can be made to lase with the potential for high power and efficiency. In a recent paper[7] we reported the emission spectrum from XeI^* at high pressure ($\gtrsim 1$ atm), and made wavelength predictions for the bands of the other rare gas monohalides. This paper reports the high pressure emission spectra of the other xenon monohalides and that of KrF.

The excited states of these molecules are predominantly ionic in character, and the predictions of the emission spectra were based on the strong similarity of the excited states of these molecules to the alkali halides. Spectra of several rare gas halides have also been obtained in low pressure discharge flow experiments by Velazco and Setser[8] and by Golde and Thrush.[9] The latter independently suggested that the emission spectra could be correlated with the aid of the alkali-halide analogy. The low pressure spectra and the high pressure spectra described in this paper substantially confirm the predictions of the alkali halide model. There are, however, distinct differences in the details of the emission spectra obtained at low pressure and those obtained at high pressures. Principally, we find that the high pressure spectra are sharper than those obtained at low pressures. The reasons for this are discussed in this paper. In addition, the high pressure spectra show considerable vibrational structure which can shed more light on the structure of both the upper and lower states. In particular, the results for XeF prove that the ground state is bound by more than very weak van der Waals forces. This result is consistent with simple chemical and thermodynamic arguments[1] and the observed electron spin resonance spectrum of XeF.[10] The bound nature of the ground state of XeF is at variance with sophisticated molecular structure calculations.[5]

A potential energy diagram for the XeI molecule is shown in Fig. 1. It is typical of most of the rare gas monohalides. At infinite internuclear separation, the energy of $Xe^* + I + e^-$ relative to $Xe + I$ is just the ionization potential of Xe, 12.127 eV. Owing to the electron affinity of I, 3.063 eV,[11] the energy of $Xe^+ + I^-$ at infinite internuclear separation is 9.064 eV. As these particles approach one another they attract along a very long range Coulomb curve which, as shown in Fig. 1, crosses, in a diabatic sense, all the excited states of both Xe and I. The ion pair $Xe^+ I^-$ is bound by 1.3 eV (relative to $Xe + I^*$) at an internuclear separation of 3.3 Å. The ground state of XeI is only weakly bound; XeF differs from the other monohalides in that its ground state is evidently more strongly bound. The strongest fluorescence band in XeI corresponds to the $^2\Sigma^+_{1/2} \rightarrow {}^2\Sigma^+_{1/2}$ transition at 254 nm. This is an allowed transition in which the electron must jump from an orbital centered on the I nucleus to one centered on the Xe nucleus. In analogy to the alkali halides, the lifetime is estimated to be $\lesssim 100$ ns. This band is also the narrowest of the fluorescence bands since it corresponds to a bound-to-weakly-bound transition. Since the lower levels of Xe + I are split into Σ and Π branches, broad, red-shifted bands appear at approximately 325 and 360 nm corresponding to the two $^2\Sigma \rightarrow {}^2\Pi$ transitions which are split by the large spin orbit forces. Although it is not shown in Fig. 1, the upper ionic level is split in a manner similar to the lower covalent level. This is because the Xe^* ion has a ^2P configuration, similar to the

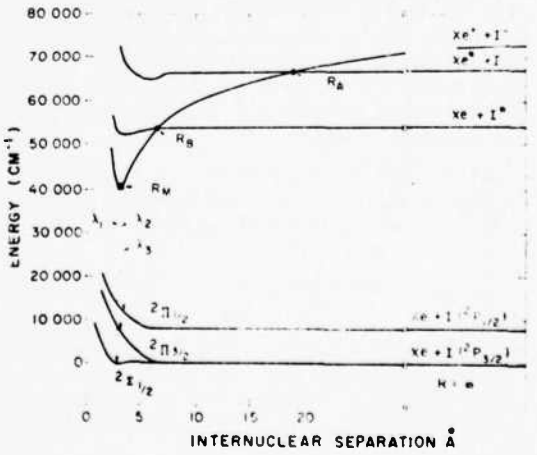

FIG. 1. Potential energy diagram showing the structure of xenon iodide.

TABLE I. Predicted features of inert gas monohalides (observed features shown in parentheses).

Molecule	R_M(Å)	E_M(cm^{-1})	λ_1(nm)	ω(cm^{-1})[a]
XeI	3.3	39135	256(254)[b]	119
XeBr	3.1	34272	292(282)[c,d]	150(180)[c]
XeCl	2.9	30860	324(308)[c,d]	214(210)[c]
XeF	2.35	25195	397(353)[c,d]	365
KrI	3.2	54000	185	138
KrBr	2.9	49353	203	170
KrCl	2.8	45592	219	233
KrF	2.27	39229	256(248)[c]	370(400)[c]
ArBr	2.8	62152	161	220
ArCl	2.7	58042	172(170)[e]	280
ArF[f]	2.17	51679	193	430
NeF	1.93	93266	107	536

[a]Vibrational spacing in the ground state of the alkali halides, Ref. 14.
[b]Reference 7.
[c]This work.
[d]Reference 8.
[e]Reference 9.
[f]A calculational error was made in Ref. 7 for the ArF molecule. The predicted E_M and λ_1 listed here are correct, and the ArF entry in Table I of Ref. 7 is incorrect.

ground state of the I atom. In the case of the Xe^+ ion, the $^2P_{1/2}$ state lies approximately 1 eV above the $^2P_{3/2}$ ground state. The $^2\Pi$ levels which arise from this splitting lead to emission which is blue shifted from the $^2\Sigma - ^2\Sigma$ transition. This emission has been observed weakly in XeF.

The analogy of the excited ion pair Xe^+X^- to the alkali halides may be used to provide a quantitative description of the structure of the excited rare gas halides.[7] According to this model, the excited rare gas halide ion pair is likened to the nearest alkali halide. This is justified by the intuitive feeling, supported, for example, by Hartree–Fock calculations,[12] that the noble gas ion and the nearest alkali ion have roughly the same size. Thus, the binding energy of XeI relative to the separated ions is taken to be equal to the ionic dissociation energy of CsI. The results of this model are summarized in Table I, along with the available experimental evidence. As may be seen from the table, the predictions are substantially confirmed by both the low and high pressure results.

In fact, other useful analogies to the alkali/halogen systems exist, and extend to the kinetics of these species. The excited ion pair states are formed by reactions of the type

$$Kr^* + F_2 - KrF^* + F \quad . \tag{1}$$

Such reactions are observed[13] to proceed very rapidly, with cross sections comparable to those observed in the analogous alkali plus halogen "harpooning" reactions.[14] This is not surprising, since the noble gas excited states have very low ionization potentials, as do the alkali atoms.

II. EXPERIMENTAL APPARATUS

The present experimental results were obtained with a high intensity electron beam which was used to pump high pressure mixtures of Ar, Kr, and Xe and the halogens. The general layout of the experiment is shown in Fig. 2. The high intensity electron beam excites gas mixtures in the high pressure cell, and the emission is monitored photoelectrically and on film. A scale drawing of the cell and the diode, used to form the high intensity electron beam, is shown in Fig. 3. The electron beam produced by the gun has an energy of about 400 keV./electron, and an intensity of about 30 A/cm^2 passing through the foil, over an area approximately 1 cm by 15 cm. For some experiments the intensity was increased to about 150 A/cm^2 through the foil at the expense of lowering the energy to about 300 keV/electron. Aside from increasing the intensities, this change had no observable effect on the fluorescence spectra. The duration of the electron beam pulse is approximately 100 ns, with a 10 ns rise time and a 20 ns fall time. The gun has proved to be very reliable, and hundreds of shots at 30 A/cm^2 are generally obtained betwee 1 foil failures.

The cell is mounted directly on the electron beam gun as shown in Fig. 3. The cell is constructed of aluminum, which is compatible with fluorine. The valves are stainless steel and the windows are sapphire or quartz. For maximum reliability, a 0.001 in. stainless steel foil is generally used. Titanium is corroded by the halogens, and aluminum is not as strong as stainless steel. However, for maximum electron beam transmission, for lasing experiments for example, an aluminized kapton film is used for the electron beam window. The cell can be warmed up using built-in car-

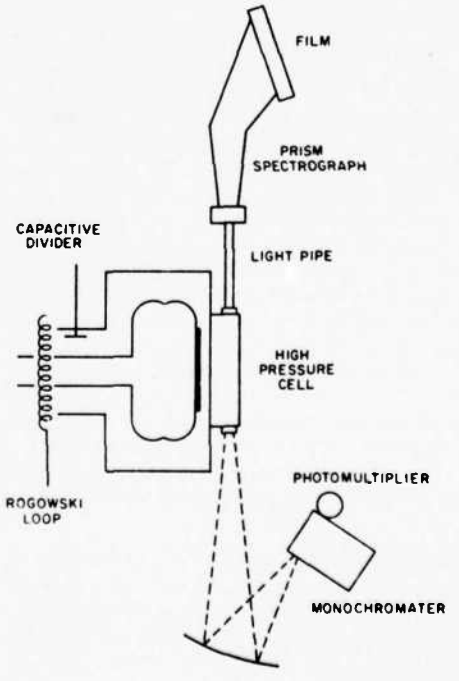

FIG. 2. Schematic diagram of electron-beam apparatus and emission diagnostics for fluorescence experiments.

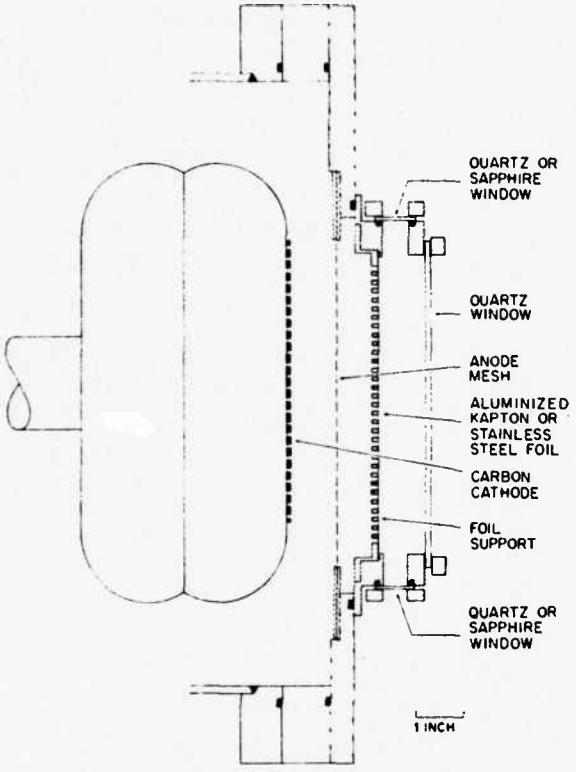

FIG. 3. Cross-sectional view of the high intensity electron-beam gun and high pressure cell.

tridge heaters to provide a mild bakeout. It can be pumped out to an ultimate vacuum of better than 10^{-5} torr with a leak rate better than 10^{-4} torr/h. Therefore, purity is not a problem.

The room-temperature gases (Ar, Kr, Xe, Cl_2, and F_2) were of research grade, obtained from Matheson, and were not purified any further. The Xe had a claimed impurity level of 50 ppm of Kr and about 10 ppm of other species. The gases, except I_2 vapor, were premixed in stainless steel tanks and allowed to stand for several hours, or even several days, to assure that they were fully mixed when used. The iodine crystals were obtained from Merck and are claimed to be >99% pure. They were placed in a small stainless steel sample cylinder attached to the cell through a stainless steel valve. The crystals and sample cylinder were repeatedly allowed to outgas at room temperature (under vacuum but valved off) and then cooled with liquid N_2 and pumped out. Owing to its low vapor pressure, it was found easier to introduce the I_2 vapor directly into the evacuated cell and allow it to come into equilibrium. The rare gases were then admitted to the desired pressure and allowed to mix. Mixing was occasionally stimulated by firing the electron beam gun to warm the gas in the irradiated region. The liquid bromine (Baker Chemical Co., no stated purity) was similarly outgassed by repeated freeze–pump–thaw cycles. Prior to making the measurements with F_2, the cell and mixing manifold were passivated by filling them with an F_2-rich mixture at low pressure (a few torr to half an atmosphere) for several hours.

The diagnostics, shown in Fig. 2, include time-integrated and time-resolved emission measurements. The time-integrated emission measurements were made with quarter-meter and half-meter Hilger quartz prism instruments, using Kodak 103-O or 103-F film. Generally, at high pressures, one shot is sufficient to provide a medium resolution spectrum using 50 μm slits. This corresponds to a wavelength resolution of approximately 0.1 nm in the larger instrument and 0.2 nm in the smaller. Time-resolved emission measurements were made with a Jarrel-Ash one-quarter meter, $f/3.5$ Ebert monochromater with a 1P28 photomultiplier tube and Tektronix 551 oscilloscopes.

III. EXPERIMENTAL RESULTS

The time-integrated spectral measurements are shown in Figs. 4–7 as microdensitometer tracings, Table I summarizes the peak wavelengths observed for the sharp $^2\Sigma - {}^2\Sigma$ bands. In the XeI spectrum, Fig. 4, we see the $^2\Sigma - {}^2\Sigma$ transition sharply peaked at about 254 nm, and shading off toward the blue with little structure. Broad, smooth bands are also evident at 325 and 360 nm. These are tentatively assigned as the $^2\Sigma - {}^2\Pi$ transitions. In the XeBr spectrum, Fig. 5, we see the $^2\Sigma - {}^2\Sigma$ band sharply peaked at 282 nm. This band shades off toward the blue with a diffuse vibrational structure superimposed on the continuum, with a spacing in the wing of the band of ~180 cm^{-1}. We interpret these fluctuations in the continuum emission intensity as due to emission from excited vibrational states of the ionic upper level. The spacing in the XeBr fluctuations is very close to the vibrational spacing in the analogous alkali-halide ground state, viz., ω_e (CsBr) = 150 cm^{-1}.[15] Such fluctuations are also observed in the absorption spectra of some alkali halides.[16] These so-called "kanneliertes" bands derive from transitions from bound states to nearly flat final states and the spacing is the vibrational spacing of the bound level.[16] Based on the nominal response of the film, the peak height ratio for the first two peaks corresponds to a vibrational temperature of about 390 °K. Thus, the

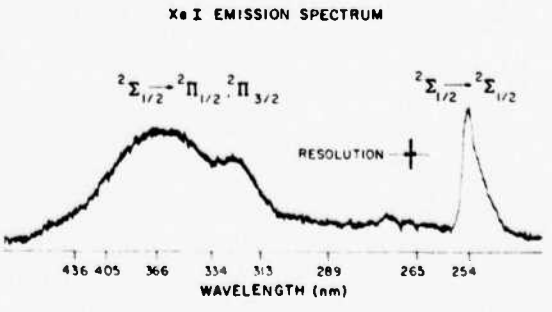

FIG. 4. Densitometer trace of XeI emission spectrum from a mixture of 20 psia Xe and 0.3 torr I_2.

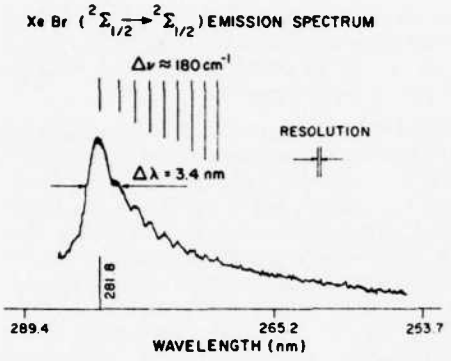

FIG. 5. Densitometer trace of XeBr ($^2\Sigma - {}^2\Sigma$) emission spectrum from a mixture of 10% Xe and 0.26% Br in Ar at a total pressure of 5 psia. The bandwidth indicated corresponds to the full-width at the half-intensity points, based on the nominal response of the film.

vibrational degrees of freedom of the excited state seem to be near equilibrium. Broad bands, not shown, also appear at 353 and 465 nm in XeBr. These are again tentatively assigned as the $^2\Sigma - {}^2\Pi$ bands. In the XeCl spectrum, Fig. 6, the $^2\Sigma - {}^2\Sigma$ band peaks at 308 nm, and shades off toward the blue with a sharper vibrational structure. From the separation of the vibration peaks we find that the vibrational spacing is approximately 210 cm^{-1}. For comparison, the vibrational spacing in CsCl is 214 cm^{-1}.[15] Based on the nominal film response, the peak height ratio for the first two peaks corresponds to a vibrational temperature of about 360 °K, again suggesting vibrational near-equilibrium in the excited state. A broad, low intensity band is also observed near 425 nm. Again, this could be the $^2\Sigma - {}^2\Pi$ band.

The $^2\Sigma - {}^2\Sigma$ band of the XeF molecule, shown in Fig.

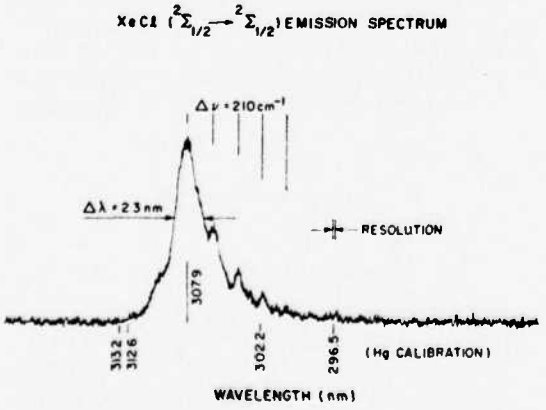

FIG. 6. Densitometer trace of XeCl($^2\Sigma - {}^2\Sigma$) emission spectrum from a mixture of 10% Xe and 0.08% Cl_2 in Ar at a total pressure of 5 psia. The bandwidth indicated corresponds to the full-width at the half-intensity points, based on the nominal response of the film.

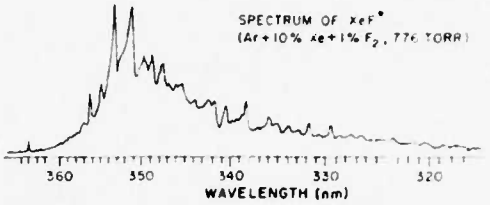

FIG. 7. Densitometer trace of XeF($^2\Sigma - {}^2\Sigma$) emission spectrum from a mixture of 10% Xe and 1% F_2 in Ar at a total pressure of 15 psia.

7, peaks near 353 nm and shades off to the blue. Although the general shape of this band is similar to that of the $^2\Sigma - {}^2\Sigma$ bands of the other molecules, much more structure is evident. This indicates that the emission is due to a bound-to-bound transition. The vibrational structure is even more apparent to the eye in the actual spectroscopic plate or in prints made from it (see Fig. 8). This is accentuated when the XeF laser spectrum is photographed. Table II lists the wavelengths of the bands one can identify from the plates. The lines observed in the XeF laser[5] are labeled with a*. The total width of the brightest bands is about 50 cm^{-1}. The two strongest peaks are separated by about 170 cm^{-1}. Rotational structure within each band could not be resolved with our spectrographs.

At very low Xe densities we observe another structured band at about 260 nm. We initially thought that this was due to ArF^*, but a careful study at various Xe mole fractions showed that Xe definitely had to be present to produce this band. However, Xe mole fractions in excess of 10^{-2} reduced the intensity of this band. The quenching of this emission with increased Xe pressure implies it comes from some state lying higher than the lowest ionic state of XeF. We assign this emission band to the transition $XeF^*\,{}^2\Pi_{1/2} - XeF^2\,\Sigma^*_{1/2}$. The splitting of the 260 nm band from the 354 nm band, 1.2 eV, is comparable to the spin orbit splitting of the Xe^* ion, 1.3 eV. The wavelengths of this system

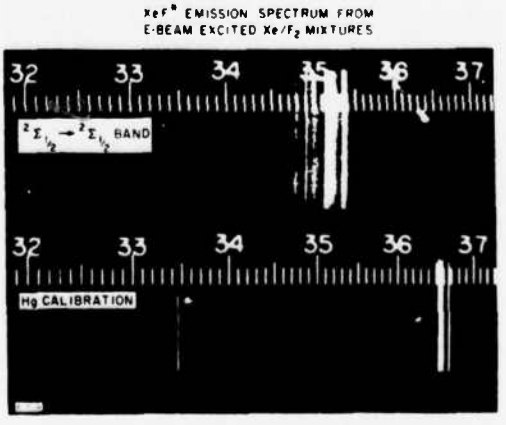

FIG. 8. Spectrum of XeF*($^2\Sigma^*_{1/2} \rightarrow {}^2\Sigma^*_{1/2}$) emission.

TABLE II. Wavelengths and energies for the 350 nm $^2\Sigma - ^2\Sigma$ band in XeF.

Estimated wavelength in Å	Estimated transition frequency (cm^{-1})	Relative intensity
3570	28 011	vw
3565	28 050	s
3550	28 169	s
3540	28 249	vw
*3535	28 288	vs
*3513	28 465	vs—overlapped on low energy side
3500	28 571	vw
3496	28 604	s (overtapped?)
3490	28 653	s
3574	28 777	s (two lines?)
3467	28 843	w
3450	28 901	Overtapping weak
3460	28 985	Overtapping weak
3437	29 095	w
3424	29 205	w
3417	29 265	w
3405	29 368	w
3402	29 394	w
3392	29 481	vw
3385	29 542	vw
3381	29 577	w
3359	29 770	vw
3349	29 860	vw
3337	29 967	w
3325	30 075	vw
3317	30 148	w
3293	30 367	w
3272	30 562	vw
3262	30 656	vw
3233	30 931	vw
3203	31 221	vw

are listed in Table III.

The 350 nm band spectra of XeF taken in our apparatus at lower pressures spread out toward the blue. We feel this is due to incomplete relaxation of the upper electronic state prior to emission. The upper state spectrum seems to be completely relaxed at pressures greater than approximately 0.5 atm.

There is also a broad smooth continuum in XeF centered near 450 nm which becomes relatively stronger at low pressures. The origin of the pressure dependence is not known, but it would seem to indicate that the band may not originate solely from the same upper level as the 354 nm band. If this is the $^2\Sigma - ^2\Pi$ band, it may be overlapped by some other band, possibly a $^2\Pi - ^2\Pi$ band.

Time-resolved emission measurements have been made on XeF using both Xe/F_2 mixtures and $Ar/Xe/F_2$ mixtures. The measurements will be described in detail elsewhere, but they show that the radiative lifetime is approximately 50 ns for XeF.

Finally, we show in Fig. 9 a densitometer tracing of the emission spectrum of KrF formed by exciting $Ar/Kr/F_2$ mixtures made up in the ratio 0.889/.01/.001 The spectra were taken at 40 psia. The $^2\Sigma - ^2\Sigma$ spectrum appears similar to that of XeCl and XeBr, with vibrational undulations occurring at a spacing of ~400 cm^{-1}. The analogous alkali halide RbF has a ground state vibrational spacing of 370 cm^{-1}.[18] A broad band also appears with a maximum at about 305 nm, possibly the $^2\Sigma - ^2\Pi$ band for this molecule.

IV. SPECTROSCOPIC INTERPRETATION

The spectra we observe are in reasonable agreement with the predictions based on the alkali-halide model of the excited state, as shown in Table I. The wavelengths of the maxima in the $\Sigma - \Sigma$ transitions also agree well with the low pressure, emission spectra published by Velazco and Setser.[8] As mentioned previously, our spectra are considerably sharper than those obtained at low pressure.

The spectra are interpreted in terms of the potential energy curves given in Fig. 10. These curves are similar to those shown for XeI with the exception that we feel that the lowest $^2\Sigma_{1/2}$ state potential energy curve of XeF is attractive rather than flat. The binding energy of the $^2\Sigma_{1/2}$ state probably increases in the sequence, XeI, XeBr, XeCl, XeF, due to the greater electronegativity of the lighter halides. For XeI and XeBr the

TABLE III. Approximate wavelengths of XeF emission near 2600 Å.

Approximate wavelength (Å)	Frequency (cm^{-1})	Relative intensity
2680	37 313	vw
2670	37 453	vw
2662	36 566	vvw
2660	37 594	vw
2650	37 736	s
2638	37 908	s
2630	38 023	w
2625	38 095	w
2622	38 139	w
2617	38 212	vw
2614	38 255	w
2600	38 462	w
2581	38 745	vw
2579	38 774	vw
2569	38 926	vw
2557	39 108	vw
2549	39 231	vw
2541	39 355	vvw
2525(2?)	39 447	vvw
2528	39 557	vvw
2512	39 809	vvw
2505	39 920	vvw
2500	40 000	vvw

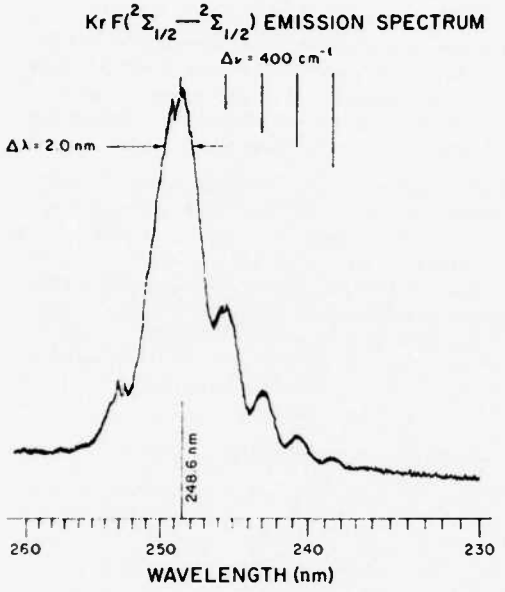

FIG. 9. Densitometer trace of KrF ($^2\Sigma \rightarrow {}^2\Sigma$) emission spectrum from a mixture of 1% Kr and 0.1% F_2 in Ar at a total pressure of 40 psia. The bandwidth indicated corresponds to the full-width at the half-intensity points, based on the nominal response of the film.

binding energy may only be of a van der Waals nature. For XeF the bond energy is claimed by some to be more like 8000 cm^{-1}.[1,17]

The errors in the simple predictions for the $^2\Sigma - {}^2\Sigma$ bands can derive from two sources, the actual amount of binding in the ionic excited state, and the deviation from flatness of the lower covalent state. The agreement of the simple theoretical predictions with experiment suggests that the binding energy relative to ions of the lowest ionic $^2\Sigma_{1/2}$ state is probably calculable to within about 10% by using the binding energy of the nearest alkali halide, viz., CsCl for $XeCl^*$. At this stage one may ask why this simple model does work so well, predicting emission frequencies of the $^2\Sigma - {}^2\Sigma$ bands to within 10%. This is a natural question since the noble gas positive ions should have slightly larger ionic radii than the neighboring alkali ions.[12] The answer is threefold. First, the small differences in ionic radii should not affect the ionic binding all that much. Calculations[12] suggest that the difference in positive ion size is only about 10%. The XeX^* and KrX^* excited states are predominantly ionic in nature, since the Coulomb curve crosses the higher lying covalent potentials that derive from $Xe^* + X$ at very large internuclear separations.[7] Since we know the separated ion energies very well and since the Coulomb attraction is basically a very long range attraction, roughly 80% of the ionic binding energy can be accounted for at large internuclear separations where the ~10% difference in size between the Xe^+ and Cs^+ ions can make no appreciable difference in the net ionic binding. This is simply a statement that Cs^+Cl^-, Cs^+Br^-, and Xe^+Br^- all follow the same potential energy curve at large R. Secondly, the energy at the minimum apparently is estimated better than one should expect because of the cancellation of two smaller effects associated with the size and angular distribution of the outermost electron cloud of the Xe^+ and Cs^+ ions. The Cs^+ ion should have a smaller radius for its outermost 5p electrons since the Cs^+ nucleus has one more nuclear charge than Xe^+. This would lead to a deeper ionic well depth (~10%) in Cs^+X^-. Partially compensating for this is the fact that in the $^2\Sigma_{1/2}$ ionic state, the Xe^+ ion has only one 5p electron on axis with the electron rich halide ion. Thus one should expect that in the $^2\Sigma_{1/2}$ state of Xe^+X^- the halide ion could approach closer and the binding energy should approach that of $^1\Sigma$ Cs^+X^-. On the other hand, the ion binding energies of the $^2\Pi$ ionic states of Xe^+X^- should be less than that pertaining to CsX since in this state the Xe^+ outermost electron radius should be larger and repulsion should begin at larger values of internuclear separation. Finally, the predictions of emission wavelength are good to within 10% because even though the lower covalent $^2\Sigma$ state could have some net binding, the minimum in the ionic curve probably occurs at a larger value of R than the minimum in the covalent curve, as we shall see shortly for XeF. Thus, the emission to the lowest covalent state probably terminates near the top of the well. In any event, the covalent binding in the heavier xenon halides is small and any errors in the predicted wavelengths will also be small.

It is the possible bound nature of the covalent $^2\Sigma_{1/2}$ state that we did not discover until we took high pressure spectra of the lighter halides of xenon. Pronounced vibrational undulations appear in our spectra of $XeBr^*$,

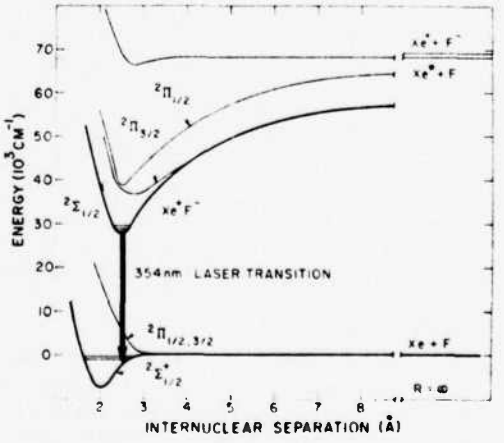

FIG. 10. Estimated potential energy curves for XeF. The lowest $X^2\Sigma_{1/2}$ curve is drawn showing the well depth and equilibrium bond length estimated from Ref. 1. The central wavelength and bandwidth of the XeF green band emission gives the approximate position and slope of the $A^2\Pi$ state's potential curve. $B^2\Sigma_{1/2}$ state's properties are estimated from the ionic model, Ref. 7, and the observed uv emission wavelength. The potential curves for the higher lying ionic and covalent states are based solely on the infinite separation energies and rough estimates of the sizes of the Xe ion and excited Xe atom.

$XeCl^*$, and KrF^*. They have a spacing one would anticipate for the upper ion pair state from comparison to the comparable ionic alkali-halide potentials. One interpretation of the undulations is that they are simply fluctuations due to transitions terminating on a very flat final state, analogous to the so-called kanneliertes bands in the alkali halides.[16] This argument is not tenable for the XeF spectra. The vibrational spacing of the Xe^+F^- excited state is expected to be of the order of 370 cm^{-1}. The observed spacing of the two prominent peaks in XeF is more like 170 cm^{-1}, completely different from the spacings anticipated for the upper states. These vibrational bands in XeF cannot be readily explained by the "kanneliertes" hypothesis. The explanation that we favor for XeF is that the $^2\Sigma - {}^2\Sigma$ transition in this species is bound-to-bound and terminates on bound vibrational levels located near the top of the *attractive* lower state $^2\Sigma_{1/2}$ potential.

One is tempted to generalize from XeF and say that the $^2\Sigma - {}^2\Sigma$ transitions may not be bound to free transitions in other xenon halides. However, these low resolution spectra cannot resolve this question. The high pressure $^2\Sigma - {}^2\Sigma$ spectra would appear continuous in XeI even if the lower level were bound because the vibrational spacings of a shallow XeI well would be fairly small as are the spacings in the upper level, ~100 cm^{-1}. Definitive statements regarding the actual depths of the lower state potentials of the other xenon halides and KrF will require further work.

The origin of the binding is easy to rationalize in the case of XeF since the well known XeF_2 has an average bond energy of 32 kcal/mole.[1] The XeF bond energy has been estimated to be in the range 10–20 kcal/mole.[1,17] The Xe–F stretching frequency in XeF_2 is 560 cm^{-1}.[1,18] The equilibrium Xe–F separation in XeF_2 is 1.977 Å,[1] considerably less than the 2.35 Å we predict for the ionic excited state. The bond length in the ion molecule XeF^+ is 1.84 Å, which should be less than that occurring in XeF_2 or XeF.[1] The vibrational frequency of the XeF^+ ion is 621 cm^{-1}, larger than expected for XeF.[1] Since the Xe–F bond lengths decrease in the sequence XeF_2 (1.98 Å), XeF_4 (1.95 Å), XeF_6 (1.89 Å), a naive extrapolation leads one to anticipate a XeF bond length of about 2.05 ± 0.1 Å. Since the bonding in the monofluoride is much weaker than the higher fluorides, the true bond length could be somewhat longer. A vibrational frequency of the order of 560 cm^{-1} would be anticipated for a bond strength of 32 kcal/mole, but somewhat less for a bond strength of 10–20 kcal/mole. Since the spontaneous and stimulated spectra show an approximate 170 cm^{-1} spacing, we presume that the XeF emission is terminating on very high states of the ground state. The potential energy curve of the lowest $^2\Sigma$ state of XeF drawn in Fig. 10 is consistent with these estimates. Clearly, an absorption spectrum of ground state XeF would be desirable, as would a rotational analysis of the bands we observe.

The dihalide species $XeCl_2$ and KrF_2[1] have been studied as well, but the binding energies for other dihalides of noble gases are apparently too small to allow isolation of these compounds. The XeCl stretching frequency in $XeCl_2$ is 313 cm^{-1}, and the mean Xe–Cl bond energy is less than 32 kcal/mole. By analogy to XeF_2 and XeF, we might expect the XeCl bonding energies to be of the order of 10 kcal/mole, roughly 4000 cm^{-1}. The vibrational spacing in XeCl would be quite small if XeCl were bound. Very small vibrational spacings in the lower level of XeCl would be consistent with the spectra we observe. The monohalide binding energy should decrease for the larger halides of xenon since they have decreased electronegativities. Similarly, a weak KrF bond is anticipated since the Kr–F bond in KrF_2 is extremely weak.[1] Also, the KrF bond in the KrF complex formed in a molecular beam is presumed to have a very shallow well because of the absence of a measurable dipole moment.[19]

Another qualitative way to rationalize a slight binding of the lower $^2\Sigma$ potential for these species follows from the molecular orbitals for these species. In the covalent binding of a halogen to Xe, one can make up molecular orbitals from the outermost p orbitals. One generates a set of molecular orbitals σ, π, π', and σ'. The σ and σ' orbitals are linear combinations of a $5p\sigma$ orbital centered on Xe and an np_σ orbital centered on the halogen. The π and π' orbitals are virtually nonbonding orbitals, one set being the p_x and p_y orbitals of the xenon the other set being the p_x and p_y orbitals of the halogen. The lowest energy configuration for a xenon halide molecule then gives the $^2\Sigma$ state: $(\sigma)^2(\pi)^4(\pi')^4(\sigma')^1$. The bond order for this species is $\frac{1}{2}$. Since the bond order is not zero, one might expect some slight binding, much like the small binding in the $^2\Sigma$ states of halogen molecular negative ions.[20] The first excited state of the xenon halide has the configuration $(\sigma)^2(\pi)^4(\pi')^3(\sigma')^2$. This state must be a $^2\Pi$ state. To the extent that the π and π' orbitals are nonbonding, the bond order for this covalent state is zero and a repulsive potential energy curve can be expected, since the two antibonding σ' electrons cancel out the bonding due to the σ electrons.

These simple molecular orbital arguments for XeF binding are not borne out by the best calculational efforts.[2] An extensive configuration interaction calculation, using 354 configurations made up of the lower lying Xe and F orbitals, shows that in the region of 2.35 Å, the approximate bond length of the Xe^+F^- excited state, the $^2\Sigma^+_{1/2}$ potential is definitely repulsive. It is possible that this CI calculation does not properly account for configuration interaction with the charge transfer state, which we know is the lowest lying excited state of XeF. Clearly, a high resolution spectrum of XeF using cold gases and isotopically pure Xe could lead to a rotational analysis and a better description of the XeF and other xenon halide potentials. We suggest that uv absorption studies of the xenon monohalides, possibly matrix isolation spectra, would also be worthwhile. Since these species show definite promise for being interesting laser systems, as well as interesting chemical species, a deeper understanding of the nature of these molecules is needed.

Finally, we give a discussion of the difference in spectral widths of the $^2\Sigma - {}^2\Sigma$ bands observed at high

and low pressures. Spectra of $XeCl^*$ and $XeBr^*$ published by Velazco and Setser[8] do not look quite the same as the high pressure spectra. Their research on the xenon halides utilizes a low pressure discharge flow technique. This approach is significantly different from our high pressure, pulsed e-beam excitation approach. In the discharge flow experiments, the total densities are purposely kept low to insure rapid mixing. Generally speaking, the low pressure spectra are considerably broader than those obtained at higher pressures. This difference derives from the fact that the emitting inert gas halide is not only formed in ionic electronically excited states, but is also formed with large amounts of vibrational and rotational excitation within the excited state manifolds. Similar vibrational excitation of an ion pair occurs in the analogous reactions of alkalis with halogen-containing species.[21,22] At the low pressures used in the flow experiments,[8,9] the inert gas halides suffer very few, if any, collisions during the excited state lifetime, of the order of 50 ns. Therefore, the XeX^* cannot be vibrationally relaxed before emission of a uv photon takes the molecule out of the higher lying $^2\Sigma$ and $^2\Pi$ ionic states and down to the lower lying covalent states. Indeed, Golde and Thrush[9] see emission from $ArCl^*$ at photon energies up to the total excess energy available to the newly formed molecules, clearly showing that they emit from many states. This emission in the short wavelength tail of the band presumably comes from unrelaxed vibrationally excited $ArCl^*$. Our experiments are done mostly at high pressures with premixed gases. Under these conditions we expect and observe partial, if not complete, vibrational relaxation during the estimated 50 ns lifetime of a typical xenon halide. At low pressures our spectra spread toward shorter wavelengths in the case of XeF. Since there are three possible excited ionic states, $^2\Sigma_{1/2}$, $^2\Pi_{1/2}$, $^2\Pi_{3/2}$, the low pressure spectra are probably also complicated by emission from the higher lying ionic states, $^2\Pi_{1/2}$, $^2\Pi_{3/2}$. At sufficiently low pressures, the excited species are probably not even rotationally relaxed. Thus, the bound-to-bound spectrum for XeF observed by us is not at variance with the unrelaxed spectrum observed by Velazco and Setser[8] and classified by them as bound to free.

ACKNOWLEDGMENT

The authors thank Jim Dodge for valuable assistance in performing these experiments.

*Supported by ARPA/ONR under Contract N00014-75-C-0063.

[1]N. Bartlett and F. O. Sladky, "The Chemistry of Krypton, Xenon and Radon," in *Comprehensive Inorganic Chemistry*, edited by J. C. Bailar (Pergamon, London, 1973).
[2]D. H. Liskow, H. F. Schaefer III, P. S. Bagus, and B. Liu, J. Am. Chem. Soc. **95**, 4056 (1973).
[3]S. K. Searles and G. A. Hart, Appl. Phys. Lett. **27**, 243 (1975).
[4]J. J. Ewing and C. A. Brau, Appl. Phys. Lett. **27**, 350 (1975).
[5]C. A. Brau and J. J. Ewing, Appl. Phys. Lett. **27**, 435 (1975).
[6]J. A. Mangano and J. H. Jacob, Appl. Phys. Lett. **27**, 495 (1975).
[7]J. J. Ewing and C. A. Brau, Phys. Rev. A **12**, 129 (1975).
[8]J. E. Velazco and D. W. Setser, J. Chem. Phys. **62**, 990 (1975).
[9]M. G. Golde and B. A. Thrush, Chem. Phys. Lett. **29**, 486 (1974).
[10]J. R. Morton and W. E. Falconer, J. Chem. Phys. **39**, 427 (1963).
[11]R. S. Berry and C. W. Reimann, J. Chem. Phys. **38**, 1540 (1963).
[12]S. Fraga, K. M. S. Saxena, and B. W. N. Lo, At. Data **3**, 323 (1971).
[13]J. E. Velazco and D. W. Setser, Chem. Phys. Lett. **25**, 197 (1974).
[14]J. L. Magee, J. Chem. Phys. **8**, 687 (1940).
[15]Y. P. Varshni and R. C. Shukla, J. Mol. Spectrosc. **16**, 63 (1965).
[16]R. S. Berry and W. Klemperer, J. Chem. Phys. **26**, 724 (1957).
[17]H. S. Johnston and R. Woolfolk, J. Chem. Phys. **41**, 269 (1964).
[18]P. A. Agron, G. M. Begun, H. A. Levy, A. A. Mason, C. Jones, and D. F. Smith, Science **139**, 842 (1963).
[19]W. Klemperer (private communication).
[20]W. F. Howard, Jr. and L. Andrews, J. Am. Chem. Soc. **97**, 2956 (1975).
[21]R. P. Marielia, D. R. Herschbach, and W. Klemperer, J. Chem. Phys. **58**, 3785 (1973).
[22]H. W. Cruse, P. J. Dagdigian, and R. N. Zare, Faraday Discuss. Chem. Soc. **55**, 277 (1973).

APPENDIX C

PHOTOIONIZATION CROSS SECTIONS FOR EXCITED STATES OF ARGON AND KRYPTON

Photoionization cross sections for excited states of argon and krypton[a)]

H. A. Hyman

Avco-Everett Research Laboratory, Inc., 2385 Revere Beach Parkway, Everett, Massachusetts 02149
(Received 28 March 1977; accepted for publication 26 April 1977)

Calculations have been carried out for the photoionization cross sections of excited states of atomic argon and krypton, relevant to the KrF laser. At $\lambda = 2486$ Å, it is found that photoabsorption due to the $^3P_{0,2}$ metastable states is relatively unimportant, while the cross sections for the first excited p states are large ($\sim 4.5 \times 10^{-18}$ cm^2).

PACS numbers: 32.80.Fb, 42.55.Hq

In order to optimize the extraction efficiency of high-power rare-gas–halide lasers, it is necessary to characterize the various photoabsorption processes for the species present in the laser medium. For this purpose, calculations have been carried out for the photoionization cross sections of excited states of atomic argon and krypton relevant to the KrF laser.[1–4]

Partial energy level diagrams for argon and krypton are shown in Fig. 1. Due to the large spin-orbit splitting in the core, the excited levels form two separate series: $mp^5(^2P_{3/2})nl$ and $mp^5(^2P_{1/2})nl'$, converging toward two different ionization limits, I and I'. If one averages over states of total angular momentum, it is found that the binding energies $I - E_{nl}$ and $I' - E_{nl'}$ are almost identical,[5] so that it is a good approximation to further average over core states. The two separate series are then effectively collapsed into one series of levels, which are simply denoted by the quantum numbers, nl, of the active electron.

Four states have been considered for the KrF laser: Ar(4s), Ar(4p), Kr(5s), and Kr(5p). The s states include the $^3P_{0,2}$ metastable levels, as well as the two $^3P_1$ levels, which are optically trapped and therefore relatively long lived in the laser. The p states can be significantly populated due to electron impact processes of the type e + Ar (4s) – e + Ar (4p), which have large cross sections. Since the laser photon has an energy of 5 eV ($\lambda = 2486$ Å), it is obvious from Fig. 1 that all four states can be photoionized.

The cross section for photoionization of the nlth state is given by the expression

$$\sigma_{nl}(\epsilon) = 2.69 \times 10^{-18}(I_{nl} + \epsilon)\left(\frac{l+1}{2l+1}R^2_{l+1} + \frac{l}{2l+1}R^2_{l-1}\right)(\text{cm}^2), \tag{1}$$

where I_{nl} is the ionization energy and ϵ is the excess energy of the free electron [all energies are in Rydbergs (1 Ry = 13.6 eV)]. R is the radial matrix element, given by

$$R_{l\pm1} = \int_0^\infty P_{nl}(r)\, r\, P_{\epsilon,l\pm1}(r)\, dr, \tag{2}$$

and $P(r)$ is the solution of the radial Schrodinger equation:

$$\left(\frac{d^2}{dr^2} - \frac{l(l+1)}{r^2} + \epsilon + V(r)\right)P(r) = 0 \tag{3}$$

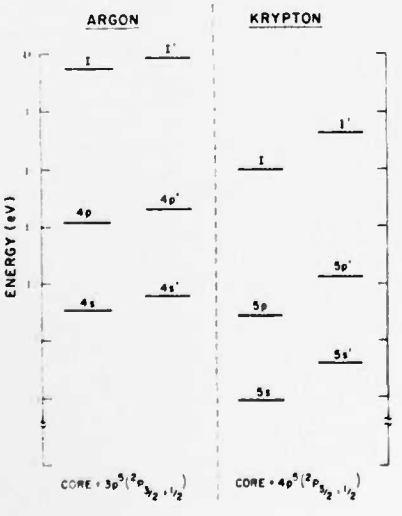

FIG. 1. Partial energy level diagrams for argon and krypton.

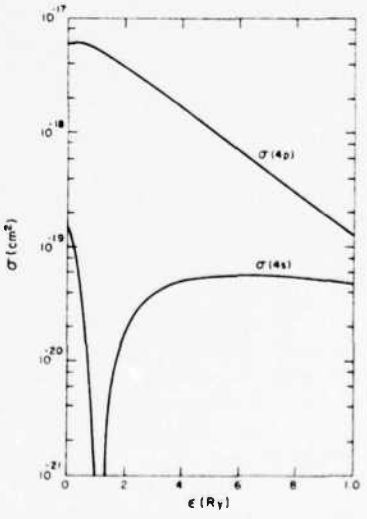

FIG. 2. Photoionization cross sections for excited states of argon.

a)Supported by ARPA/ONR under Contract N0001-1-75-C-0063.

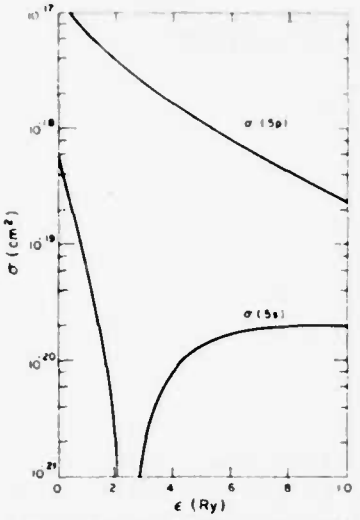

FIG. 3. Photoionization cross sections for excited states of krypton.

with $V(r)$ being the atomic potential. We have used a central-field approximation, which is consistent with our scheme for representing the excited states (i.e., neglecting spin-orbit effects); we thus obtain

$$V(r) = V_{\text{ion}}(r) + \alpha/(r^2 + r_0^2)^2. \tag{4}$$

The first term in Eq. (4) is the central-field potential of the parent ion, which was constructed from the Hartree-Fock wave functions of Clementi and Roetti.[6] The second term is a polarization potential, where α is the core polarizability and r_0 is an effective cutoff radius. The scaling law,[7] $\alpha \sim Zr_0^4$, has been used to estimate the core polarizabilities of Ar and Kr from the known polarizabilities of the alkali ions and halogens.[8,9] The value of r_0 was taken to be the Hartree-Fock mean radius of the outer shell of the core. The parameters used in the calculations were as follows: for Ar, $r_0 = 1.56a_0$ and $\alpha = 8.85a_0^3$; for Kr, $r_0 = 1.84a_0$ and $\alpha = 14.9a_0^3$ (where a_0 is the Bohr radius). The Schrodinger equation (3) was solved numerically subject to the boundary conditions: $P(0) = 0$, and for large r, $P(r) \to 0$ for the bound states and $P(r) \to \pi^{-1/2}\epsilon^{-1/4}$ $\sin[\epsilon^{1/2}r - \frac{1}{2}l\pi - \epsilon^{-1/2}\ln(2\epsilon^{1/2}r) + \arg\Gamma(l+1-i\epsilon^{-1/2}) + \delta_l(\epsilon)]$ for the continuum states, where $\delta_l(\epsilon)$ is the phase shift The same potential, $V(r)$, was used for all bound and continuum states, so that the wave functions are orthogonal.

The results for argon are shown in Fig. 2 and for krypton in Fig. 3. For the s states, the cross sections drop rapidly to zero just above threshold, where the matrix element R changes sign. Qualitatively, this behavior is very similar to that of the alkali photoionization cross sections,[10] which also have minima close to threshold. Although, in the present approximation the cross sections go to zero, including spin-orbit effects would give a small nonzero value at the minimum, as in the case of the alkalis.[10,11] Since the s-state cross sections are rapidly varying near threshold, they are very sensitive to the details of the model, and a much more elaborate theory, including both spin-orbit and configuration interaction effects, would be required to obtain a greater degree of accuracy. By contrast, the cross sections for the p states are relatively insensitive to the model and are therefore expected to be more accurate. In Table I we have listed the relevant photoionization cross sections at $\lambda = 2486$ Å; it is apparent that photoionization from the p states is the dominant process under conditions where they are significantly populated.

TABLE I. Photoionization cross sections for excited states of argon and krypton at $\lambda = 2486$ Å.

Atomic states	Cross section (cm²)
Ar(4s)	2.1×10^{-20}
Ar(4p)	4.3×10^{-18}
Kr(5s)	1.3×10^{-19}
Kr(5p)	4.5×10^{-18}

Dunning and Stebbings[12] have reported upper bounds for the Ar ($4s\ ^3P_{0,2}$) and Kr ($5s\ ^3P_{0,2}$) photoionization cross sections at threshold ($\epsilon = 0$). The values they give are 1.1×10^{-18} cm² for Ar and 4.9×10^{-19} cm² for Kr. The present calculations agree quite well with their value for krypton, but are considerably lower for argon, presumably due to the sensitivity of the s-state cross sections close to the threshold, as discussed earlier. If we renormalize our results for the Ar (4s) state to agree with Dunning and Stebbings's upper bound at threshold, the corresponding value at 2486 Å becomes $\sim 1.5\times10^{-19}$ cm², which is still a factor of ~30 smaller than the calculated Ar (4p) value of 4.3×10^{-18} cm².

The principal conclusions to be drawn from the present calculations are that photoionization directly from the Ar ($4s\ ^3P_{0,2}$) and Kr ($5s\ ^3P_{0,2}$) metastable states is relatively unimportant, while photoionization from the Ar (4p) and Kr (5p) levels is likely to be a significant process in the KrF laser.

The author wishes to acknowledge helpful discussions with J. Jacob and J. Mangano.

[1] J.J. Ewing and C.A. Brau, Appl. Phys. Lett. **27**, 350 (1975).
[2] M.L. Bhaumik, R.S. Bradford, Jr., and E.R. Ault, Appl. Phys. Lett. **28**, 23 (1976).
[3] J.M. Hoffman, A.K. Hays, and G.C. Tisone, Appl. Phys. Lett. **28**, 538 (1976).
[4] J.A. Mangano and J.H. Jacob, Appl. Phys. Lett. **27**, 495 (1975).
[5] P.S. Ganas and A.E.S. Green, Phys. Rev. A **4**, 182 (1971).
[6] E. Clementi and C. Roetti, At. Data Nucl. Data Tables **14**, 177 (1974).
[7] M.M. Klein and K.A. Brueckner, Phys. Rev. **111**, 1115 (1958).
[8] A. Dalgarno, Adv. Phys. **11**, 281 (1962).
[9] R.R. Teachout and R.T. Pack, At. Data **3**, 195 (1971).
[10] G.C. Marr and D.M. Creek, Proc. R. Soc. (London) A **304**, 233 (1968).
[11] M.J. Seaton, Proc. R. Soc. (London) A **208**, 418 (1951).
[12] F.B. Dunning and R.F. Stebbings, Phys. Rev. A **9**, 2378 (1974).

APPENDIX D

HIGH EFFICIENCY UV LASERS

HIGH EFFICIENCY UV LASERS

J. J. Ewing and C. A. Brau
Avco Everett Research Laboratory, Inc.
2385 Revere Beach Parkway
Everett, Massachusetts 02149 U.S.A.

Abstract

The potential of the rare gas halide lasers for high efficiency is briefly reviewed. The spectroscopy and kinetics of these lasers is emphasized.

Introduction

Within the past year it has become clear that UV lasers having high efficiency are practically realizable. This paper will briefly review the research that is leading to this revolution in UV lasers. The paper will also emphasize the underlying physics that determines the efficiency of electronic transition lasers. We will draw examples from recent work on rare gas halide lasers.

The biggest gains towards the goal of high efficiency at short wavelengths have been made in a new class of molecules and molecular lasers, the rare gas monohalides. The spectra of some of these species were first taken within the past two years[1, 2, 3, 4, 5] and a solid understanding of the spectroscopy and the formation mechanisms is developing.[3, 4, 5, 6, 7, 8] Specifically, lasing on XeBr at 282 nm,[9] XeF at 354 nm,[10] XeCl at 308 nm,[11] KrF at 248 nm,[11] ArF at 193 nm[12] and KrCl at 222 nm[13, 14] has been observed. Electric discharge pumping of some of these species has also been observed, on KrF[15] and XeF[16] up to now, although one assumes that some of the other members of the class can be pumped by discharges as well.

A complementary set of lasers operating on halogen molecules formed in certain rare gas/halogen mixtures has also been demonstrated. I_2 lases at 342 nm,[17] Br_2 at 292 nm,[18] and Cl_2 is projected to lase near 260 nm,[19] although it has not lased in our laboratory or others[20] despite substantial effort. Discharge production of Br_2^* and I_2^* lasers has also been achieved.[21, 22]

Although the halogen systems are very efficient as flourescence sources,[23, 24] they have not yet performed as well as the best rare gas halide lasers. The reasons for this decreased performance are not yet quantitatively established.

The most efficient lasers to date in this class are the KrF and XeF lasers. High intrinsic efficiencies[25,26] as well as high wall socket efficiencies[26,27] have been obtained. The KrF laser has also produced the highest total energy outputs to date although the ArF laser is also capable of comparably high energy outputs.[12]

Most of these exciting results in novel high efficiency UV lasers have developed out of lasers utilizing ground state dissociation, so called "excimer" lasers.[28] As we will discuss later, excimer lasers have the advantage that the kinetic extraction efficiency can be made large because the intra cavity flux can be large without causing bottlenecking. Although this is the current state of the art, we caution that two other methods of lower level removal, predissociation and collisional quenching, can in principle provide sufficiently rapid lower level quenching to allow a high cavity flux to efficiently extract upper laser levels.

What is High Efficiency

The words "high efficiency" mean different things for various laser applications. However, a definition of the term within the context of a particular application can serve as an important guideline in pursuing the goal. This is so because various applications require different pulse energies and average powers, and very often the application itself dictates the techniques needed to achieve the desired overall laser system efficiency. Two examples illustrate this point. Some laser isotope separation schemes require higher powers and efficiencies than currently available. However, for the near term and the long term, a high efficiency laser for UV uranium isotope separation probably only needs to be of order 1% efficient, operate at about the 1J per pulse level, with ultimate power levels of order 5 kW.[29] This efficiency and power level is clearly higher than what is currently available in the UV or visible. However, it does not place severe constraints on either the excitation methods or the nature of the laser medium and a variety of solutions appear feasible. As a contrast, for the projected laser needs for an ultimate high average power laser for a laser fusion application, energy outputs per laser amplifier of order 2000 J or more are of interest.[30] Economics presumably will dictate ultimate efficiencies as high as possible, (>10%) as well as some modest pulse repetition frequency. Clearly a combination of laser medium and excitation scheme applicable to the isotope separation effort need not be directly applicable to the higher power fusion application.

An important, if obvious point is that the overall efficiency of a laser is a product of efficiencies. To maximize the overall laser efficiency it is important that each element of the efficiency be high simultaneously. Roughly speaking the overall efficiency is a product of a quantum efficiency, an upper laser level production efficiency, an extraction efficiency, an efficiency for producing the initial excited states by the pump, and an energy coupling efficiency which describes the efficiency with which energy gets from a wall socket into the gas medium. The extraction efficiency is comprised of both spectroscopic and kinetic extraction efficiencies depending on the ratio of net gain to loss and the ratio of rates of stimulated emission of upper laser levels to the quenching and spontaneous loss of upper levels. Certain rare gas halide lasers have potential for high power and high efficiency because they have high efficiency in each of the above mentioned elements. Depending on the application requirements, one may accept a lower efficiency of one of these elements if the compromise allows for some simplification of the laser. Typically this tradeoff usually involves coupling and excited state production efficiencies.

Let us briefly summarize some of the means available for exciting UV or visible laser transitions and the ultimate efficiencies they can yield. For the very high powers and high efficiencies, as in the fusion application, one clearly requires a volumetrically scalable excitation technique. Three broad approaches are currently possible for making large volume UV or visible devices: E-beam (or possibly UV) ionized electric discharges, pure E-beam pumping, and optical excitation.[31] Of the above, experience with IR lasers shows that the discharge approach offers the potential for the highest efficiencies (> 10%), with high energy outputs and average powers. However, the discharge pumping approach imposes certain constraints on the laser medium. One key constraint of larger volume electric discharge lasers is that the coupling efficiency improves as the pumping duration increases. An excited medium having constant impedance is also a desirable feature for a high coupling efficiency. The pure E-beam pumping technique is versatile, but is limited in terms of overall systems efficiency and repetition rate. Overall efficiencies up to about 10% are probably possible in suitable media. Optical excitation schemes are inherently limited by the efficiency and repetition rate of the optical pump being used. However, as the overall efficiencies of UV and visible lasers and incoherent pumps improve, the potential and scope of optically pumped lasers will broaden. One can project optically excited high energy visible lasers with efficiencies of order 1-3% based on a hypothetical 10% efficient ArF or KrF UV laser.

At lower average power levels, all of the above methods or combinations thereof are suitable and can yield efficiencies of order 1% or greater. More convenient for efficiencies near 1%, however, is the use of self sustained discharges such as the fast pulse Blumlein devices which are performing so well with the XeF laser.[27] These devices typically run with an unstable discharge, one which becomes an arc after a short time, and the principal source of inefficiency lies in the "coupling" efficiency. These lasers do not lend themselves to scaling to large volumes and as such are limited in total energy outputs. Currently, these devices are excellent for producing high peak powers and short pulses. Since similar pumping techniques yield higher efficiencies in CO_2 IR lasers, improving the performance of short pulse UV lasers is currently an active area of research.

In general, it is true that the longer pulse, larger volume, highest efficiency excitation schemes place the most stringent constraints on the intrinsic aspects of the laser medium. For example, there is one very important difference in the required laser kinetics of an allowed UV or visible laser transition excited by an E-beam stabilized discharge for a large volume device, contrasted to a short pulse, small scale discharge. As noted above the coupling efficiency of a large scale, very efficent laser improves with long excitation pulses, $t \gtrsim 300$ ns. The fast pulse discharges can operate well with very short excitation times, $t \lesssim 50$ ns. Because the radiative lifetimes of typical allowed electronic transitions are roughly equal to the transient turn on time of a large scale discharge, the long pulse devices must have rapid removal of the lower laser level for a laser operating on an allowed transition. Obviously one cannot expect to have an efficient large scale device if the laser medium shuts off before the electrical circuitry is efficiently coupled to the laser plasma. The long pulse high efficiency lasers require one to look for means of removing the lower laser level, a natural venue for the excimer concept. The short pulse devices, can, however, work quite well on transitions that bottleneck such as the 510.6 nm Cu laser line, or the

Let us briefly summarize some of the means available for exciting UV or visible laser transitions and the ultimate efficiencies they can yield. For the very high powers and high efficiencies, as in the fusion application, one clearly requires a volumetrically scalable excitation technique. Three broad approaches are currently possible for making large volume UV or visible devices: E-beam (or possibly UV) ionized electric discharges, pure E-beam pumping, and optical excitation.[31] Of the above, experience with IR lasers shows that the discharge approach offers the potential for the highest efficiencies (> 10%), with high energy outputs and average powers. However, the discharge pumping approach imposes certain constraints on the laser medium. One key constraint of larger volume electric discharge lasers is that the coupling efficiency improves as the pumping duration increases. An excited medium having constant impedance is also a desirable feature for a high coupling efficiency. The pure E-beam pumping technique is versatile, but is limited in terms of overall systems efficiency and repetition rate. Overall efficiencies up to about 10% are probably possible in suitable media. Optical excitation schemes are inherently limited by the efficiency and repetition rate of the optical pump being used. However, as the overall efficiencies of UV and visible lasers and incoherent pumps improve, the potential and scope of optically pumped lasers will broaden. One can project optically excited high energy visible lasers with efficiencies of order 1-3% based on a hypothetical 10% efficient ArF or KrF UV laser.

At lower average power levels, all of the above methods or combinations thereof are suitable and can yield efficiencies of order 1% or greater. More convenient for efficiencies near 1%, however, is the use of self sustained discharges such as the fast pulse Blumlein devices which are performing so well with the XeF laser.[27] These devices typically run with an unstable discharge, one which becomes an arc after a short time, and the principal source of inefficiency lies in the "coupling" efficiency. These lasers do not lend themselves to scaling to large volumes and as such are limited in total energy outputs. Currently, these devices are excellent for producing high peak powers and short pulses. Since similar pumping techniques yield higher efficiencies in CO_2 IR lasers, improving the performance of short pulse UV lasers is currently an active area of research.

In general, it is true that the longer pulse, larger volume, highest efficiency excitation schemes place the most stringent constraints on the intrinsic aspects of the laser medium. For example, there is one very important difference in the required laser kinetics of an allowed UV or visible laser transition excited by an E-beam stabilized discharge for a large volume device, contrasted to a short pulse, small scale discharge. As noted above the coupling efficiency of a large scale, very efficent laser improves with long excitation pulses, $t \gtrsim 300$ ns. The fast pulse discharges can operate well with very short excitation times, $t \lesssim 50$ ns. Because the radiative lifetimes of typical allowed electronic transitions are roughly equal to the transient turn on time of a large scale discharge, the long pulse devices must have rapid removal of the lower laser level for a laser operating on an allowed transition. Obviously one cannot expect to have an efficient large scale device if the laser medium shuts off before the electrical circuitry is efficiently coupled to the laser plasma. The long pulse high efficiency lasers require one to look for means of removing the lower laser level, a natural venue for the excimer concept. The short pulse devices, can, however, work quite well on transitions that bottleneck such as the 510.6 nm Cu laser line, or the

337.1 nm N_2 (C→B) transition. A second kinetic constraint typical of the long pulse electric discharges derives from the preference for constant laser plasma impedance, implying constant electron number density. In the rare gas halide lasers this constraint is neatly managed by using electron attachment by the halogen species to balance the avalanching of electron number density caused by the high steady state number density of low ionization potential rare gas excited states.[32]

Since the highest efficiency pumping schemes by and large place the most stringent constraints on the laser medium, our discussion of new high efficiency lasers will be oriented towards E-beam and E-beam controlled discharge excitation of laser media. For each of these pumping techniques a set of guidelines can be drawn up that allows one to focus on key elements required to obtain overall high efficiency. Listed below are a set of such guidelines convenient for discussing potential as high efficiency electric discharge lasers.

Guidelines for an Efficient UV Electric Discharge Laser

- Quantum Efficiency

  Maximize Quantum Efficiency
  Usually a Fixed Parameter within a Pumping Scheme

- Upper Laser Level Production

  Minimize Branching into the Useless Channels

- Extraction

  Net Gain Much Greater than Loss (Minimize Excited State Absorption)
  Cavity Flux Large Enough to Beat Quenching and Spontaneous Emission

- Initial Excited State Production

  Minimize Production of Ions and Useless Excitations

- Coupling

  Stable, Constant Impedance Laser Plasma, Long Excitation Pulses

For a pure E-beam laser or an optically pumped laser the guidelines within the first three areas will be the same. For E-beams there is little control over the excited state production efficiency, whereas with optical excitation one can hope to choose the best wavelength for exciting the medium. The coupling efficiency for optical or E-beam pumping will be limited by desired homogeneity of excitation and the fraction of the primary electron range or optical depth utilized. The coupling efficiency will also include the efficiency with which the E-beam or laser beam itself is produced from electrical energy drawn from the wall socket.

In the following sections we will consider the spectroscopy and kinetics of the rare gas halide lasers and show how various components of the overall efficiency of each laser compares to the "ideals" stated in the

above guidelines. Similar comparisons for other classes of UV or visible lasers can be drawn.

Rare Gas Halide Spectroscopy

The potential for high efficiency of the rare gas monohalides derives from both kinetic and spectroscopic aspects. Since the spectroscopy is somewhat better understood than the laser kinetics, we will describe it first. The spectroscopy impacts on the above mentioned efficiency areas in several ways. Obviously with the choice of an excitation scheme, the laser wavelength determines the quantum efficiency. The upper laser level production efficiency is primarily a kinetic phenomena, but certain aspects of high branching ratios can be traced directly to the almost unique spectroscopic features of these molecules. Spectroscopy impacts the extraction efficiency in two ways. The position of the molecular potential energy curves determines the amount of excited state absorption competing with stimulated emission. Obviously, the less absorption one has the better the extraction. Secondly, the shape of the lower level potential energy curve determines to a first approximation the emission spectrum bandwidth and as such impacts the stimulated emission coefficient and, correspondingly, stimulated emission rates. It is important to note that among UV excimer lasers the stimulated emission cross sections for the sharp bands in the rare gas monohalides are very large, $\sigma \approx 10^{-16}$ cm^2. This large cross section makes it possible to extract upper laser levels on time scales of order 1 ns with flux levels of order 5 MW/cm^2. The rapid stimulation of the upper laser levels effectively competes with kinetic quenching and is a key component of attaining high efficiency with these species.

Figure 1 shows a schematic molecular potential energy level diagram for a rare gas monohalide. One can see that these lasers utilize lower level dissociation. Unlike the rare gas excimer lasers there are two lower branches. For the simplified case shown here emission is centered near two wavelengths, λ_1 and λ_2. The two dissociative levels are designated as a $^2\Sigma$ state and a $^2\Pi$ state. Spin orbit splitting of the lower $^2\Pi$ states is neglected but is important in rare gas bromides and iodides. The $^2\Sigma$ lower state corresponds to having one halogen "hole" in a p orbital on axis with the rare gas atom. The $^2\Pi$ state places the partially occupied atomic p orbital perpendicular to the molecular axis. The $^2\Pi$ state is strongly repulsive at the equilibrium internuclear configuration of MX^*, R_o, because more electrons are between the halogen and rare gas nuclei. Emission terminating on the $^2\Pi$ state, near wavelength λ_2, is characterized by a relatively broad continuum band width. The $^2\Sigma$ lower level has a fairly flat potential energy curve at R_o, and the emission bandwidth for this transition is narrow. Assuming comparable radiative transition rates to both states, the gain on the transition near λ_1 is higher because the bandwidth is lower. To date rare gas monohalide lasers have operated on the sharper, higher gain bands. As noted above, a "high gain" excimer laser which utilizes a fairly flat lower laser level has many significant advantages because the higher stimulated emission cross section increases the rate at which stimulated emission can remove the upper laser level. This allows laser emission on the sharp band to effectively compete with quenching of the excited state. This benefit would not accrue as readily on the broad, lower cross section bands that terminate on very repulsive lower laser levels. The dissociative nature of the relatively flat lower level still allows for the rapid removal of the lower level, thus maintaining the population inversion.

sociation into an inert gas atom M and an excited halogen atom, X^*. It is also bound with respect to $M^* + X$. The ionic nature of these excited states has been discussed.[1, 2, 3, 4, 5] The excited state is nothing more than a positively charged inert gas ion, M^+, and a negative halogen ion, X^-, held together by coulombic rather than covalent forces. Predications of various properties of these excited species are based on the similarity of these excited states to the ionic ground states of the nearly isoelectronic alkali halide ground states.[3] These predictions are accurate to within a few percent.[4, 5] The similarity of the excited ionic states of the rare gas monohalides to ground state alkali halides derives from the fact that a rare gas halide ionic excited state differs by only one electron from an alkali halide. KrF^* is simply the ion pair $Kr^+ F^-$. Kr^+ is only different by one electron from Rb^+. Thus, the properties of KrF^* are very close to those of the ionic RbF molecules. A number of other useful analogies exist as well. For instance, the rare gas excited states, such as Kr^* have low ionization potentials and as a result the chemistry of Kr^*, both kinetically and generically, is very similar to that of Rb.

The simplified potential curves shown in Fig. 1 do not illustrate the other ionic excited states, which lie very close to the ionic $^2\Sigma_{1/2}$ state. Two other curves having symmetry $^2\Pi_{3/2}$, $^2\Pi_{1/2}$ lie within 1 eV of the upper laser level. The splitting depends on the amount of spin orbit coupling, being largest for the Xe halides. A priori calculations show that a substantial amount of mixing occurs between the $\Omega = 1/2$ states, and as such the $^2\Sigma$ notation given in Fig. 1 is an over simplification.[33] Emission from the higher ionic states has been observed.[5, 8, 13] In fact, the broad bands are probably super positions of emission from the $^2\Sigma_{1/2}$ and the $^2\Pi_{3/2}$ states to the repulsive $^2\Pi$.

Note the high quantum efficiency that is intrinsic to the rare gas monohalide lasers. Assuming the process begins with production of an excited metastable, such as Kr^*, quantum efficiencies of order 50% can be achieved. The lost energy goes into chemical potential by dissociation of a weakly bound halogen source, such as F_2, and excess vibrational energy initially invested in producing the rare gas monohalide excited state. Discharge excitation of Kr^* is capable of fairly high excited state production efficiencies. Boltzmann code calculations[32, 34] suggest that the efficiency of producing excited rare gas atoms could be as high as 70% for an excitation level sufficiently high to produce useful laser gain on rare gas halides in a reasonable length device. Thus, before accounting for losses due to extraction and energy coupling, a discharge pumped rare gas halide laser could have an efficiency of order 35%.

For E-beam pumping the quantum efficiencies are not as high as with discharge pumping. Moreover, the production efficiencies are much lower than with discharge excitation because the primary electron beam looses roughly twice the energy of ionization of the dominant species to produce an ion with some atomic excitation.[35] Thus the product of production efficiency with quantum efficiency is about 25% for typical rare gas halides. Power coupling efficiency lowers the overall potential system efficiency for an E-beam device relative to a discharge.

Naturally, the development of new lasers and new molecules is leading to increased research on these species. The exact dependence on internuclear separation as well as the locations and assignments of the potential curves for many of the states of the rare gas halides remains to be done. The lowest $^2\Sigma$ covalent state, the lower laser level, is not truly dissociative for XeF and XeCl. The lasing transitions are, in fact, bound to bound,[5, 6, 36] for these species since these molecules have shallow wells

in the lowest states. Because the wells are fairly shallow, depopulation of the lower level can take place via rapid collisional dissociation. The binding of the XeF ground state was not anticipated theoretically.[37] Refined calculations on the XeF ground state show that inclusion of the long range Vander Waals attraction is important in calculating the properties of the bound ground state of XeF.[38]

As seen in Fig. 1, there are higher lying potential curves that derive from $M^* + X$ and $X^* + M$. Not drawn are the potential curves for the ion MX^+, which are typically at higher energies. The exact energy and shape of the curves coming from $M^* + X$ has an important impact on the possibility of self absorption. Xenon bromide is probably a fine example of a rare gas haide that fluoresces very efficiently but lases very poorly. This is possibly due to self absorption as shown in Fig. 2. Note that the self absorption is a photodissociation process rather than photoionization which plagues the rare gas excimer lasers such as Xe_2^*. The positions of the upper and lower laser levels can be determined by the wavelength and shape of the $XeBr^*$ emission bands. The exact position of the potential curves and the wavelength dependence of the absorption bands relative to the stimulated emission cross section is not known. However, it is reasonably clear that absorption is possible in the $XeBr^*$ case since a 282 nm photon has ample energy to produce an $Xe^* + Br$ from the ionic upper laser level. Rough considerations of the atomic orbitals that the electrons occupy in the various states suggests that absorption plays a major role in decreasing gain and efficiency in this system. Recall that the upper laser level is an ion $Xe^+ Br^-$. In making a transition to the lower laser level an electron hops out of a p orbital of Br^- into the lowest vacant orbital of Xe^+, a 5 p orbital. This produces ground state Xe and Br atoms. However, in making a transition upward to $Xe^* + Br$ the electron hops from Br^- into a

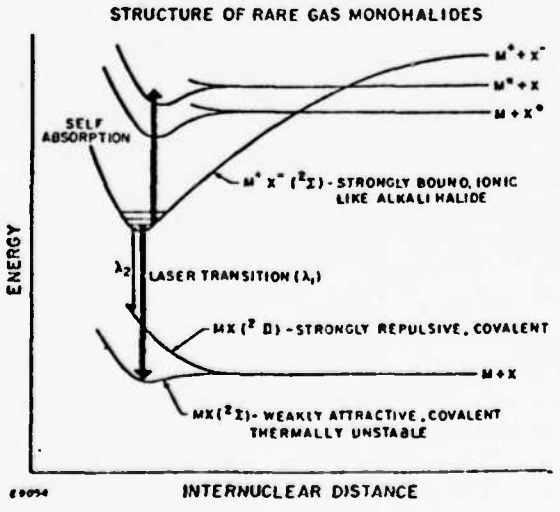

Fig. 1 Schematic of rare gas monohalide potential energy curves

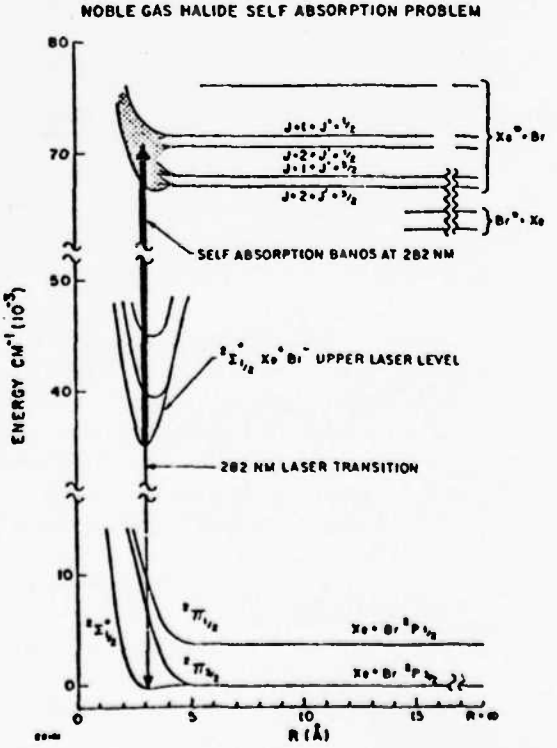

Fig. 2 Estimated potential curves for NeBr showing the possibility of strong absorption band overlapping the lasing transition

large 6 s orbital of Xe. By virtue of the fact that the final electron orbitals centered on Xenon for states of Xe^* are larger than those in which a ground state Xe atom is produced, one expects that the total transition dipole moment for absorption is larger than that corresponding to the lasing transition. The absorption is probably spread out over a broader band than the sharp laser transition, thus allowing for net gain to occur. Such absorption, as in the case of $XeBr^*$, obviously limits the spectroscopic component of the extraction efficiency as well as lowering the gain. A similar absorption can occur in other rare gas halide lasers, even in the high efficiency KrF laser. The KrF^* 248 nm photon barely allows the molecule to reach the energetic limit for forming Kr^*+ F. Such absorption would clearly limit the scalability and efficiency of a larger KrF laser. Small signal gain and loss measurements through the KrF laser band would shed light on this problem. That absorption is a problem in the KrF laser can be shown simply by measuring laser power out as a function of output coupling.[25] For $Ar/Kr/F_2$ mixtures the maximum efficiency is derived with large output coupling, for example when using the 15% feedback of a quartz flat as one of the laser reflectors. Similar results obtained with $Ar/Kr/NF_3$ mixtures suggest that the F_2 by itself was not the only absorbing species (NF_3 does not absorb at 248 nm). As mentioned above KrF^* self absorption could be the cause of this effect, or possibly photoionization of the excited atoms Ar^* or Kr^*, absorption by ArF, Ar_2^*, or Kr_2^* molecules.

The XeCl laser is another case where absorption strongly limits laser performance. With the use of Cl_2 as an oxidizer, absorption is clearly a problem because of its strong photodissociation band at 308 nm. However, use of alternate sources such as HCl, while improving performance relative to Cl_2, does not make the XeCl laser as efficient as either XeF or KrF.[6, 39]

Spectroscopically speaking, even the best of the rare gas halide lasers is far from ideal. Quantum efficiencies, while excellent, are lower than that of the CO infrared laser. Spectroscopically efficient extraction requires high output coupling in the best of cases to date. The use of high output coupling lowers the intra cavity flux for a fixed total energy input. This can lower kinetic extraction efficiency of a KrF laser if the flux drops below that required for reasonable saturation. The simultaneous observation of efficient discharge pumping of excited states, high flux levels for efficient kinetic extraction, and high output couplings for good extraction relative to losses has yet to be shown for KrF.

Rare Gas Halide Kinetics

The mechanism for producing the excited states of the rare gas halide lasers are not yet fully understood or quantitatively documented. However, the general ways in which excited states can be produced can be given and estimates of pertinent rates made. Producing excited states from the primary excitation products, ions and excited atoms, is only a part of the overall laser kinetics. This part is becoming well understood. From an efficiency point of view, the kinetics are ideal, since branching ratios are near unity for many cases. Electron attachment rates are very important in electric discharge lasers because attachment is usually the dominant mechanism for removing electrons. Moreover, attachment provides a mechanism for maintaining a constant impedance discharge in strongly excited rare gas mixtures.[32,34] The kinetics of this process is critical to the attainment of high efficiency at high average powers. The quenching kinetics and radiative lifetimes of these species are poorly understood but are clearly important because they determine the flux level needed for a kinetically efficient extraction.

Table I gives a simplified mechanism for the KrF laser. This laser operates most efficiently in $Ar/Kr/F_2$ mixtures. Left out of this mechanism is any specification of the excited states. Since a manifold of states are excited and can react with different reaction rates for forming excited states, this is possibly an oversimplification. The three body loss of excited states into excimers is not tabulated, and this is an important reaction when the halogen number densities are below optimal. Three body loss will decrease the upper laser level production efficiency. Ionization of Ar and Kr excited states has been left out of the Table, and this is a very important rate for efficient discharge pumped rare gas halide lasers.[32, 34]

With the above mention of the simplifications in the mechanism, we discuss the reaction kinetics as they are understood at this stage. We begin with a discussion of the "classical" route to rare gas halide excited states, reactions of rare gas excited states with halogenated species.

The first public mention of the potential of these new molecules as "excimer" lasers was a result of fundamental rate constant measurements for the quenching of inert gas metastables.[1, 2] Groups in Kansas and Cambridge, England, were attempting to look at the energy partioning in these reactions by monitoring product fluorescence. Both observed new UV and VUV luminescence due to quenching reactions of rare gas excited states with halogens. These new, bright emission spectra were attributed to bound-free continua of rare gas monohalides. The prototypical reactions are

$$Ar^* + Cl_2 \rightarrow ArCl^* + Cl$$
$$ArCl^* \rightarrow Ar + Cl + h\nu \quad (172\ nm) \qquad (1)$$

and

$$Xe^* + Cl_2 \rightarrow XeCl^* + Cl$$
$$XeCl^* \rightarrow Xe + Cl + h\nu \quad (308\ nm) \qquad (2)$$

These reactions all tend to proceed with large cross sections. This is not surprising since the corresponding reactions of alkali metal atoms with halogens and halogenated species also have large cross sections. As mentioned earlier, a noble gas in its excited state is very similar in properties to an alkali ground state. A low ionization potential is the key to the similarity of reaction chemistry and chemical compounds.

Species such as KrF^*, are nothing more than short lived "pseudo alkali halides", i.e., diatomic molecules in which one electrical charge has been transferred from the rare gas atom to the halogen. The formation of alkali halide molecules and rare gas halide excited states can all proceed along chemically similar pathways. This similarity derives from the fact that metastable rare gas atoms, Kr^* for example, or any highly excited state of an atom have low ionization potentials and chemically will behave like ground state atoms that have low ionization potentials, viz the alkali atoms. The chemical kinetics of alkalis reacting with halogen molecules has a long history and this chemistry is understood in much detail. The mechanism for such alkali/halogen reactions is discussed in detail elsewhere.[40] The reaction of a Kr^* with a halogen containing molecule should produce an ionic species. A graphic explanation of these reactions, thought to proceed by way of an ionic-covalent curve crossing, is called the "harpooning" mechanism.[1, 2, 40] In such reactions the low ionization potential of the

Table I

Simplified mechanism for rare gas halide lasers
($Ar/Kr/F_2$ mixture)

EXCITATION REACTIONS

Discharge Pumping

- Metastable Formation

$$e + Ar \rightarrow Ar^* + e$$

$$e + Kr \rightarrow Kr^* + e$$

- Reaction with Halogen

$$Ar^* + F_2 \rightarrow ArF^* + F$$

$$Kr^* + F_2 \rightarrow KrF^* + F$$

- Displacement

$$Kr + ArF^* \rightarrow KrF^* + Ar$$

E-Beam Pumping

- All of the Above
- Ion Recombination

$$e + F_2 \rightarrow F + F^-$$

$$F^- + Ar^+ + M \rightarrow ArF^* + M$$

$$F^- + Kr^+ + M \rightarrow KrF^* + M$$

LOSS REACTIONS

- Quenching

$$KrF^* + \begin{Bmatrix} Ar \\ Kr \\ F_2 \\ e \end{Bmatrix} \rightarrow Kr + F + \begin{Bmatrix} Ar \\ Kr \\ 2F \\ e \end{Bmatrix}$$

$$KrF^* + e \rightarrow Kr, Kr^* + F^-$$

- Radiation

$$KrF^* \rightarrow Kr + F + h\nu$$

$$h\nu + KrF^* \rightarrow Kr + F + 2h\nu$$

alkali or excited species and the high electron affinity of the halogen molecules allows an ionic potential curve of the form $M^+ + X_2^-$ to cross that of $M^* + X_2$ at fairly large internuclear separations, distances of order 5 Å. The X_2^- ion formed by an electron hop, when the ionic and covalent potentials become degenerate, is unstable with respect to dissociation into $X^- + X$ in the presence of the large electric field of the M^+ ion. As a result, the $M^+X_2^-$ temporary triatomic species fall apart into an ion pair M^+X^- leaving behind an X atom. The term "harpooning" mechanism derives from considering the electron that hops from the M^* over to X_2 as the harpoon that creates an extremely large coulombic force that pulls the old X_2 molecule apart and forms the new ionic, M^+X^- species. The prime difference between reactions of halogen molecules with alkali metal atoms and the corresponding chemistry with excited states such as Kr^* is that in the alkali reactions only one electronic state can be formed while several potential product channels can exist in certain excited state/halogen molecule reactions.

The cross sections and exit channel branching ratios for a number of excited metastable inert gas atoms reacting with halogens are now being measured.[7,8] The bulk of this work is being done at low pressures. The spectra observed are similar but not identical to those at high pressure as in E-beam or discharge excited lasers. A brief compendium of some of the relevant reaction rates for reaction of metastable inert gases with halogen containing compounds is given in Table II. The key phenomenon, from an efficiency viewpoint, is that the kinetic branching ratios for forming rare gas halide excited states are unity for several of the most important reactions: viz $Xe^* + F_2$, $Xe^* + NF_3$, $Xe^* + Cl_2$, $Kr^* + F_2$ and $Kr^* + Cl_2$. Thus, if one makes rare gas excited states and does not lose excitation into excimer states such as Xe_2^*, Kr_2^*, or Ar_2^*, one has a very efficient means of producing the upper laser level from a species which can be produced directly, and hopefully efficiently in a discharge. At typical F_2 mole fractions, 0.3%, and total pressures of 2 atm, the characteristic time for Ar^* or Kr^* reaction with F_2 is about 10 ns. The Kr_2^* excimers formation time is longer than this because of the use of Ar/Kr mixtures. Some Ar_2^* excimers are made from Ar^* initially produced, but because of the large cross section for producing Kr^* upon collision of Kr with Ar_2^* excimers, the formation of Ar_2^* does not constitute a kinetic branching loss mechanism. Thus for suitable mixtures of rare gases and halogens the production channel involving rare gas metastables can provide upper laser levels with branching ratios that appear to be unity.

The reactions tabulated above pertain, to some degree, to discharge pumping of a rare gas halide laser. In a discharge, however, one can have several other excited states produced, and the reaction kinetics of other states may differ, possibly even having larger cross sections. The low pressure E-beam excited $XeBr^*$ experiments of Searles and Hart suggest this since their modeling of the production and decay of $XeBr^*$ from E-beam excited Xe/Br_2 mixtures gives a rate constant for an undefined ensemble of Xe^* excited states reacting with Br_2 that is a factor of 4 times larger than the rate measured out of Xe metastables.[9]

Not all reactions of rare gas metastables give high yields of rare gas halide excited states. In fact, a number of reaction pairs, such as $Ar^* + Br_2$[7] give halogen atom emission.

Table II

Some kinetic rate constants for
rare gas metastable/halogen reactions

		k_Q[a.]	σ_Q[b.]	Ref.	Comments
$Xe^*(^3P_2)$ +	Cl_2	6.5	193	(2)	
	Br_2	6.0	202	(2)	
	CF_3I		184	(2)	
	F_2	7.3	156	(8)	Produces XeF^* with unit quantum yield.
	NF_3	.86	23	(8)	
$Kr^*(^3P_2)$ +	F_2	8.1	163	(8)	Produces KrF^* with unit yield.
	Cl_2	6.0	147	(8)	
	NF_3	1.6	39	(8)	
$Ar^*(^3P_2)$ +	Br_2	6.5	147	(7)	Produces Br^*
	Cl_2	7.1	142	(7)	Produces $ArCl^*$ and Cl^*
	F_2	8.5	148	(8)	Should produce ArF^* with near unit yield.
	Kr	.06	1.3	(51)	
	Xe	1.8	40	(51)	

a. Rate constants, k_Q, given in units of 10^{-10} cm^3/ molecule sec.

b. Cross sections, σ_Q, given in units of 10^{-16} cm^2.

A simple understanding of why some reactions produce halogen atom excited states and others produce rare gas halide emission can be gained by inspecting approximate potential curves for a rare gas halide. In the measured case of Ar^* + Br_2 chemistry, the $ArBr^*$ is presumably formed with energy up to that available from the combining reactants, in this case $E(Ar^*)$ - $DE(Br_2)$ where DE is the dissociation energy of the halogen bearing fuel.[1] Sketching up the $ArBr^*$ potential curves shows that the energy available by this reaction is sufficient to populate a number of exit channels that can yield Br^* by predissociation. Making a statistical argument, which has been found excellent in the analogous alkali dimer/halogen atom reactions,[41,42,43] one would say that every state accessible via some curve crossing will be produced. For the case of Ar^* + Br_2 or Ar^* + an iodine containing compound such as I_2 or HI there are many more accessible states that put the energy into electronically excited halogen atoms rather than rare gas halide excited states. For the case of ArI^*, whose potential energy curves are schematically shown in Fig. 3, no net binding of ArI^* relative to Ar + I^* is expected[3] and one predicts that Ar^* + RI reactions should produce primarily high lying iodine atom excited states. In marked contrast to this is the reaction of Ar^*, Kr^*, and Xe^* with F_2 and Xe^* with Cl_2. The rare gas halides formed in these cases cannot predissociate into any F^* or Cl^* excited states since the rare gas halides produced by reactions all have lower energy than any halogen atom excited state.[3] Reactions of these species should then lead primarily to rare gas halide emission. This, of course, is one reason for the high efficiency of the KrF laser.

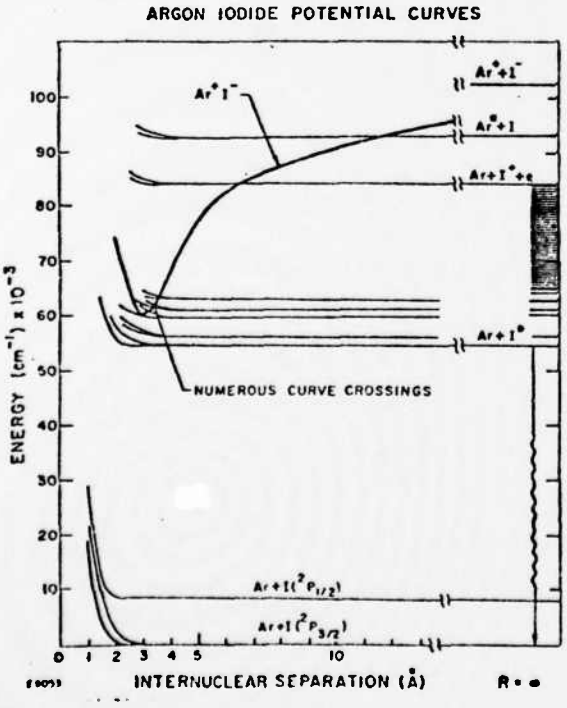

Fig. 3 Gross estimate of the potential curves for ArI. Note that the ionic state is not bound relative to Ar + I^*. As a result quenching reactions of Ar^* with iodine containing molecules such as CF_3I, or ion recombination of Ar^+ with I^- should yield I^* excited states

Since the upper levels of rare gas halide lasers are ionic in nature, positive-negative ion recombination can also feed the upper laser level. In E-beam excited Ar/F_2 mixtures the Ar^+ ions are formed by the relativistic electrons. F^- ions can be formed by attachment of the secondary electrons. Recombination then yields ArF^*. For those rare gas halides that have very large radii curve crossings with M^* + X or M + X^*,[3] theory and experiments with alkali halide dissociation show that these species should recombine entirely into ions.[44,45] For the recombination of Ar^+ + I^- or Ar^+ + Br^-, however, ion recombination should simply yield electronic excitation of the various atoms. Because of the long range of the coulomb potential these ion recombination reactions have huge three body rates, ~10^{-25} cm^3 sec.[46] These three body rates become diffusion limited two body rates at high pressures. The degree to which ion-ion recombination occurs rather than ion-electron recombination (typically

by way of $Ar_2^+ + e$ at high pressure) depends on the rate constants for dissociative attachment

$$e + RX \rightarrow R + X^- \qquad (4)$$

where R is anything bonded to a halogen. For mixtures containing F_2, HI, and CF_3I attachment is fast and negative ion-positive ion recombination dominates for mixtures with halogen pressures of order 3 torr.[47] Br_2 and I_2, however, attach slowly[48] and rare gas mixtures with these halogen sources will be dominated by neutral chemistry.

Displacement reactions should be very important in rare gas halide lasers, although little is yet known quantitatively. These come about when a light rare gas halide excited state collides with a heavier rare gas atom:

$$ArF^* + Kr(Xe) \rightarrow KrF^* (XeF^*) + Ar \qquad (5)$$

ArF^* is simply an ion pair, $Ar^+ F^-$. Kr and Xe have lower ionization potentials than Ar. ArF^* has a higher energy than KrF^* or XeF^*. These facts suggests that these exothermic "knockout" reactions could have large reaction rate constants, at least as large as 3×10^{-10} cm^3 sec^{-1}. These reactions must be accounted for to properly model the rare gas halide lasers. They will be important in both E-beam pumped lasers where ArF^* will form by ion recombination, and also in discharge pumped KrF lasers where ArF^* forms by way of $Ar^* + F_2$ reactions. Electron-beam pumped KrF lasers, using F_2 as the flourine source, are excited primarily by ion recombination. Thus the branching ratio for the reaction $ArF^* + Kr \rightarrow KrF^* + Ar$ must be unity since Ar^+ is the dominant ion formed, and since the intrinsic efficiency of the KrF laser is so high.[25]

The excited states of these species can also be pumped by neutral recombination, for example, Br^* recombining with Ar, Kr, or Xe. Such reactions are important in E-beam pumped mixtures where the attachment rate is low leading to Ar^* or Ar_2^* chemistry and a primary reaction leads to an excited halogen rather than a rare gas halide.

The radiative lifetimes of these species are not well known. Searles modelled the kinetics of his low pressure, E-beam excited Xe/Br_2 system to give a radiative lifetime of 17 ns.[8] This lifetime is quite reasonable for an allowed charge transfer transition corresponding to an oscillator strength of about 0.1. Preliminary measurements at AERL have suggested an upper limit of 40 ns for the radiative lifetime of XeF.[49] This corresponds to an oscillator strength of about 0.05, which also is consistent with experience with alkali halides or the recently measured lifetime of an analogous charge transfer band in I_2.[50] Since the radiative lifetime is needed to determine the gain and saturation parameters of these lasers it is anticipated that calculations and measurements of radiative lifetimes will appear in the next year. Dunning and Hay have given a theoretical calculation of the KrF^* lifetimes for the various ionic excited states.[33] For the intense laser band a lifetime of about 6 ns is calculated. This corresponds to a stimulated emission cross section, $\sigma \sim 4 \times 10^{-16}$ cm^2.

The quenching kinetics of the upper laser levels of rare gas halides and halogens is not yet completely understood. However, it is known that the laser efficiency of KrF is much higher than its fluorescence efficiency. High cavity fluxes should in principal be capable of competing with any quenching, but from an academic point of view it is important to identify

the quenching mechanisms. The obvious quenchers are the rare gas atoms present in the excited mixtures. Quenching in the KrF laser occurs about four times faster than radiation.[25] This implies a quenching frequency of about 5×10^8 sec^{-1}. If the quenching is ascribed wholly to Ar or Kr, rate constants of 5×10^{-12} and 8×10^{-11} cm^3 sec^{-1} would be required. This seems rather large for what must be an E → T process with almost 4 eV of energy appearing in the relative translational energy of 2 Kr atoms and an F atom. F_2 could also quench KrF* and at the typical mole fractions used this would correspond to a rate constant of 8×10^{-10} cm^3 sec^{-1}. This seems at first to be too large also, but is within the range of rate constants one can have for a long range dipole interaction.[51] This is not unreasonable since F_2 does absorb in the 248 nm band and a continuum of final states is accessible. The cross section for such a process is about 200 Å^2. Larger cross sections are known for the transfer of energy from Kr_2^* and Ar_2^* excimers to Xe by a similar mechanism.[51] Finally electrons can quench these excited states. Recall that the excited state in both halogen and rare gas halide lasers is an ion pair. The permanent electric dipole moment of rare gas halides is hugh, ~10D. The charge-dipole interaction then at large distances, ~5 Å, can exert a significant force and initial and final states can be mixed together by passing electrons. Also, a dissociative attachment process such as

$$KrF^* + e \rightarrow Kr^* + F^- \qquad (6)$$

can occur with electrons of energy ~1 eV. If the entire quenching of excited states was due to electrons, a rate constant of order 2×10^{-7} cm^3 sec^{-1} corresponding to a cross section of ~200 Å^2 is inferred. This is a little bit larger than most dissociative attachment rates, but not outside the realm of possibility. The total quenching is probably due to contributions from each of the above, and detailed modeling will require definitive measurements of these quenching rates individually.

In terms of the guidelines given earlier, the kinetics of the rare gas halides is nearly ideal. Coupling efficiencies can be large for several reasons. Attachment of electrons to halogens balances the avalanching of electron number density. The net rate of ionization, and consequent change in plasma impedance, and the state population of excited rare gas atoms can also be minimized because the halogens react rapidly with excited states. Because the stimulated emission cross-sections are sufficiently high, excited state number densities can be kept lower than those required for broader band excimer lasers, such as Xe_2^* or Hg_2^*. Naturally, since the lower levels, excepting possibly XeF, are rapidly removed, the inversion can be maintained while the discharge circuitry is being switched. Upper laser level production efficiencies are large. Both ion recombination and direct reactions can yield certain rare gas halides with unit branching ratios. The displacement reaction apparently also has a high branching ratio. Loss into other excimer channels is minimized. At sufficiently low excitation levels, $< 10^{-2}$%, the initial excited states can be produced at roughly 80% efficiency.[32, 34] The area of extraction efficiency is the only aspect of rare gas halide lasers that critically taxes the kinetics of the system. Quenching of excited states does occur, but reasonable flux levels can be used to extract efficiently. Since the lower level is dissociative, no bottlenecking occurs even when the stimulated rate is significant.

Conclusions

The growth of research in the rare gas/halogen systems has been phenomenal over the past year. This is not surprising since the potential of these species as lasers and as fluorescence sources is quite large. The rare gas monohalide molecules themselves are intrinsically interesting because of their novelty. It is not hard to predict that practical lasers based on the schemes discussed here will evolve over the next few years. If indeed practical UV lasers with overall efficiencies well in excess of 1% become available, UV photochemistry, and other areas requiring coherent UV light, should be dramatically enhanced.

Nothing with similar laser potential has been demonstrated yet as a coherent visible source. However, the potential for higher efficiency clearly exists. Aside from finding systems analogous to the rare gas halides that might work in the visible, one can hope to find systems with higher efficiencies by overcoming some of the shortcomings of the rare gas halides. The rare gas halides do have fairly low quantum efficiencies and have problems with spectroscopic extraction, and these areas would have to be improved on if one hopes to find visible or UV lasers with even higher efficiency.

There is no reason, however, to doubt that practical, high efficiency lasers can also be found in the visible, as well as the UV and IR.

Acknowledgments

The authors are indebted for numerous stimulating conversations with his co-workers at Avco Everett: J. D. Daugherty, H. Hyman, J. Jacob, and J. Mangano. Also they thank D. W. Setser for providing preprints of very important rate constant measurements prior to their publication. A variety of other workers in the field have provided the authors with preprints and comments prior to final publication and these are acknowledged: R. Gordon, Y. T. Lee, J. Murray, M. McCusker, M, Krauss, A. K. Hays, S. Suchard, N. Djeu, and R. Hunter. Support of ARPA/ ONR through Contract No. N00014-75-C-0062 is acknowledged.

References

1. M. F. Golde and B. A. Thrush, Chem. Phys. Lett. 29, 486 (1974).

2. J. E. Velazco and D. W. Setser, J. Chem. Phys. 62, 1990 (1975).

3. J. J. Ewing and C. A. Brau, Phys. Rev. A12, 129 (1975).

4. M. F. Golde, J. Mol. Spectry 58, 261 (1975).

5. C. A. Brau and J. J. Ewing, J. Chem. Phys. 63, 4640 (1975).

6. J. Tellinghuisen, J. W. Hoffman, G. C. Tisone, and A. K. Hays, J. Chem. Phys. 64, 2484 (1976).

7. L. A. Gundel, D. W. Setser, M. A. A. Clyne, J. A. Coxon, and W. Nip, J. Chem. Phys. 64, 4390 (1976).

8. J. E. Velazco, J. H. Kolts and D. W. Setser, "Quenching Rate Constants for Metastable Argon, Krypton and Xenon Atoms by Fluorine Containing Molecules and Branching Ratios for XeF and KrF Formation," to be published.

9. S. K. Searles and G. A. Hart, Appl. Phys. Lett. 27, 243 (1975).

10. C. A. Brau and J. J. Ewing, Appl. Phys. Lett. 27, 435 (1975).

11. J. J. Ewing and C. A. Brau, Appl. Phys. Lett. 27, 350 (1975).

12. J. M. Hoffman, A. K. Hays, and G. C. Tisone, Appl. Phys. Lett. 28, 538 (1976).

13. J. R. Murray and H. T. Powell, "KrCl Laser Oscillation at 222 nm," to be published.

14. S. Searles, private communication.

15. J. A. Mangano and J. H. Jacob, Appl. Phys. Lett. 27, 495 (1975).

16. R. Burnham, N. W. Harris and N. Djeu, Appl. Phys. Lett. 28, 86 (1976).

17. J. J. Ewing and C. A. Brau, Appl. Phys. Lett. 27, 557 (1975).

18. J. R. Murray, J. C. Swingle, and C. E. Turner, Appl. Phys. Lett. 28, 530 (1976).

19. C. H. Chen and M. G. Payne, Appl. Phys. Lett. 28, 219 (1976).

20. J. R. Murray, private communication.

21. J. J. Ewing, J. H. Jacob, J. A. Mangano and H. Brown, Appl. Phys. Lett. 28, 656 (1976).

22. J. Jacob, private communication.

23. M.V. McCusker, R.M. Hill, D.L. Huestis, D. C. Lorents, R.A. Gutchek and H.H. Nakano, Appl. Phys. Lett. 27, 363 (1975).

24. M. V. McCusker, private communication.

25. C. A. Brau and J.J.Ewing, "Rare Gas Monohalide Lasers: Performance and Spectroscopy," Second Summer Colloquium on Electronic Transition Lasers, Woods Hole, Massachusetts, Sept., 1975.

26. M.L.Bhaumik, R.S. Bradford, Jr., and E.R. Ault, Appl. Phys. Lett. 28, 23 (1976).

27. R. Burnham, F.X.Powell and N. Djeu, Appl. Phys. Lett. 29, 30 (1976).

28. The term "excimer" is standard chemical nomenclature for dimers which are bound in the excited state and free in the lower state. In standard nomenclature dimer means two of the same thing. Thus, Xe_2^*, Ar_2^*, etc. are excimers. Species that are heteronuclear such as $LiXe^*$ or KrF^* can also have bound excited states and dissociative lower states. The accepted chemical nomenclature for such species is "exiplex" short for excited complex. Unfortunately, the laser community has not uniformly utilized good scientific English and typically calls all species with dissociative lower states, and even some like XeF with bound lower states, "excimers."

29. J.H. Birely, D.C. Cartwright and J. Marinuzzi, "Application of High Power Lasers to Problems in the Nuclear Fuel Cycle," to be published.

30. K. Brueckner and S. Jorna, Rev. Mod. Phys. 46, 325 (1974).

31. Chemical production of excited states and a corresponding visible chemical laser is a volumetrically scalable excitation technique. However, chemical pumping of a UV or visible laser has not yet been demonstrated.

32. J.D. Daugherty, J. A. Mangano and J.H. Jacob, Appl. Phys. Lett. 28, 581 (1976).

33. T. H. Dunning, Jr., and P. J. Hay, Appl. Phys. Lett. 28, 649 (1976).

34. J.H. Jacob and J.A.Mangano, Appl. Phys. Lett. 28, 724 (1976).

35. D. C. Lorents and R.E. Olson, Stanford Research Institute Project PYU-2018 Semi annual Report, 1972 (unpublished).

36. J. Tellinghuisen, G. C. Tisone, J. M. Hoffman and A. K. Hays, J. Chem. Phys. 64, 4796 (1976).

37. D. H. Liskow, H. F. Schaefer III, P. S. Bagus and B. Liu, J. Am. Chem. Soc. 95, 4056 (1973).

38. M. Krauss, private communication.

39. J. J. Ewing and C. A. Brau, unpublished.

40. Keith J. Laidler, "Theories of Chemical Reaction Rates," McGraw Hill Book Co., New York (1969).

41. J. R. Krenos and J. C. Tully, J. Chem. Phys. 62, 420 (1975).

42. W. S. Struve, J. R. Krenos, D. L. McFaddlen and D. R. Herschbach, J. Chem. Phys. 62, 404 (1975).

43. D. O. Ham. J. Chem. Phys. 60, 1802 (1974).

44. J. J. Ewing, R. Milstein, and R.S. Berry, J. Chem. Phys. 54, 1752 (1971).

45. A. Mandl, J. Chem. Phys. 55, 2918, 2922 (1971).

46. D. R. Bates and M. R. Flannery, Proc. Roy. Soc. (London) A302, 367 (1968).

47. L. G. Christophorou and J. A. D. Stockdale, J. Chem. Phys. 48, 1956 (1968).

48. D. W. Trainor, private communication.

49. C. A. Brau and J. J. Ewing, "Radiative Lifetime of XeF," unpublished.

50. D. L. Rousseau, J. Mol. Spectry. 58, 481 (1975).

51. A. Gedanken, J. Jortner, B. Raz and A. Szoke, J. Chem. Phys. 57, 3456 (1972).

52. L. G. Piper, J. E. Velazco and D. W. Setser, Chem. Phys. Lett. 25, 197 (1974).

DISTRIBUTION LIST

Office of Naval Research, Department of the Navy, Arlington, VA 22217 - Attn: Physics Program (3 copies)

Naval Research Laboratory, Department of the Navy, Washington, D.C. 20375 - Attn: Technical Library (1 copy)

Office of the Director of Defense, Research and Engineering, Information Office Library Branch, The Pentagon, Washington, D.C. 20301 (1 copy)

U.S. Army Research Office, Box CM, Duke Station, Durham, N.C. 27706 (1 copy)

Defense Documentation Center, Cameron Station, Alexandria, VA 22314 (12 copies)

Defendar Information Analysis Center, Battelle Memorial Institute, 505 King Avenue, Columbus, OH 43201 (1 copy)

Commanding Officer, Office of Naval Research Branch Office, 536 South Clark Street, Chicago, IL 60615 (1 copy)

New York Area Office, Office of Naval Research, 715 Broadway (5th Floor), New York, NY 10003 - Attn: Dr. Irving Rowe (1 copy)

San Francisco Area Office, Office of Naval Research, 760 Market Street, Room 447, San Francisco, CA 94102 (1 copy)

Air Force Office of Scientific Research, Department of the Air Force, Washington, D.C. 22209 (1 copy)

Office of Naval Research Branch Office, 1030 East Green Street, Pasadena, CA 91106 - Attn: Dr. Robert Behringer (1 copy)

Code 102 IP (ONRL), Office of Naval Research, 800 N. Quincy Street, Arlington, VA 22217 (6 copies)

Defense Advanced Research Projects Agency, 1400 Wilson Blvd., Arlington, VA 22209 - Attn: Strategic Technology Office (1 copy)

Office Director of Defense, Research & Engineering, The Pentagon, Washington, D.C. 20301 - Attn: Assistant Director (Space and Advanced Systems) (1 copy)

Office of the Assistant Secretary of Defense, System Analysis (Strategic Programs), Washington, D.C. 20301 - Attn: Mr. Gerald R. McNichols (1 copy)

U.S. Arms Control and Disarmament Agency, Dept. of State Bldg., Rm. 4931, Washington, D.C. 20451 - Attn: Dr. Charles Henkin (1 copy)

Energy Research Development Agency, Division of Military Applications, Washington, D.C. 20545 (1 copy)

National Aeronautics and Space Administration, Lewis Research Center, Cleveland, OH 44135 - Attn: Dr. John W. Dunning, Jr. (1 copy)
(Aerospace Res. Engineer)

National Aeronautics & Space Administration, Code RR, FOB 10B, 600 Independence Ave., SW, Washington, D.C. 20546 (1 copy)

National Aeronautics and Space Administration, Ames Research Center, Moffett Field, CA 94035 - Attn: Dr. Kenneth W. Billman (1 copy)

Department of the Army, Office of the Chief of RD&A, Washington, D.C. 20310 - Attn: DARD-DD (1 copy)
DAMA-WSM-T (1 copy)

Department of the Army, Office of the Deputy Chief of Staff for Operations & Plans, Washington, D.C. 20310 - Attn: DAMO-RQD - (1 copy)

Ballistic Missile Defense Program Office (BMDPO), The Commonwealth Building, 1300 Wilson Blvd., Arlington, VA 22209 - Attn: Mr. Albert J. Baat, Jr. (1 copy)

U.S. Army Missile Command, Research & Development Division, Redstone Arsenal, AL 35809 - Attn: Army High Energy Laser Programs (2 copies)

Commander, Rock Island Arsenal, Rock Island, IL 61201, Attn: SARRI-LR, Mr. J.W. McGarvey (1 copy)

Commanding Officer, U.S. Army Mobility Equipment R&D Center, Ft. Belvoir, VA 22060 - Attn: SMEFB-MW (1 copy)

Commander, U.S. Army Armament Command, Rock Island, IL 61201 - Attn: AMSAR-RDT (1 copy)

Director, Ballistic Missile Defense Advanced Technology Center, P.O. Box 1500, Huntsville AL 35807 - Attn: ATC-O (1 copy)
ACT-T (1 copy)

Commander, U.S. Army Material Command, Alexandria, VA 22304 - Attn: Mr. Paul Chernoff (AMCRD-T) (1 copy)

Commanding General, U.S. Army Munitions Command, Dover, NH 07801 - Attn: Mr. Gilbert F. Chesnov (AMSMU-R) (1 copy)

Director, U.S. Army Ballistics Res. Lab, Aberdeen Proving Ground, MD 21005 - Attn: Dr. Robert Eichenberger (1 copy)

Commandant, U.S. Army, Air Defense School, Ft. Bliss, TX 79916 - Attn: Air Defense Agency (1 copy)
ATSA-CTD-MS (1 copy)

Commanding General, U.S. Army Combat Dev. Command, Ft. Belvoir, VA 22060 - Attn: Director of Material, Missile Div. (1 copy)

Commandar, U.S. Army Training & Doctrine Command, Ft. Monroe, VA 23651 - Attn: ATCD-CF (1 copy)

Commander, U.S. Army Frankford Arsenal, Philadelphia, PA 19137 - Attn: Mr. M. Elnick SARFA-FCD Bldg. 201-3 (1 copy)

Commandar, U.S. Army Electronics Command, Ft. Monmouth, NJ 07703 - Attn: AMSEL-CT-L, Dr. R.G. Buser (1 copy)

Commandar, U.S. Army Combined Arms Combat Developments Activity, Ft. Leavenworth, KS 66027 (1 copy)

National Security Agency, Ft. Geo. G. Meade, MD 20755 - Attn: R.C. Foss A763 (1 copy)

Deputy Commandant for Combat & Training Developments, U.S. Army Ordnance Center and School, Aberdeen Proving Ground, MD 21005
Attn: ATSL-CTD-MS-R (1 copy)

Commanding Officer, USACDC CBR Agency, Ft. McClellan, AL 36201 - Attn: CDCCRR-MR (Mr. F.D. Poer) (1 copy)

DISTRIBUTION LIST (Continued)

Department of the Navy, Office of the Chief of Naval Operations, The Pentagon 5C739, Washington, D.C. 20350 - Attn: (OP 982F3) (1 copy)

Office of Naval Research Branch Office, 495 Summer Street, Boston, MA 02210 - Attn: Dr. Fred Quelle (1 copy)

Department of the Navy, Deputy Chief of Navy Material (Dev.), Washington, D.C. 20360 - Attn: Mr. R. Gaylord (MAT 032B) (1 copy)

Naval Missile Center, Point Mugu, CA 93042 - Attn: Gary Gibbs (Code 5352) (1 copy)

Naval Research Laboratory, Washington, D.C. 20375 - Attn: (Code 5503-EOTPO) (1 copy)
Dr. P. Livingston - Code 5560 (1 copy)
Dr. A. I. Schindler - Code 6000 (1 copy)
Dr. H. Shenker - Code 5504 (1 copy)
Mr. D.J. McLaughlin - Code 5560 (1 copy)
Dr. John L. Walsh - Code 5503 (1 copy)

...h Energy Laser Project Office, Department of the Navy, Naval Sea Systems Command, Washington, D.C. 20360 - Attn: Capt. A. Skolnick, USN (PM 22) (1 copy)

Superintendent, Naval Postgraduate School, Monterey, CA 93940 - Attn: Library (Code 2124) (1 copy)

Navy Radiation Technology, Air Force Weapons Lab (NLO), Kirtland AFB, NM 87117 (1 copy)

Naval Surface Weapons Center, White Oak, Silver Spring, MD 20910 - Attn: Dr. Leon H. Schindel (Code 310) (1 copy)
Dr. E. Leroy Harris (Code 313) (1 copy)
Mr. K. Enkenhaus (Code 034) (1 copy)
Mr. J. Wise (Code 047) (1 copy)
Technical Library (1 copy)

U.S. Naval Weapons Center, China Lake, CA 93555 - Attn: Technical Library (1 copy)

HQ USAF (AF/RDPS), The Pentagon, Washington, D.C. 20330 - Attn: Lt. Col. A.J. Chiota (1 copy)

HQ AFSC/XRLW, Andrews AFB, Washington, D.C. 20331 - Attn: Maj. J.M. Walton (1 copy)

HQ AFSC (DLCAW), Andrews AFB, Washington, D.C. 20331 - Attn: Maj. H. Axelrod (1 copy)

Air Force Weapons Laboratory, Kirtland AFB, NM 87117 - Attn: LR (1 copy)
AL (1 copy)

HQ SAMSO (XRTD), P.O. Box 92960, Worldway Postal Center, Los Angeles, CA 90009 - Attn: Lt. Dorian DeMaio (XRTD) (1 copy)

AF Avionics Lab (TEO), Wright Patterson AFB, OH 45433 - Attn: Mr. K. Hutchinson (1 copy)

Dept. of the Air Force, Air Force Materials Lab. (AFSC), Wright Patterson AFB, OH 45433 - Attn: Maj. Paul Elder (LPS) (1 copy)
Laser Window Group

HQ Aeronautical Systems Div., Wright Patterson AFB, OH 45433 - Attn: XRF - Mr. Clifford Fawcett (1 copy)

Rome Air Development Command, Griffiss AFB, Rome, NY 13440 - Attn: Mr. R. Urtz (OCSE) (1 copy)

HQ Electronics Systems Div. (ESL), L.G. Hanacom Field, Bedford, MA 01730 - Attn: Mr. Alfred E. Anderson (XRT) (1 copy)
Technical Library (1 copy)

Air Force Rocket Propulsion Lab., Edwards AFB, CA 93523 - Attn: B.R. Bornhorst, (LKCG) (1 copy)

Air Force Aero Propulsion Lab., Wright Patterson AFB, OH 45433 - Attn: Col. Walter Moe (CC) (1 copy)

Dept. of the Air Force, Foreign Technology Division, Wright Patterson AFB, OH 45433 - Attn: PDTN (1 copy)

Commandant of the Marine Corps, Scientific Advisor (Code RD-1), Washington, D.C. 20380 (1 copy)

Aerospace Research Labs., (AP), Wright Patterson AFB, OH 45433 - Attn: Lt. Col. Max Duggins (1 copy)

Defense Intelligence Agency, Washington, D.C. 20301 - Attn: Mr. Seymour Berler (DT1B) (1 copy)

Central Intelligence Agency, Washington, D.C. 20505 - Attn: Mr. Julian C. Nall (1 copy)

Analytic Services, Inc., 5613 Leesburg Pike, Falls Church, VA 22041 - Attn: Dr. John Davis (1 copy)

Aerospace Corp., P.O. Box 92957, Los Angeles, CA 90009 - Attn: Dr. G.P. Millburn (1 copy)

Airesearch Manuf. Co., 9851-9951 Sepulvada Blvd., Los Angeles, CA 90009 - Attn: Mr. A. Colin Stancliffe (1 copy)

Atlantic Research Corp., Shirley Highway at Edsall Road, Alexandria, VA 22314 - Attn: Mr. Robert Naismith (1 copy)

Avco Everett Research Lab., 2385 Revere Beach Parkway, Everett, MA 02149 - Attn: Dr. George Sutton (1 copy)
Dr. Jack Daugherty (1 copy)

Battelle Columbus Laboratories, 505 King Avenue, Columbus, OH 43201 - Attn: Mr. Fred Tietzel (STPIAC) (1 copy)

Bell Aerospace Co., Buffalo, NY 14240 - Attn: Dr. Wayne C. Solomon (1 copy)

Boeing Company, P.O. Box 3999, Seattle, WA 98124 - Attn: Mr. M.J. Gamble (2-, 460, MS 8C-88) (1 copy)

Electro-Optical Systems, 300 N. Halstead, Pasadena, CA 91107 - Attn: Dr. Andrew Jensen (1 copy)

ESL, Inc., 495 Java Drive, Sunnyvale, CA 94086 - Attn: Arthur Einhorn (1 copy)

DISTRIBUTION LIST (Continued)

General Electric Co., Space Division, P.O. Box 8555, Philadelphia, PA 19101 - Attn: Dr. R.R. Sigismonti (1 copy)

General Electric Co., 100 Plastics Avenue, Pittsfield, MA 01201 - Attn: Mr. D.G. Harrington (Rm. 1044) (1 copy)

General Research Corp., P.O. Box 3587, Santa Barbara, CA 93105 - Attn: Dr. R. Holbrook (1 copy)

General Research Corp., 1501 Wilson Blvd., Suite 700, Arlington, VA 22209 - Attn: Dr. Giles F. Crimi (1 copy)

Hercules, Inc., Industrial System Dept., Wilmington, DE 19899 - Attn: Dr. R.S. Voris (1 copy)

Hercules, Inc., P.O. Box 210, Cumberland, MD 21502 - Attn: Dr. Ralph R. Preckel (1 copy)

Hughes Research Labs., 3011 Malibu Canyon Road, Malibu, CA 90265 - Attn: Dr. D. Forster (1 copy)

Hughes Aircraft Co., Aerospace Group - Systems Division, Canoga Park, CA 91304 - Attn: Dr. Jack A. Alcalay (1 copy)

Hughes Aircraft Co., Centinela and Teale Streets, Bldg. 6, MS E-125, Culver City, CA 90230 - Attn: Dr. William Yates (1 copy)

Institute for Defense Analyses, 400 Army-Navy Drive, Arlington, VA 22202 - Attn: Dr. Alvin Schnitzler (1 copy)

Johns Hopkins University, Applied Physics Lab., 8621 Georgia Avenue, Silver Spring, MD 20910 - Attn: Dr. Albert M. Stone (1 copy)

Lawrence Livermore Laboratory, P.O. Box 808, Livermore, CA 94550 - Attn: Dr. R.E. Kidder (1 copy)
Dr. E. Taller (1 copy)
Dr. Joe Fleck (1 copy)

Los Alamos Scientific Laboratory, P.O. Box 1663, Los Alamos, NM 87544 - Attn: Dr. Keith Boyer (1 copy)

Lulejian and Associates, Inc., Del Amo Financial Center, 21515 Hawthorne Blvd. - Suite 500, Torrance, CA 90503 (1 copy)

Lockheed Palo Alto Res. Lab., 3251 Hanover St., Palo Alto, CA 94303 - Attn: L.R. Lunsford, Orgn. 52-24, Bldg. 201 (1 copy)

Mathematical Sciences Northwest, Inc., P.O. Box 1887, Bellevue, WN 98009 - Attn: Dr. Abraham Hertzberg (1 copy)

Martin Marietta Corp., P.O. Box 179, Mail Station 0471, Denver, CO 80201 - Attn: Mr. Stewart Chapin (1 copy)

Massachusetts Institute of Technology, Lincoln Laboratory, P.O. Box 73, Lexington, MA 02173 - Attn: Dr. S. Edelberg (1 copy)
Dr. L.C. Marquet (1 copy)

McDoonell Douglas Astronautics Co., 5301 Bolsa Avenue, Huntington Beach, CA 92647 - Attn: Mr. P.L. Klevatt, Dept. A3-830-BBFO, M/S 9 (1 copy)

McDonnell Douglas Research Labs., Dept. 220, Box 516, St. Louis, MO 63166 - Attn: Dr. D.P. Ames (1 copy)

MITRE Corp., P.O. Box 208, Bedford, MA 01730 - Attn: Mr. A.C. Cron (1 copy)

North American Rockwell Corp., Autonetics Div., Anaheim, CA 92803 - Attn: Mr. T.T. Kumagi, C/476 Mail Code HA18 (1 copy)

Northrop Corp., 3401 West Broadway, Hawthorne, CA 90250 - Attn: Dr. Gerard Hasserjian, Laser Systems Dept. (1 copy)

Dr. Anthony N. Pirri, Physical Sciences, Inc., 18 Lakeside Office Park, Wakefield, MA 01880 (1 copy)

RAND Corp., 1700 Main Street, Santa Monica, CA 90406 - Attn: Dr. C.R. Culp/Mr. G.A. Carter (1 copy)

Raytheon Co., 28 Seyon Street, Waltham, MA 02154 - Attn: Dr. F.A. Horrigan (Res. Div.) (1 copy)

Raytheon Co., Boston Post Road, Sudbury, MA 01776 - Attn: Dr. C. Sonnenschien (Equip. Div.) (1 copy)

Raytheon Co., Bedford Labs, Missile Systems Div., Bedford, MA 01730 - Attn: Dr. H.A. Mehlhorn (1 copy)

Riverside Research Institute, 80 West End Street, New York, NY 10023 - Attn: Dr. L.H. O'Neill (1 copy)
Dr. John Bose (1 copy)
(HPEGL Library) (1 copy)

R&D Associates, Inc., P.O. Box 3580, Santa Monica, CA 90431 - Attn: Dr. R.E. LeLevier (1 copy)

Rockwell International Corporation, Rocketdyne Division, Albuquerque District Office, 3636 Menaul Blvd., NE, Suite 211, Albuquerque, NM 87110 - Attn: C.K. Kraus, Mgr. (1 copy)

SANDIA Corp., P.O. Box 5800, Albuquerque, NM 87115 - Attn: Dr. Al Narath (1 copy)

Stanford Research Institute, Menlo Park, CA 94025 - Attn: Dr. F.T. Smith (1 copy)

Science Applications, Inc., 1911 N. Ft. Meyer Drive, Arlington, VA 22209 - Attn: L. Peckam (1 copy)

Science Applications, Inc., P.O. Box 328, Ann Arbor, MI 48103 - Attn: R.E. Meredith (1 copy)

Science Applications, Inc., 6 Preston Court, Bedford, MA 01703 - Attn: R. Greenberg (1 copy)

Science Applications, Inc., P.O. Box 2351, La Jolla, CA 92037 - Attn: Dr. John Asmus (1 copy)

Systems, Science and Software, P.O. Box 1620, La Jolla, CA 92037 - Attn: Alan F. Klein (1 copy)

Systems Consultants, Inc., 1050 31st Street, NW, Washington, D.C. 20007 - Attn: Dr. R.B. Keller (1 copy)

Thiokol Chemical Corp., WASATCH Division, P.O. Box 524, Brigham City, UT 84302 - Attn: Mr. J.E. Hansen (1 copy)

TRW Systems Group, One Space Park, Bldg. R-1, Rm. 1050, Redondo Beach, CA 90278 - Attn: Mr. Norman Campbell (1 copy)

United Technologies Research Center, 400 Main Street, East Hartford, CT 06108 - Attn: Mr. G.H. McLafferty (3 copies)

DISTRIBUTION LIST (Continued)

United Technologiee Reeearch Center, Pratt and Whitney Aircraft Div., Florida R&D Center, Weet Palm Beach, FL 33402 Attn: Dr. R.A. Schmidtke (1 copy)
Mr. Ed Pinsley (1 copy)

VARIAN Aeeociates, EIMAC Divieion, 301 Induetrial Way, San Carlos, CA 94070 - Attn: Mr. Jack Quinn (1 copy)

Vought Syeteme Divieion, LTV Aeroepace Corp., P.O. Box 5907, Dallae, TX 75222 - Attn: Mr. F.G. Simpeon, MS 254142 (1 copy)

Weetinghouse Elactric Corp., Defeoee and Space Center, Balt-Waeh. International Airport - Box 746, Baltimore, MD 21203 - Attn: Mr. W.F. Liet (1 copy)

Weetinghouee Reeearch Labs., Beulah Road, Churchill Boro, Pitteburgh, PA 15235 - Attn: Dr. E.P. Riedel (1 copy)

United Technologiee Reeearch Center, Eaet Hartford, CT 06108 - Attn: A.J. DeMaria (1 copy)

Airborne Inetrumente Laboratory, Walt Whitorian Road, Melville, NY 11746 - Attn: F. Pace (1 copy)

General Elactric R&D Center, Schenectady, NY 12305 - Attn: Dr. Donald White (1 copy)

Cleveland Stats Univereity, Cleveland, OH 44115 - Attn: Dean Jack Soules (1 copy)

EXXON Reeearch and Engineering Co., P.O. Box 8, Linden, NJ 07036 - Attn: D. Grafetein (1 copy)

Univereity of Maryland, Department of Phyeice and Aetronomy, College Park, MD 20742 - Attn: D. Currie (1 copy)

Sylvania Elactric Producte, Inc., 100 Fergeeon Drive, Mountain View, CA 94040 - Attn: L.M. Oeterink (1 copy)

North Amarican Rockwell Corp., Autonetice Divieion, 3370 Miraloma Avenue, Anaheim, CA 92803 - Attn: R. Gudmundeen (1 copy)

Maeeachusetts Instituts of Tachnology, 77 Maeeachueette Avenue, Cambridge, MA 02138 - Attn: Prof. A. Javan (1 copy)

Lockheed Missils & Spaca Co., Palo Alto Reeearch Laboratoriee, Palo Alto, CA 94304 - Attn: Dr. R.C. Ohlman (1 copy)

ILC Laboratoriee, Inc., 164 Commercial Street, Sunnyvale, CA 94086 - Attn: L. Nobie (1 copy)

Univereity of Texae at Dallae, P.O. Box 30365, Dallae, TX 75230 - Attn: Prof. Carl B. Collins (1 copy)

Polytechnic Institute of New York, Rt. 110, Farmingdale, NY 11735 - Attn: Dr. William T. Walter (1 copy)